

# CHALMERS



## **Chassis Strength Evaluation and Rollover Analysis of a Single Seat Electric Car**

*Master of Science Thesis in Automotive engineering*

**ESWAR VIJAYAKUMAR**

Department of Applied mechanics  
*Division of Automotive engineering*  
*Vehicle dynamics group*  
CHALMERS UNIVERSITY OF TECHNOLOGY  
Gothenburg, Sweden, 2013  
Report No. 2013:61



Master's thesis in *Automotive Engineering*

# **Chassis Strength Evaluation and Rollover Analysis of a Single Seat Electric Car**

ESWAR VIJAYAKUMAR

Department of Applied Mechanics  
Division of Automotive engineering  
Vehicle dynamics group  
CHALMERS UNIVERSITY OF TECHNOLOGY  
Goteborg, Sweden  
2013

**Chassis Strength Evaluation and Rollover Analysis of a Single Seat Electric Car**  
ESWAR VIJAYAKUMAR

© ESWAR VIJAYAKUMAR, 2013.

Master's Thesis  
2013:61  
ISSN 1652-8557  
Department of Applied Mechanics  
Division of Automotive engineering  
Vehicle Dynamics group  
Chalmers University of Technology  
SE-412 96 Göteborg  
Sweden  
Telephone: + 46 (0)31-772 1000

Commissioned by: Volvo Group Advanced Technology & Research  
Department of Mechatronics and Software  
Volvo Group Trucks Technology  
SE- 412 58 Göteborg  
Sweden

Cover:  
Concept CAD model of the electric demonstration vehicle, developed at Volvo GTT [1]  
Printed at Chalmers Reproservice  
Goteborg, Sweden 2013

# **Chassis Strength Evaluation and Rollover Analysis of a Single Seat Electric Car**

ESWAR VIJAYAKUMAR

Department of Applied Mechanics

Division of Automotive engineering

Chalmers University of Technology

## **ABSTRACT**

This thesis work is the part of project “EDV (electric demonstration vehicle)” at Volvo group trucks technology, Mechatronics and Software division, which aims at building a single seat electric car. The car will later, primary, be used for function development.

In this thesis, mass of the vehicle and the center of gravity position of the static vehicle are estimated and are used to perform the chassis strength analysis and rollover analysis of the vehicle. For chassis strength analysis, three frame variants are analyzed with various beam cross sections and frame features such as fillets and gussets to optimize for torsional stiffness, bending stiffness, stress generated and weight. For steady state rollover analysis, the vehicle is tested for rollover propensity on various maneuver conditions, road friction conditions, bank angles and vehicle property such as center of gravity location of the vehicle.

Though, the results of this thesis work pertain to a specific single seat electric car, but, the results are extrapolated to provide a general overview. Beam cross sections and structures of chassis are proposed in the chapter chassis strength evaluation. Here, both analytical model and finite element analysis models are presented. The results of rollover analysis pertain to the limitations of the vehicle in terms of road friction, possible maneuver proportions, possible speed limits, bank angles and vehicle property such as center of gravity height.

Keywords: Chassis strength, rollover, dynamic, stiffness, friction, center of gravity, fillets, gussets, stress, finite element analysis, steady state cornering



## PREFACE

In this study, chassis strength evaluation and rollover analysis of a single seat electric car has been performed. The thesis has been carried out from January 2013 to July 2013. The study is a part of a project “Electric Demonstration Vehicle (EDV)” at Volvo group trucks technology, mechatronics and software division, rooting to study and improvise on functional developments of a vehicle. The project is carried out at the Department of Applied mechanics, Automotive engineering division, Chalmers University of Technology, Sweden. The project is financed by Volvo Group Trucks Technology, Sweden.

This thesis wouldn't have been possible without help and support of a lot of people around me. Though it is not possible to mention everyone here, nonetheless, all the contributions are much appreciated.

First of all, I would like to thank Dr. Jonas Hellgren of Volvo GTT, division mechatronics and software, for providing me with this thesis work at Volvo GTT and unconditional help whenever it was required. Without his excellent academic and managerial supervision, it would have been hard task to complete this thesis.

Next, I would like to thank Prof. Bengt Jacobson, division of vehicle dynamics to provide me with support from the University and clarifying all the doubts on all the problems I encountered pertaining to vehicle dynamics.

One of the important people I would like to mention is Mr. V. Vijayakumar, my father, who provided with me with information on regular industrial practices on chassis strength evaluation.

This work was performed under the financial support of Volvo Group Trucks Technology, Gothenburg, Sweden.

I further want to express my gratitude towards my mother, Mrs. K. Vijayarani and Grandmother Mrs. Nagalakshmi for their unconditional love and helping me keep the balance in life under stress.

Eswar Vijayakumar  
Gothenburg, August 2013





# CONTENTS

ABSTRACT .....	V
PREFACE.....	VII
CONTENTS .....	IX
INTRODUCTION .....	XI
NOTATIONS.....	XIII
1 Mass estimation.....	1
1.1 Data setting.....	1
1.2 Modeling .....	1
1.3 Results .....	3
2 Center of gravity evaluation.....	4
2.1 Data setting.....	4
2.2 Modeling .....	5
2.3 Results .....	6
3 Rollover analysis .....	7
3.1 Data setting.....	8
3.2 Modeling .....	9
3.2.1 Steady state modeling .....	9
3.3 Results and discussion .....	13
3.3.1 Steady state model results and discussion.....	14
3.3.2 Discussion .....	18
4 Frame strength evaluation using analytical method.....	19
4.1 Methodology.....	19
4.1.1 Mid beam shear stress.....	20
4.1.2 Mid beam bending stress.....	20
4.1.3 Mid beam deflection .....	20
4.1.4 Floor structure mass.....	21
4.1.5 Floor torsional stiffness.....	21
4.2 Data setting.....	23
4.3 Results .....	24
4.3.1 Total frame mass .....	25
5 FEM based frame strength evaluation.....	26
5.1 Methodology.....	26
5.1.1 Approach .....	26
5.1.2 Target criteria .....	27
5.1.3 Frame variants .....	28
5.1.4 Frame features .....	28

5.1.5	Boundary conditions .....	30
5.2	Results .....	31
5.3	Discussion .....	34
6	Result summary .....	35
Appendix A	.....	A-1
A.1	Fixed mass values of components .....	A-2
A.2	Mass estimation of battery pack .....	A-2
A.3	Mass estimation of electric motor module .....	A-3
A.4	Mass estimation of passenger module .....	A-4
A.5	Mass estimation of front suspension module .....	A-5
A.6	Mass estimation of rear suspension module .....	A-6
A.7	Mass estimation of transmission module .....	A-7
A.8	Mass estimation of genset module .....	A-8
A.9	Mass estimation of frame module .....	A-8
A.10	Miscellaneous mass module estimation .....	A-9
A.11	Mass estimation of the rims .....	A-10
A.12	Mass estimation of tire module .....	A-11
Appendix B	.....	B-1
Appendix C	.....	C-1
C.1	Suspension kinematics .....	C-1
C.2	Roll stiffness estimation .....	C-4
C.3	Road bank angle modeling .....	C-6
C.4	Steady state rollover simulation results .....	C-7
C.5	Transient rollover modeling .....	C-12
C.6	Transient maneuver results .....	C-18
Appendix D	.....	D-1
Appendix E	.....	E-1
E.1	Approach .....	E-1
E.2	Boundary conditions .....	E-1
E.2.1	Torsional stiffness .....	E-1
E.2.2	Bending stiffness .....	E-4
E.3	Beam shortlist .....	E-6
REFERENCES	.....	36

# INTRODUCTION

Single seat Electric vehicles (EV's) might become an alternative mode of transportation for short distant travel these days with an increase in the demand for non-renewable resource of energy. There are many electric cars are available in the market, such as Renault Twizy, Mahindra Reva, Kewet Buddy and Qbeak. These cars serve as a platform to keep abreast the revolution in battery technology. Similarly, Volvo group trucks technology have come up with an idea of “Electric demonstration vehicle (EDV)”, which will serve as a platform to test technologies and functions. For example, development of battery technology.

For a conceptual look of the vehicle, refer to Figure 1.



Figure 1: Conceptual picture of EDV.

## Deliverables

The tasks, sub tasks and deliverables of this thesis work refer Figure 2.

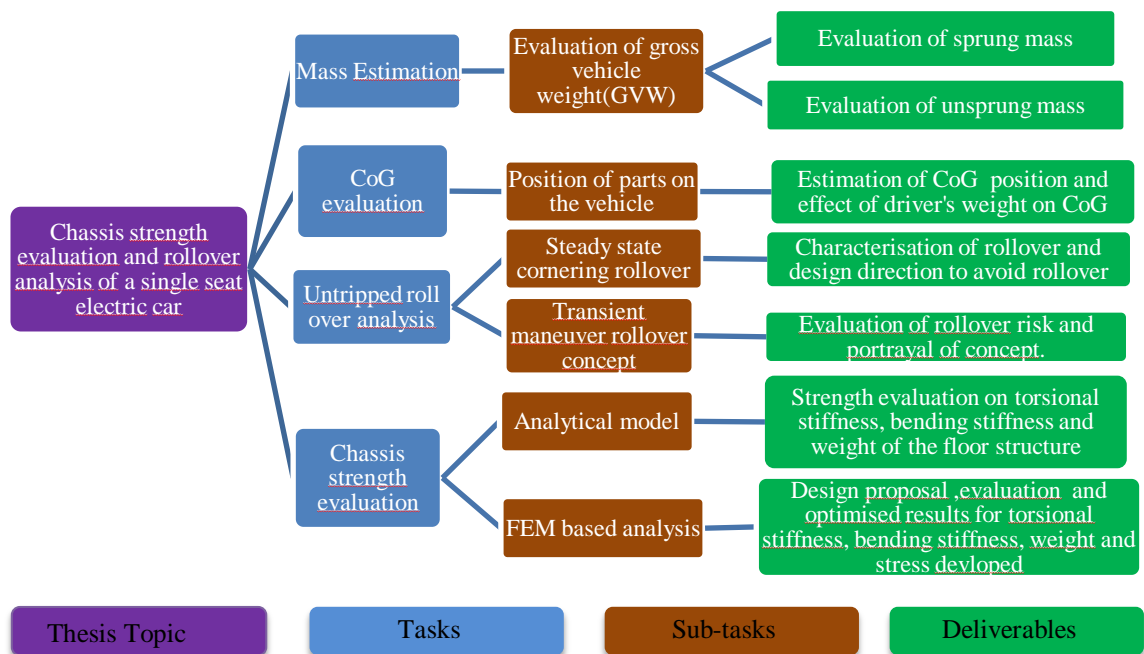


Figure 2: Tasks, subtasks and deliverables

## **Delimitations**

The objective of this section is to enlist the limitations of this thesis. Some of the delimitations are

- Chapter 1 gives approximate masses of the vehicle, as mass of certain parts of vehicle were not measured and have been considered using references.
- Chapter 2 does not consider the effects of suspension.
- Transient modeling in Appendix C for Chapter 3 does not aim to study rollover in worst possible maneuvers. Just step steer inputs are considered. It just depicts another method to predict rollover.
- In Chapters 4 and 5 , effects of vehicle handling are not taken into consideration. The strength of the chassis is evaluated using steady state load cases and static load cases.

## NOTATIONS

For Chapters 1 ,2 and 3 .

### Roman letters

$GVW^e$	Expected gross vehicle weight
$GVW^{max}$	Maximum gross vehicle weight
$GVW^{min}$	Minimum gross vehicle weight
$m_{ref}^e$	Expected reference mass
$m_{ref}^{max}$	Maximum reference mass
$m_{ref}^{min}$	Minimum reference mass
$m_{curb}^e$	Expected curb mass
$m_{curb}^{max}$	Maximum curb mass
$m_{curb}^{min}$	Minimum curb mass
$m_{sprung}^e$	Expected sprung mass
$m_{sprung}^{max}$	Maximum sprung mass
$m_{sprung}^{min}$	Minimum sprung mass
$m_{unsprung}^e$	Expected unsprung mass
$m_{unsprung}^{max}$	Maximum unsprung mass
$m_{unsprung}^{min}$	Minimum unsprung mass
$m_{driver}^e$	Expected driver's mass
$m_{driver}^{max}$	Maximum driver's mass
$m_{driver}^{min}$	Minimum driver's mass
$m_{baggage}^e$	Expected baggage mass
$m_{baggage}^{max}$	Maximum baggage mass
$m_{baggage}^{min}$	Minimum baggage mass

$h_{cog}^{vehicle}$	Height of center of gravity of the vehicle
$L$	Wheelbase of the vehicle
$t_w$	Track width of the vehicle
$C_\alpha$	Cornering stiffness
$F_x$	Longitudinal force along X axis
$F_y$	Lateral force along Y axis
$F_z$	Normal force along Z axis
$h_{rollc}$	Height of the roll axis from the ground at the plane of center of gravity
$h_{roll}$	Distance between roll axis and center of gravity
$h_{rcf}$	Height of roll center of the front axle
$h_{rcr}$	Height of roll center of the rear axle
$J_{zz}$	Polar moment of inertia
$K_s$	Spring stiffness
$K_{st}$	Suspension stiffness
$v_x$	Longitudinal velocity of the vehicle
$R$	Radius of the corner
$SSF$	Static stability factor
$a_x$	Acceleration along X axis
$a_y$	Acceleration along Y axis
$K_\phi$	Roll stiffness of the vehicle
$T_\phi$	Torque acting on the vehicle about X axis
$\Delta z$	Displacement along Z axis
$K_{lat}^{tyre}$	Tire lateral stiffness

#### **Greek letters**

$\mu$	Road tire coefficient of static friction
-------	--

$\alpha$	Tire side slip angle
$\psi$	Yaw angle
$\varphi$	Body roll angle
$\beta$	Body slip
$\gamma$	Angle between center of contact patch and instantaneous center
$\delta$	Wheel steered angle
$\phi$	Road bank angle

### Subscripts

$\cdot$	Derivation with respect to time
$\ddot{\phantom{x}}$	Second derivation with respect to time
$x$	X axis direction
$y$	Y axis direction
$z$	Z axis direction
$i$	Wheel (left/right)
$j$	Axle (front/rear)
$1$	Front axle
$2$	Rear axle
$l$	Left wheel
$r$	Right wheel
$c$	Component module

For Chapters 4 and 5 the notations are given below.

### Roman letters

$T$	Torque
$E$	Young's modulus
$G$	Shear modulus

$K_t$	Torsional stiffness
$K_b$	Bending stiffness
$B$	Outer width of the beam
$b$	Inner width of the beam
$H$	Depth of the beam
$h$	Inner depth of the beam
$t$	Thickness of the beam
$L_x$	Length of the floor beam structure along X axis
$L$	Distance between the load points
$z$	Displacement in Z direction
$F$	Force
$F_v$	Vertical force along Z direction
$m_{floor}$	Mass of floor structure
$I$	Area moment of inertia
$T_{simulation}$	Simulation torque input

### **Greek Letters**

$\sigma_v$	von Mises Stress or equivalent stress
$\delta$	Deflection
$\sigma_y$	Yield Strength
$\varphi$	Deflection angle about an axis
$\rho$	Density of the material
$\nu$	Poisson's ratio

### **Subscripts**

$x$	X axis direction
$y$	Y axis direction



<i>z</i>	Z axis direction
13	Corresponds to beam 1 and 3
2	Corresponds to beam 2



# 1 Mass estimation

The objective of this chapter is to evaluate the vehicle mass. GVW, reference mass, curb mass, sprung mass and unsprung mass, refer Table 1.1 for definitions. Results with and without genset (range extender) are also presented. Terms used in the chapter are defined in Table 1.1.

Table 1.1: Terms and definitions

Term	Description
GVW (kg)	Gross vehicle weight. Maximum operating mass. Typically it includes driver/passenger(s) and baggage. The fuel tank is filled. This mass is used in performance analysis, e.g. acceleration analysis.
Reference mass (kg)	This mass is the typical operating mass, used in energy/fuel consumption analysis.
Curb mass (kg)	Vehicle mass without driver/passenger(s) or baggage. This one is defined because it is included both in reference mass and GVW.
Sprung mass(kg)	Sprung mass of an automobile is defined as the portions of the vehicle's mass that lies above the suspension system.
Unsprung mass(kg)	Unsprung mass is the portion of the vehicle's mass that lies below the sprung mass and ground when the vehicle is said to be in a stand still position.

## 1.1 Data setting

For further details on definition of variables and setting, the mass limits are defined in Appendix A. The results presented contain results pertaining to wheel motors (WM) and axle motors (AM), as at the beginning of the thesis, the configuration wasn't decided. Pictorial representations of these two models are illustrated in Figure 1.1.



Figure 1.1: Left- Axle mounted motors; second from left- Wheel motors, third from left- Torsion bar suspension, Extreme right- Double wishbone suspension

## 1.2 Modeling

Expected, maximum and minimum GVW is defined by (1. 1) - (1. 3). In this mass, both driver and baggage are added to the curb mass. Expected, maximum and minimum reference mass by (1. 4)-(1. 6). Driver mass is added to curb mas for defining reference mass. Expected, maximum and minimum curb mass by (1. 7)-(1. 9). More motivation about the component modules and their masses are given in Appendix A.

$$GVW^e = m_{curb}^e + m_{driver}^e + m_{baggage}^e \quad (1.1)$$

$$GVW^{max} = m_{curb}^{max} + m_{driver}^{max} + m_{baggage}^{max} \quad (1.2)$$

$$GVW^{min} = m_{curb}^{min} + m_{driver}^{min} + m_{baggage}^{min} \quad (1.3)$$

$$m_{ref}^e = m_{curb}^e + m_{driver}^e \quad (1.4)$$

$$m_{ref}^{max} = m_{curb}^{max} + m_{driver}^{max} \quad (1.5)$$

$$m_{ref}^{min} = m_{curb}^{min} + m_{driver}^{min} \quad (1.6)$$

$$m_{curb}^e = \sum_{c=1}^k m_c^e \quad (1.7)$$

$$m_{curb}^{max} = \sum_{c=1}^k m_c^e + m_c^d \quad (1.8)$$

$$m_{curb}^{min} = \sum_{c=1}^k m_c^e - m_c^d \quad (1.9)$$

$$m_{sprung}^{min} = \sum_{c \in x} m_c^e - m_c^d \quad (1.10)$$

$$m_{sprung}^{max} = \sum_{c \in x} m_c^e + m_c^d \quad (1.11)$$

$$m_{sprung}^e = \sum_{c \in x} m_c^e \quad (1.12)$$

$$m_{unsprung}^{min} = \sum_{c \in y} m_c^e - m_c^d \quad (1.13)$$

$$m_{unsprung}^{max} = \sum_{c \in y} m_c^e + m_c^d \quad (1.14)$$

$$m_{unsprung}^e = \sum_{c \in y} m_c^e \quad (1.15)$$

Here, x stands for all the component modules corresponding to the sprung mass and y to the unsprung mass. Assessment of sprung and unsprung mass is relevant, as it could be used to get a clear idea on their average masses for different chassis proposals, which will be used in the Chapters 2 , 3 , 4 and 5 .

### 1.3 Results

From the data setting and modeling in previous sections, the mass estimation results in Figure 1.2 are derived. It was decided to further the development of EDV with the axle mounted motor and wishbone suspension configuration. As the figure shows,  $m_{curb} \sim 318 \text{ kg}$ ,  $m_{reference} \sim 398 \text{ kg}$ ,  $GVW \sim 418 \text{ kg}$ ,  $m_{unsprung}^e \sim 63 \text{ kg}$  and  $m_{sprung}^e \sim 355 \text{ kg}$  for the current vehicle setup, wishbones with axle mounted motors. The variation in the GVW is high due to high uncertainty in the weight of the driver and baggage.

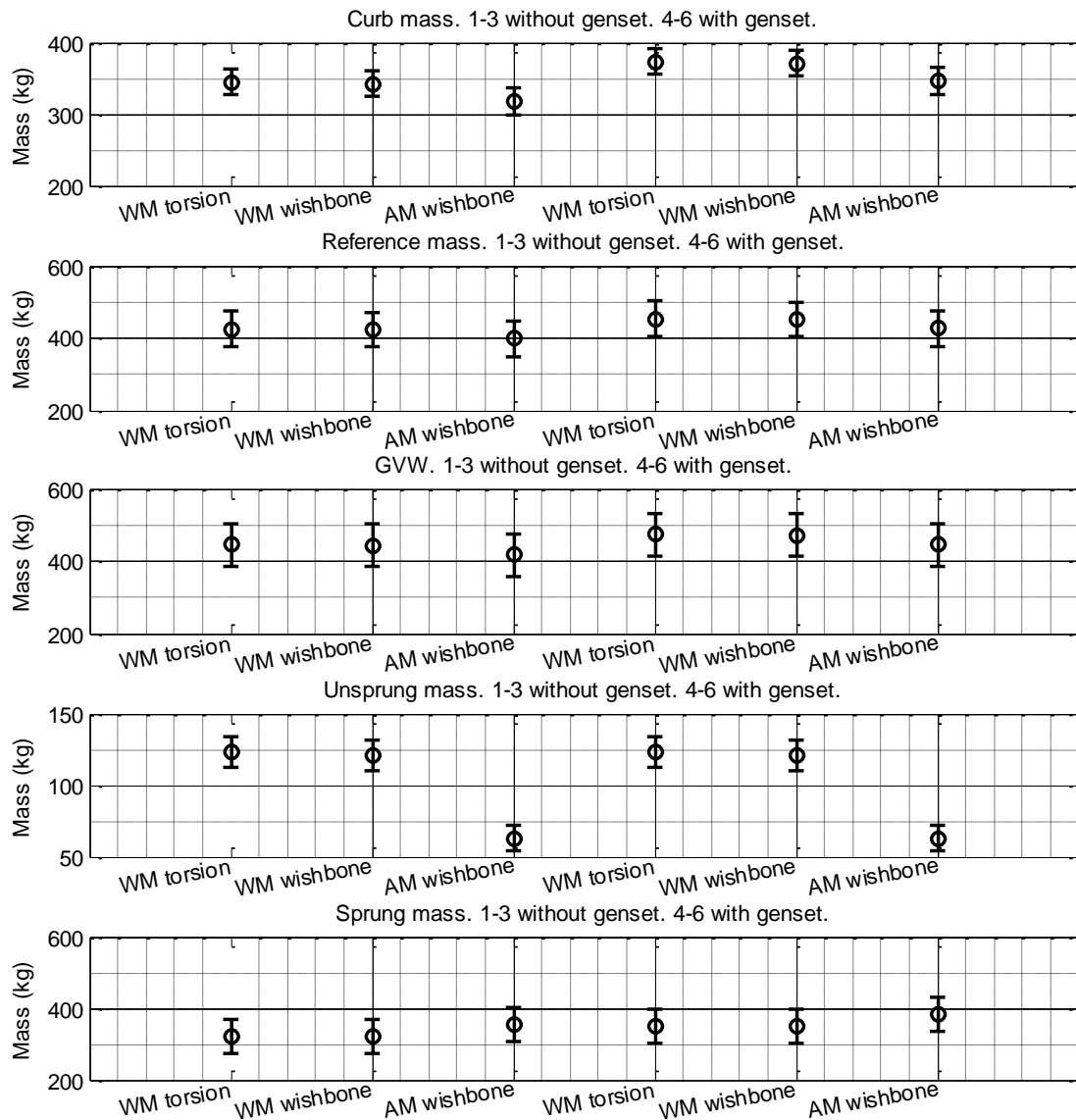



Figure 1.2: Mass estimation results. The error bars show the expected (circle), minimum and maximum masses for every design variant. The first three variants are without genset and the rest are with genset.

## 2 Center of gravity evaluation

The objective of this chapter is to evaluate the position of center of gravity (CoG) of the static vehicle. This chapter also throws light on the effects on vehicle's CoG due to position of various components. This chapter shows results of current position of static CoG of the vehicle. The terms used in this chapter are shown in Figure 2.1. It is to be noted that, the static and dynamic effects of suspension travel are not taken into consideration.

Table 2.1: Term definitions

Terms	Definition
CoG	For every system at every instant in time, there is a unique position in space that is the average position of the systems mass. This position is either called the center of mass, Center of gravity (CoG), system with unified gravity or  .
Module	When a component is specified with term "module", it accounts for the respective part and small components that are associated with that particular assembly. Example: front suspension module means, the upper wishbones, lower wishbones, tie rods, uprights, bearings, bushings and etc.

### 2.1 Data setting

For position of CoG in each and every component module on the frame structure, refer Appendix B. For position of the components in the current vehicle specification refer Appendix B. For axis system refer Figure 2.1.

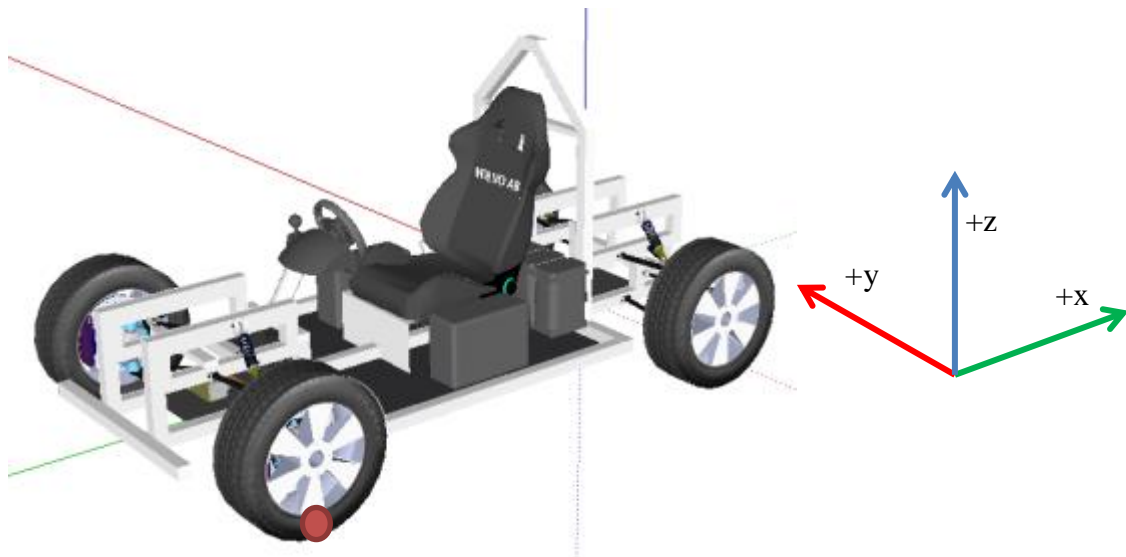


Figure 2.1: Axis system corresponding to chapter Center of gravity evaluation

The origin of the axis system is shown in Figure 2.1 and is denoted by the red dot, which is positioned at the front left wheel-center's projection on the ground. All the dimensions inside the vehicle from the origin are considered positive.

The mass of each and every component module estimated was taken from the Chapter 1 . The results from this chapter give an approximation of the CoG value.

The considered distance between the frame and the ground (ground clearance) was 200mm. This was set, considering suspension travel and general heights of speed bumps and curbs from [2], [3] and [4]. This ground clearance serves as a direction for suspension design (setting ride height) and is considered to be fixed.

## 2.2 Modeling

Since the objective of this chapter is to find out the static CoG location, the whole vehicle as a system is considered to be built with discrete masses of component modules. For each component module, the CoG is determined and based on the position of these component modules, the position of the final CoG of the whole system can be determined. It is to be noted that, all the CoG of all the component modules are given importance, which means that all the component modules are considered as point masses.

For a discrete system, the CoG [5] is given by (2. 1).

$$\overline{r_{cm,axis}} = \frac{\sum \overline{r_{i,axis}} \cdot m_c}{m_{tot}} \quad (2. 1)$$

$$m_{tot} = \sum m_c \quad (2. 2)$$

In equation (2. 1) and (2. 2),  $r$  is the distance of the COG of component modules with respect to the origin and subscript  $axis$  represents the direction along axis (X, Y or Z). Here,  $m_{tot}$  is the total mass of all the component modules. From equations (2. 1) and (2. 2), the CoG location of the system (vehicle) in x, y and z-axis are calculated. It is to be noted that the effects of suspension travel during static condition were not modeled. Also, the height of driver's center of gravity from ground is given by (2. 3).

$$h_{cog}^{driver} = \text{ground clearance} + \text{height of the middle floor structure beam} \\ + \text{height of seat mount} + \text{height of seat} \\ + \text{height of CoG of driver above the seat} \quad (2. 3)$$

$$\text{ground clearance} = \text{loaded wheel radius} \pm \text{ride height} \quad (2. 4)$$

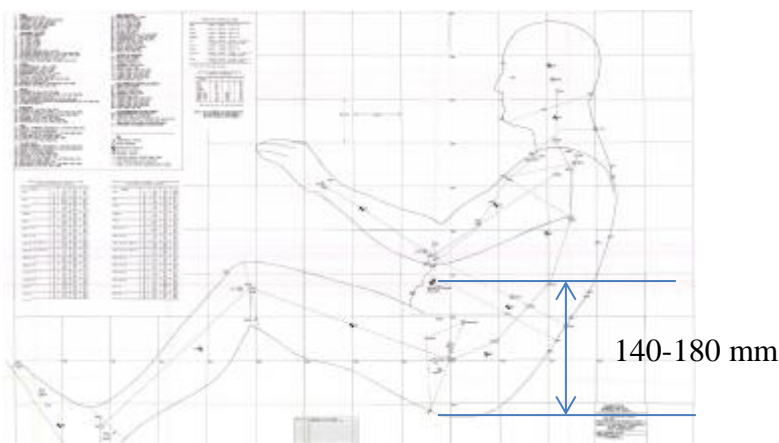


Figure 2.2: CoG position of various parts of a 95 percentile human being [6]

Height of center of gravity of a 95 percentile human being on a sitting posture varies from 140-180mm [6]. For a worst case scenario it is considered to be 180mm from the seat.

The height of seat mount and height of seat is given by [7]. The ride height is defined by the minimum distance between the axle center and the vehicle's under tray. This has not been decided yet. Ride height will be based on spring stiffness and spring inclination. For now the considered ride height is -250mm just to account for low CoG.

### 2.3 Results

For the current vehicle, the position of COG is given by Figure 2.3

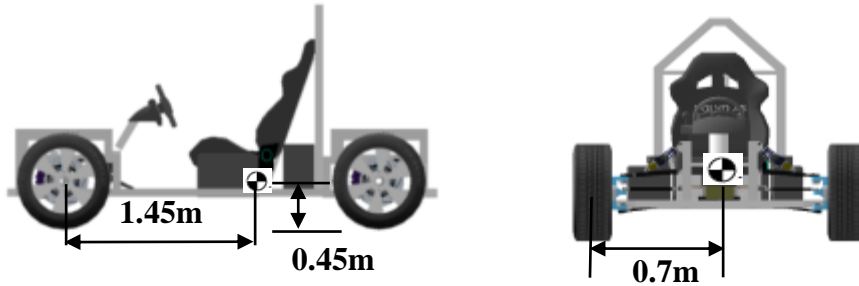


Figure 2.3: Left -Position of CoG in XZ plane of the vehicle; Right- Position of CoG in YZ plane

The load distribution in the front and rear axle is 37 percent and 63 percent respectively. Figure 2.4 gives better understanding of variation of the CoG position with respect to increase or decrease in driver's mass.

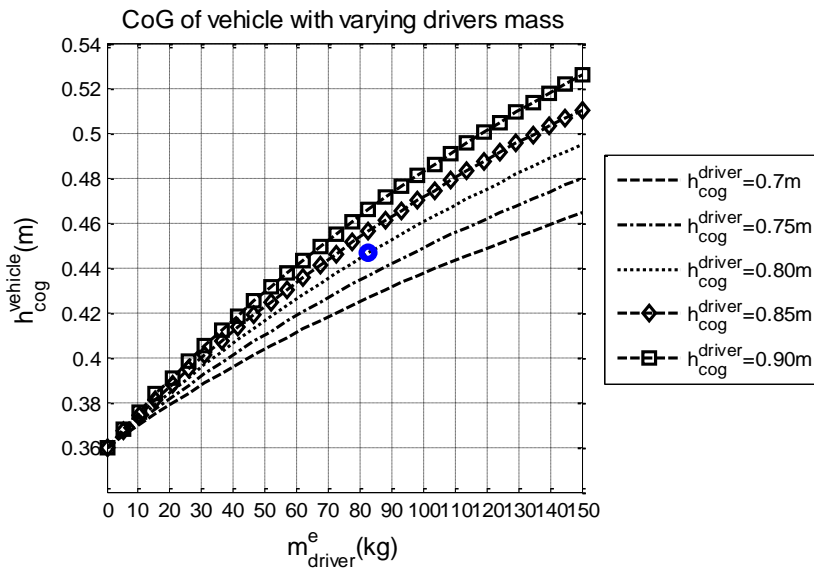


Figure 2.4: Variation of vehicle's CoG height from ground with respect to weight of the driver and his/her position from the ground.

For a driverless vehicle,  $h_{cog}^{vehicle} \cong 0.355m$ . (Considering no suspension effects)

It can be seen from Figure 2.4 that, with an increase in weight of the driver, the height of CoG of the vehicle increases. This effect reduces, as the driver's CoG is closer to the vehicle's CoG. For the current configuration and position of the driver, the CoG of the vehicle is represented by a blue dot in Figure 2.4.

For the current vehicle setup and an expected driver's mass of 82kg, the position of CoG location is shown in Figure 2.3. These figures include the mass of the driver and baggage.



### 3 Rollover analysis

The purpose of this chapter is to evaluate friction/untripped rollover behavior of the vehicle. This chapter includes the basic mechanics of a rollover propensity and results pertaining to steady state rollover mechanics are produced. For steady state rollover, the effects of roll angle, change in half-track width, effects of jacking forces on height of center of gravity and effects of suspension kinematics on the rollover threshold are modeled and are presented. The varying parameters of this section are height of center of gravity, road friction and banking angle. The limitations with this chapter are braking and accelerating in corners is not modeled and tipped rollover is not modeled. Additionally, banking corresponding to centrifugal force is not modeled. (Refer Table 3.1)

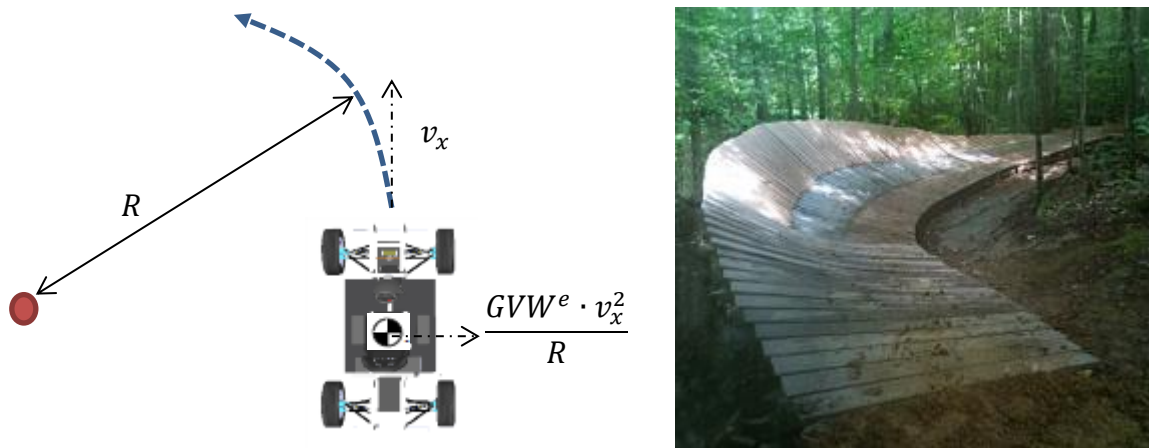


Figure 3.1: Left- Steady state cornering; Right- Inward bank corner

Certain important definitions used in this Chapter are mentioned in Table 3.1.

Table 3.1: Terms and definitions

Terms	Definitions
Rollover threshold	The lateral acceleration at which the rollover takes place. Defined in terms of lateral acceleration normalized with gravitational force.
Roll axis	It is the imaginary line that connects the roll centers of the front and rear suspensions.
Roll center	Roll center of a suspension is a point around which all the suspension hard points rotate and it's the point at which all the suspension forces act.
Instantaneous center	It is the imaginary point around which all the suspension hard points rotate when the vehicle body experiences roll.
Half-track width	The lateral distance between centerline of the vehicle and the center of contact patch of the tires.
Cornering stiffness	Initial linear slope of $\mu$ vs. side slip curve; $C_\alpha = -\left(\frac{\partial}{\partial \alpha} F_y\right)\Big _{\alpha=0}$
Slip angle	The difference between intended wheel heading direction and wheel travel direction.(considered SAE system for positive and negative slip angles)
Normal force	Vertical force acting on the tire /axle/vehicle.
Banking angle	The inclination of the road in the Y-Z plane of a vehicle.

Centripetal force	Tendency of an object following a curved path to fly away from the center of curvature. The direction is from center of the circle towards the object.
Centrifugal force	Reaction force that keeps the object moving in a circular path. The direction of the force is from the object towards the center of circle.

### 3.1 Data setting

For rollover analysis, the following parameters have been taken into account, listed in Table 3.2.

Table 3.2: Fixed vehicle parameters

S.no	Fixed parameter	Value	Unit	Comment/Reference
1	Vehicle mass( $GVW^e$ )	418	$kg$	Chapter 1
2	Wheelbase( $L$ )	2.3	$m$	Vehicle parameter(given)
3	Steering ratio	11	-	[8]
4	Roll center height front( $h_{rcf}$ )	0	$m$	Appendix C
5	Roll center height rear( $h_{rcr}$ )	0	$m$	Appendix C
6	Spring stiffness( $K_s$ )	10	$kN/m$	[8]
7	Polar moment of inertia( $J_{zz}$ )	984	$Kgm^2$	Evaluation from frame CAD model [1]
8	Load distribution(front/rear)	37/63	%	Chapter 2
9	Tire cornering stiffness( $C_\alpha$ )	36	$kN/rad$	[9]
10	Lateral Tire stiffness( $K_{lat}^{tire}$ )	90	$kN/m$	[10] for tire 195/60R15
11	Track width( $t_w$ )	1.4	$m$	[7] [4]

Table 3.3: Varying vehicle parameters

S.no	Varying parameters	Min value	Max value	Units	Comment/Reference
1	Friction coefficient( $\mu$ )	0.4	1.3	-	Ice, wet road and dry road [11]
2	Center of gravity height ( $h_{cog}^{vehicle}$ )	0.4	0.5	m	Chapter 2 .Driver's weight of 50kg, 100kg and 150 kg. <sup>1</sup>
3	Road bank angle( $\phi$ )	0	11	degrees	Refer Appendix C.

All the roads these days are not flat. They either have an inward bank (just like closed loop racing circuits) which generates centrifugal force, or with an outward bank (not common) which generates centripetal force. Outward banks usually result in faster rollovers than in an inward bank, as lateral acceleration threshold required for the vehicle to rollover is less. For definition of forces, refer Table 3.1.

As a “worst case scenario”, banking angles which generates centripetal force are modeled in this chapter. Refer Figure 3.2. For a clear view on the critical case modeled here. For more motivation on selection of bank angle, refer Appendix C.

<sup>1</sup> 50kg corresponds to 0.4m COG, while 150kg corresponds to 0.5m COG

The relation between  $K_s$  and roll stiffness of the vehicle ( $K_\phi$ ) is given in Appendix C. A linear spring model is considered.

Table 3.4: Minimum and maximum radius and velocity setting

	Minimum	Maximum	Comment/Reference
$R(m)$	5	100	Refer Appendix C and refer [8]
$v_x(kmph)$	10	100	From [4]

Table 3.4 gives the minimum and maximum radius and velocity settings under which, the vehicle model is simulated for both steady state and transient simulations.

## 3.2 Modeling

This section consists of two parts i.e. steady state cornering modeling and transient maneuver modeling.

### 3.2.1 Steady state modeling

This section consists of steady state rollover mechanics of the vehicle and various effects that contribute towards enhancing rollover such as body roll angle, change in half-track width, effects of jacking forces on height of center of gravity and effects of suspension kinematics. Though this might not go deep into all the topics, it gives a better understanding of these effects on rollover situations.

#### Rigid body rollover

The vehicle is considered to be a rigid body and no suspension effects are taken under consideration. This chapter introduces to a term called steady state factor (SSF), which describes the rollover of a rigid vehicle.

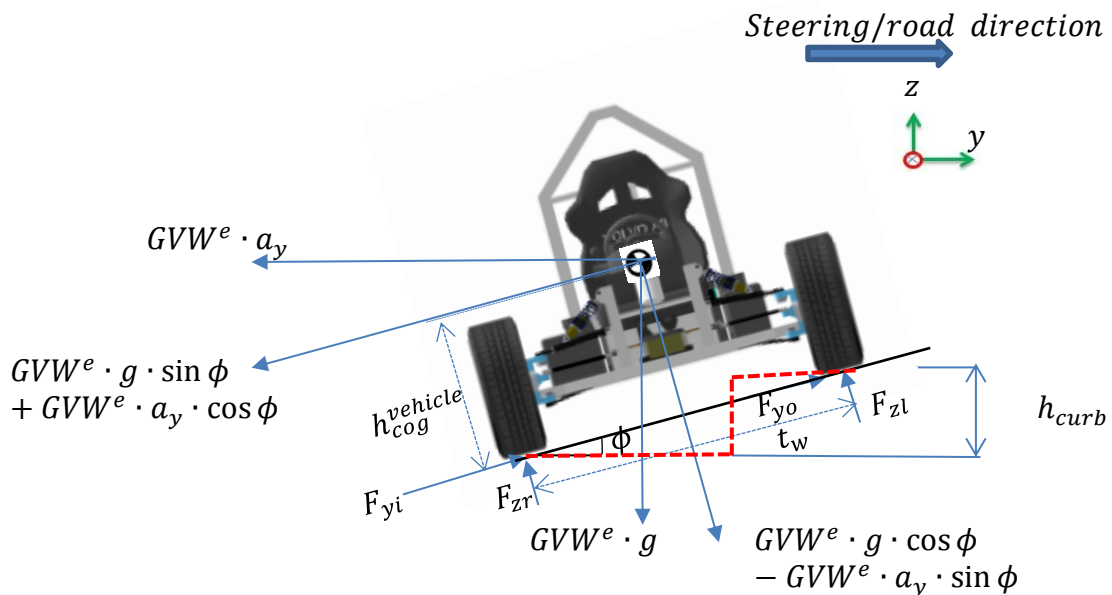


Figure 3.2: Rigid body rollover

Moment equilibrium about the outside wheel (left wheel) is given by (3. 1)

$$\sum T = GVW^e \cdot a_y \cdot h_{cog}^{vehicle} \cdot \cos \phi - GVW^e \cdot g \cdot \frac{t_w}{2} \cdot \cos \phi + GVW^e \cdot g \cdot h_{cog}^{vehicle} \cdot \sin \phi + GVW^e \cdot a_y \cdot \frac{t_w}{2} \cdot \sin \phi + F_{zr} \cdot t_w = 0 \quad (3.1)$$

The lateral acceleration at which the rollover begins is the rollover threshold. In this case, the rollover threshold is defined at a lateral acceleration at  $F_{zr} = 0$ .  $GVW^e$  stands for expected gross vehicle weight (refer Chapter 1 ).

$$\left. \frac{a_y}{g} \right|_{F_{zr}=0} = \frac{t_w \cdot \cos \phi - 2 \cdot h_{cog}^{vehicle} \cdot \sin \phi}{2 \cdot h_{cog}^{vehicle} \cdot \cos \phi + t_w \cdot \sin \phi} \quad (3.2)$$

$$\left. \frac{a_y}{g} \right|_{F_{zr}=0, \phi=0} = a_y^{rigid} = \frac{t_w}{2 \cdot h_{cog}^{vehicle}} = SSF \quad (3.3)$$

Where, SSF stands for static stability factor. Equation (3. 2) gives SSF with a bank angle as shown in Figure 3.2.

The static stability factor does not give accurate results as it does not take the effects of body roll, suspension and tire compliances, change in half-track width and wheel jacking into consideration. This significantly reduces the rollover threshold lateral acceleration of the vehicle.

### Effects of body roll

Vehicle body roll angle for the current suspension setup is given by (3. 4).

$$\varphi = \frac{T_\varphi}{K_\varphi} = \frac{m_{sprung}^e \cdot h_{cog}^{vehicle} \cdot a_y \cdot \cos \phi + m_{sprung}^e \cdot g \cdot h_{cog}^{vehicle} \cdot \sin \phi}{K_\varphi} \quad (3.4)$$

$T_\varphi$  is the roll moment acting around the roll axis of the vehicle on the vehicle body,  $m_{sprung}^e$  is the expected sprung mass,  $h_{roll}$  is the height of center of gravity over the roll axis,  $K_\varphi$  is the total roll stiffness of the vehicle including the cornering stiffness of the tires and suspension,  $\varphi$  is the roll angle of the sprung mass with respect to the roll center and  $\phi$  is the bank angle of the road.

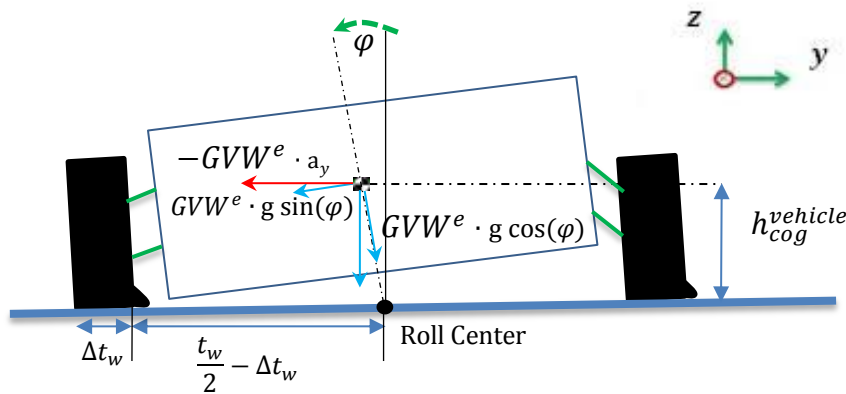


Figure 3.3: Vehicle body roll free body diagram

For more reference on the position of roll center, refer Appendix C. Vehicle body roll results in the lateral shift of center of gravity which results in the sinus component of the body weight ( $GVW^e \cdot g \sin(\phi)$ ) which aids in the moment of the body roll around the roll axis and also gives rise to the reduction in half-track width of the vehicle.

### Effects of change in half track width

Tire compliance results in reduction of half-track width given by (3. 5)

$$\Delta t_{w1} = \frac{GVW^e \cdot a_y \cdot \cos \phi + GVW^e \cdot g \cdot \sin \phi}{K_{lat}^{tyre}} \quad (3. 5)$$

Where  $K_{lat}^{tyre}$  is the lateral stiffness of both the outside tires. The suspension lateral compliances are not taken into consideration to make it simpler and to avoid indulgence of unknown data.

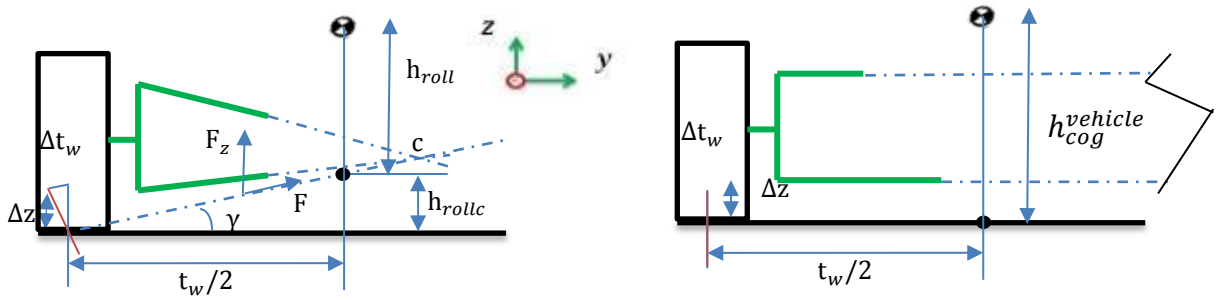


Figure 3.4: Left- Suspension (double wishbone with non-parallel unequal arms) set up and dimensions, Right- Current vehicle suspension setup (double wishbone with parallel unequal arms) for EDV

For the current suspension setup (parallel and unequal arms) as shown Figure 3.4 (right), the roll center lies on the ground. This means that,  $h_{rollc} = 0$ .

Increase in half-track width due to suspension compression ( $\Delta z$ ) is given by equation

$$\Delta t_{w2} = \Delta z \cdot \tan \gamma = \frac{2 \cdot \Delta z \cdot h_{rollc}}{t_w} \quad (3. 6)$$

During cornering, the outside spring's compression is proportional to roll angle ( $\Delta z = \phi \cdot t_w/2$ ) and lateral acceleration as given in (3. 4). Hence, (3. 6) can be rewritten as (3. 7). For the current suspension setup  $h_{roll} = h_{cog}^{vehicle}$  (Refer Figure 3.4).

$$\Delta t_{w2} = \frac{(m_{sprung}^e \cdot h_{cog}^{vehicle} \cdot a_y \cdot \cos \phi + m_{sprung}^e \cdot g \cdot h_{cog}^{vehicle} \cdot \sin \phi) \cdot h_{rollc}}{K_\phi} \quad (3. 7)$$

The overall change in half-track width is given by

$$\Delta t_w = \Delta t_{w1} - \Delta t_{w2} \quad (3. 8)$$

### Effects of wheel jacking

When a vehicle is cornering, the wheels are subjected to normal loads which are called wheel jacking forces. These forces are transmitted through the suspension to the body and lift the center of gravity above the prevailing position. These are caused by two phenomenons in the suspension. One is due to the spring, which is nonlinear in stiffness and the other is through the rigid suspension links. To avoid complexity to the situation, only the rigid suspension arms are used to see the effects of jacking.

From Figure 3.4 (left) it can be inferred that, for both the front and rear wheels,

$$\tan \gamma = \frac{2 \cdot h_{rollc}}{t_w} \quad (3.9)$$

This equation considers that all the wheels have similar suspension geometry assigned. For different suspension geometries, different equations need to be used. To account for the normal forces acting on the wheel (jacking force),

$$F_z = F_y \cdot \tan \gamma = \frac{2 \cdot h_{rollc} \cdot (m_{sprung}^e \cdot a_y \cdot \cos \phi + m_{sprung}^e \cdot g \cdot \sin \phi)}{t_w} \quad (3.10)$$

$$\Delta h = \frac{F_z}{K_{st}} = \frac{2 \cdot h_{rollc} \cdot (m_{sprung}^e \cdot a_y \cdot \cos \phi + m_{sprung}^e \cdot g \cdot \sin \phi)}{t_w \cdot K_{st}} \quad (3.11)$$

Where,  $K_{st}$  is vertical suspension stiffness.

### Effective model - Cumulative model considering all the forces

The cumulative model sums up all the effects mentioned in this section. The effective solution is further used for analysis of the vehicle. Referred from [12], applying all the effects mentioned in (3.4) to (3.11) in (3.1) and by using Figure 3.3, calculating moment about the outer wheel for a rollover scenario yield (3.12).

$$\begin{aligned} \sum T = & (GVW^e \cdot g \cdot \sin \phi + GVW^e \cdot a_y \cdot \cos \phi) \cdot (h_{cog}^{vehicle} + \Delta h) \\ & - (GVW^e \cdot g \cdot \cos \phi - GVW^e \cdot a_y \cdot \sin \phi) \cdot \cos \phi \\ & \cdot \left( \frac{t_w}{2} - \Delta t_w \right) + (GVW^e \cdot g \cdot \cos \phi - GVW^e \cdot a_y \cdot \sin \phi) \\ & \cdot \sin \phi \cdot h_{cog}^{vehicle} \cdot \cos \phi = 0 \end{aligned} \quad (3.12)$$

Now using (3.4) to (3.11), considering roll angles are small ( $< \pm 10^\circ$ ) and  $\Delta h = 0$  the quadratic equation for the lateral acceleration threshold is given by

$$\begin{aligned} & (GVW^e \cdot g \cdot \sin \phi + GVW^e \cdot a_y^{effective} \cdot \cos \phi) \cdot (h_{cog}^{vehicle}) - \\ & (GVW^e \cdot g \cdot \cos \phi - GVW^e \cdot a_y^{effective} \cdot \sin \phi) \cdot \\ & \left( \frac{t_w}{2} - \left( \frac{GVW^e \cdot a_y^{effective} \cdot \cos \phi + GVW^e \cdot g \cdot \sin \phi}{K_{lat}^{tyre}} \right) \right) + (GVW^e \cdot g \cdot \cos \phi - \\ & GVW^e \cdot a_y^{effective} \cdot \sin \phi) \cdot \\ & \left( \frac{m_{sprung}^e \cdot h_{cog}^{vehicle} \cdot a_y^{effective} \cdot \cos \phi + m_{sprung}^e \cdot g \cdot h_{cog}^{vehicle} \cdot \sin \phi}{K_\phi} \right) \cdot h_{cog}^{vehicle} = 0 \end{aligned} \quad (3.13)$$

## Model reasoning

This section gives reasoning behind steady state rollover analysis. It shows the difference between vehicle spinout and rollover.

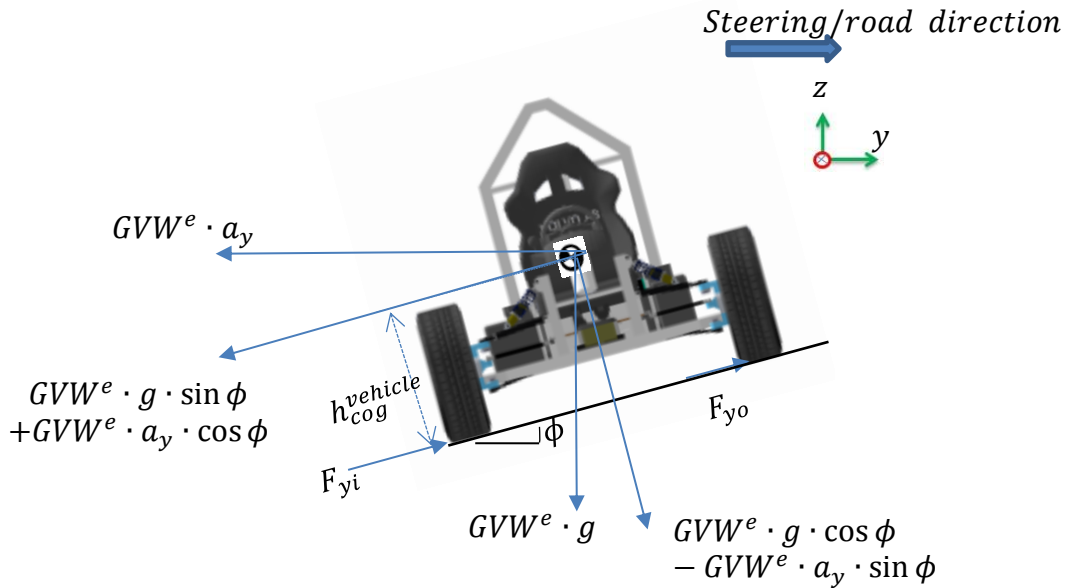


Figure 3.5: Steady state cornering

Table 3.5 gives a clear view on how the results will be formulated for the steady state rollover analysis.

For a clear understanding, in Figure 3.5 let us consider  $GVW^e \cdot g \cdot \sin \phi + GVW^e \cdot \frac{v^2}{R} \cdot \cos \phi$  as the “Centripetal force”,  $\mu \cdot (GVW^e \cdot g \cdot \cos \phi - GVW^e \cdot \frac{v^2}{R} \cdot \sin \phi)$  is the “friction threshold” and  $GVW^e \cdot a_y^{effective}$  is the “rollover threshold”. Table 3.5 is explained based on these definitions explained. Further, Table 3.5 is used for framing the results and conclusions.

Table 3.5: Steady state cornering conditions

Event	Conditions
Regular Maneuver	$Centripetal\ force < friction\ threshold;$ $Centripetal\ force < rollover\ threshold$
Vehicle Spinout	$Centripetal\ force > friction\ threshold;$ $Centripetal\ force < rollover\ threshold$
Vehicle Rollover	$Centripetal\ force < friction\ threshold;$ $Centripetal\ force > rollover\ threshold$

It is to be noted that  $a_y^{effective}$  is the rollover acceleration threshold of the vehicle considering all the effects mentioned Section 3.2.1.

### 3.3 Results and discussion

This section of rollover analysis pertains to the results of untripped steady state rollover. The results presented gives guidelines to vehicle design, for example CoG height. Motivation on bank angles, center of gravity height and friction coefficient and their role in rollover of the current vehicle are also provided in the discussion.

### 3.3.1 Steady state model results

This section gives a clear idea on the safety limits of the vehicle i.e. the best radius and velocity setting possible for the vehicle to maneuver, from the existing possibilities (refer Table 3.4) in a cornering condition. This model describes if the vehicle will reach the possible limits of friction with or without rollover. It also describes if the vehicle spins out first or rolls over first according to conditions given in Table 3.5. It is to be noted that if the vehicle spins out first (at comparatively lower sets of velocity and radius settings), the rollover event would not occur and is considered invalid. If the rollover event occurs first (at comparatively lower sets of velocity and radius settings), the spin out event is considered to be invalid.

From papers presented by [13], [14] and [15] and figures extrapolated, it shows a conclusive proof that the realistic possible lateral acceleration (mentioned as a constant) of a utility vehicle (refer Figure 3.6) and small electric vehicles can never go above 1.1g. This maximum realistic possible lateral acceleration is mentioned in graphs in Table 3.7 and Table 3.8 by the term “poss. Maneuver”. Although paper presented by [16] and similar papers pertaining to track performance cars show a lateral acceleration reach of 2g, it is safe to assume 1.1g, as this car is not built for track racing purposes.



Figure 3.6: Picture of the utility vehicle mentioned previously [14]

Table 3.6: Explanation for steady state cornering graphs

————	Vehicle spinout/slide threshold	$\mu \cdot GVW^e \cdot g$
.....	Rollover threshold of corresponding configuration	$GVW^e \cdot a_y^{effecyive}$
— —	Possible maximum lateral acceleration	1.1 g

The maneuver is considered safe if the vehicle spins out before it rolls over, or the spinning out and rollover event occurs beyond maximum realistic possible lateral acceleration curve, as it is not reachable.

One of the most interesting cases is shown in Table 3.7. The friction rollover usually takes place at high friction limits. Low friction limits usually result in vehicle spinout (will be discussed later in this section). Since vehicle spinout is not the prioritized criteria here, high friction limit is considered. For more motivation on friction limits, refer Table 3.3. The height of center of gravity is referred from Chapter 2 for a heavy driver with mass 150kg.

Another most important point to be noted is the weight of the driver. An increase in driver’s mass, the static position of vehicle’s CoG increases. This results in higher chance of rollover. The reflections of rollover with driver’s mass are given in the discussion section in this chapter.



Table 3.7: Steady state cornering results comparison with  $h_{cog}^{vehicle}=0.5, \mu = 1.3$

Road friction ( $\mu$ )	$h_{cog}^{vehicle}$ (m)	$h_{curb}$ (mm)	$\phi$ (degrees)	Plots
1.3	0.5	No curb	0	
		200	5.5	
		400	11	

Table 3.8 gives the situation of a rollover in a wet and dry road condition similar to Gothenburg's weather condition during autumn. Hence the road friction was considered as 0.8. Here, a heavy driver is considered and the CoG position is fixed at 0.5m. The references are taken from [17] and [11].

Table 3.8: Steady state cornering results comparison with  $h_{cog}^{vehicle}=0.5, \mu = 0.8$

Road friction ( $\mu$ )	$h_{cog}^{vehicle}$ (m)	$h_{curb}$ (mm)	$\phi$ (degrees)	Plots
0.8	0.5	Flat road		
		5.5		
		11		

For more details on results different data setting, refer to Appendix C.

### Observations for steady state modeling

From Table 3.8 and it can be seen that for any road friction below 0.8, the vehicle spins out on flat roads and on outward bank angles. It can also be seen that with a decrease in vehicle's weight (driver with less mass), the ability to spin off increases reducing the risk of a rollover. This is due to reduction of CoG (neglecting the effects of suspension) and reduction in Z-axis mass component of the vehicle which leads to lesser force required for the vehicle to spinout.

Results pertaining to  $\mu = 0.8$  are presented in this section because the weather in Gothenburg during autumn varies between rain and dry weather, and it was referred from [17] and Figure C.11 . Also, the lists of results are summarized in Table 3.9. It is to be noted that, the results pertaining to transient rollover (refer Appendix C) corresponds to only flat road maneuver. Steady state results are more significant as many aspects are covered in this section (refer Section 3.2.1).

Table 3.9: Results summary

Road friction ( $\mu$ )	$h_{cog}^{vehicle}$ (m)	$\phi$ (degrees)	$\frac{a_y^{effective}}{g}$	Safety	
				Steady state	Transient
0.4	0.4	Flat road	1.29	Safe	-
		5.5	1.09	Safe	-
		11	0.93	Safe	-
	0.45	Flat road	1.12	Safe	-
		5.5	0.95	Safe	-
		11	0.80	Safe	-
	0.5	Flat road	0.98	Safe	-
		5.5	0.83	Safe	-
		11	0.70	Safe	-
0.8	0.4	Flat road	1.29	Safe	-
		5.5	1.09	Safe	-
		11	0.93	Safe	-
	0.45	Flat road	1.12	Safe	-
		5.5	0.95	Safe	-
		11	0.80	Safe	-
	0.5	Flat road	0.98	Safe	-
		5.5	0.83	Safe	-
		11	0.70	Safe	-
1.3	0.4	Flat road	1.29	Safe	Safe
		5.5	1.09	Marginal/risky	-
		11	0.93	Marginally safe	-
	0.45	Flat road	1.12	Unsafe	Safe
		5.5	0.95	Unsafe	-
		11	0.80	Unsafe	-
	0.5	Flat road	0.98	Unsafe	Safe
		5.5	0.83	Unsafe	-
		11	0.70	Unsafe	-

For more clarity of Table 3.9, refer Figure 3.7

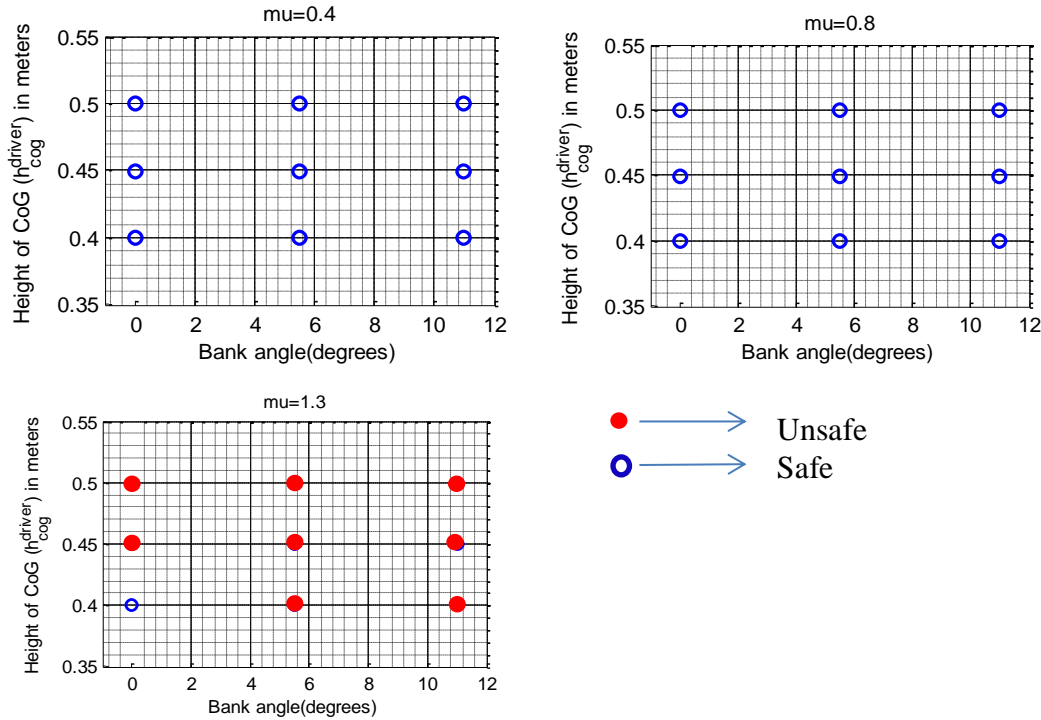


Figure 3.7: Graphical compilation and summary; Top left-Results pertaining to a road with snow; Top left- Results pertaining to a semi wet road; Bottom left; Dry road. Refer [11].

It can be theoretically understood that by decreasing the  $h_{cog}^{vehicle}$ , the rollover limits gets reduced i.e. the vehicle gets more stable. This also enhances the capability of the vehicle to withstand high amounts of lateral accelerations. It can also be learnt that by increasing bank angles the lateral acceleration threshold reduces which results in an earlier rollover. Whereas, for the current vehicle specification, banking in a corner with low coefficient of friction (0.4-0.8) results in a spinout, rather than a friction rollover.

### 3.3.2 Discussion

Comparing steady state cornering results it can be seen that reducing the CoG height of the vehicle has a significant effect on the rollover threshold. It is also advised that, banking on a platform or in a road bank angle with high coefficient of static friction has an adverse effect on the stability of the vehicle. Since the mass of the vehicle is not in par compared to a passenger car (whereas the dimensions are), the chances of the vehicle spinning out it more as the lateral force generated often exceeds the friction limits of the vehicle. Since this is not a series production vehicle which will run inside the city, there are no limitations on  $h_{cog}^{vehicle}$ . Additionally it is also to be noted that the rollover chances are higher with a driver's mass higher than 100Kg. Therefore, drivers with higher mass should be cautious if they intend to perform evasive maneuvers on banks and flat roads on dry roads ( $\mu \geq 1.3$ ). Important specification that can be adopted for the current vehicle design is mentioned in Table 3.10.

Table 3.10: Interesting specifications that can be adopted

Parameters	Lower limit	Upper limit	Comment
$h_{cog}^{vehicle}$	<0.4m	0.45m	

## 4 Frame strength evaluation using analytical method

The objective of this chapter is to evaluate floor structure of the proposed frame design from a strength perspective. The analysis in this section pertains only to static strength analysis. No handling analysis pertaining to vehicle is accomplished in this chapter. There are two load case scenarios, which are taken under consideration: 1) torsion loading and 2) vertical bending. These are described by Figure 4.1.

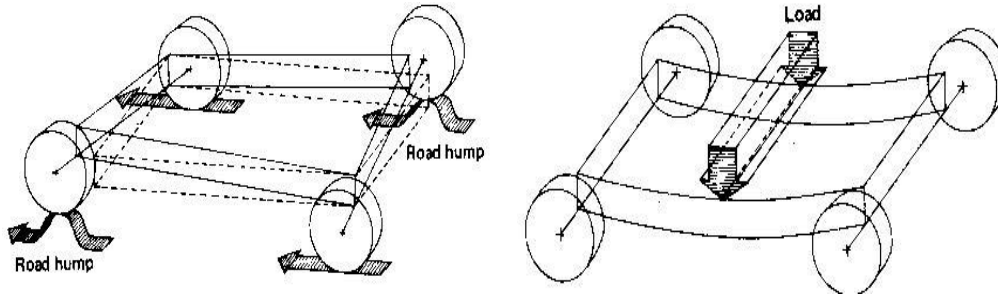


Figure 4.1: Torsional loading (left) and vertical bending (right).

### 4.1 Methodology

Figure 4.2 shows how the problem has been approached. A frame design is proposed and from the strength properties, it is decided if it is acceptable or not. The lightest frame that is strong shall be regarded as most appropriate.

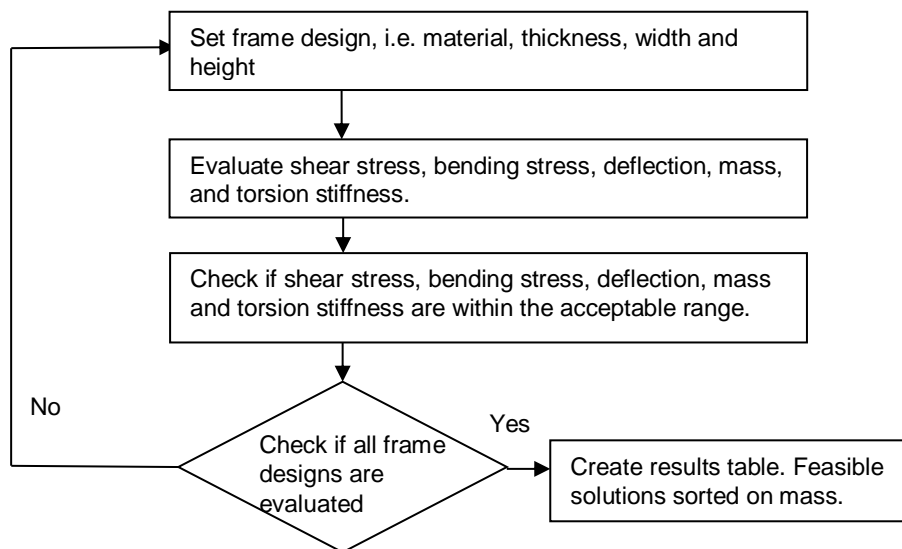


Figure 4.2: Methodology flow chart

From Figure 4.5 the floor structure is mainly constituted by the three beams connecting the front and rear wheel axle. The mid beam is in this section subscribed by 2 the other two beams by 13. The reason is to enable differing design of the mid beam compared to the other two beams. Here, only rectangular beams are considered, for the simplicity of cutting and welding.

Figure 4.3 gives some important dimensions considered for the analytical method calculations.

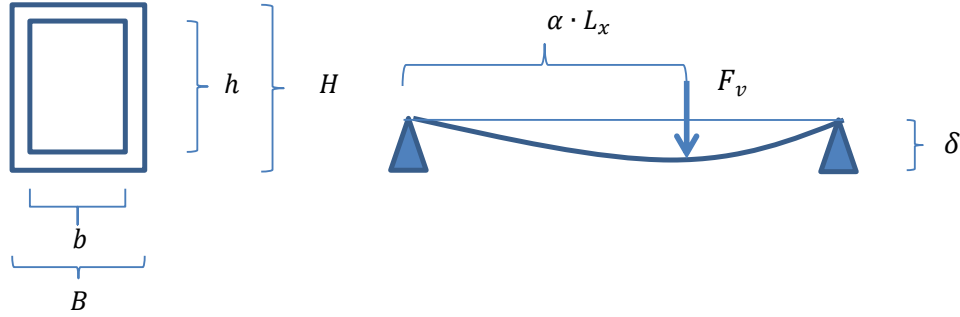


Figure 4.3: Important dimensions of the beam structure

#### 4.1.1 Mid beam shear stress

[18] (page 75) gives (4. 1). It is assumed that vertical force  $F_v$  is loaded on mid-beam only.

$$\sigma_{shear} = \frac{|F_v|}{A} \quad (4. 1)$$

$$A = B_2 \cdot H_2 - b_2 \cdot h_2 \quad (4. 2)$$

#### 4.1.2 Mid beam bending stress

[18], (page 18 and 75) gives (4. 3). It is assumed that vertical force  $F_v$  is loaded on mid-beam only.

$$\sigma_{bend} = \frac{|T_{max}|}{W_w} = \frac{|F_v| \cdot L_x \cdot \alpha}{W_w} \quad (4. 3)$$

$$W_w = \frac{I_2}{z_{max}} \quad (4. 4)$$

$$I_2 = \frac{B_2 \cdot H_2^3 - b_2 \cdot h_2^3}{12} \quad (4. 5)$$

#### 4.1.3 Mid beam deflection

[18] (page 76) gives (4. 6). It is assumed that vertical force  $F_v$  is loaded on mid-beam only.

$$\delta = \frac{F_v \cdot L_x^3}{3 \cdot E \cdot I_2} \cdot \alpha^2 \cdot (1 - \alpha)^2 \quad (4. 6)$$

#### 4.1.4 Floor structure mass

The floor mass is expressed by 0.

$$m_{floor} = \rho_{steel} \cdot L_x \cdot [(B_2 \cdot H_2 - b_2 \cdot h_2) + 2 \cdot (B_{13} \cdot H_{13} - b_{13} \cdot h_{13})] \quad (4. 7)$$

#### 4.1.5 Floor torsional stiffness

As per Figure 4.5 the three beams connecting the front and rear wheel axle mainly constitute the floor. The objective of this section is to study the torsional stiffness of these three beams combined Figure 4.4 shows schematically the geometry at torsional bending. The approach is to let the total torque affecting the floor  $T$  be divided into three torques, one for each beam. The two outer beams are assumed to resist the floor rotation by their “unwillingness” to undergo endpoint deflection, i.e. bending. The middle one resists by torsional stiffness.

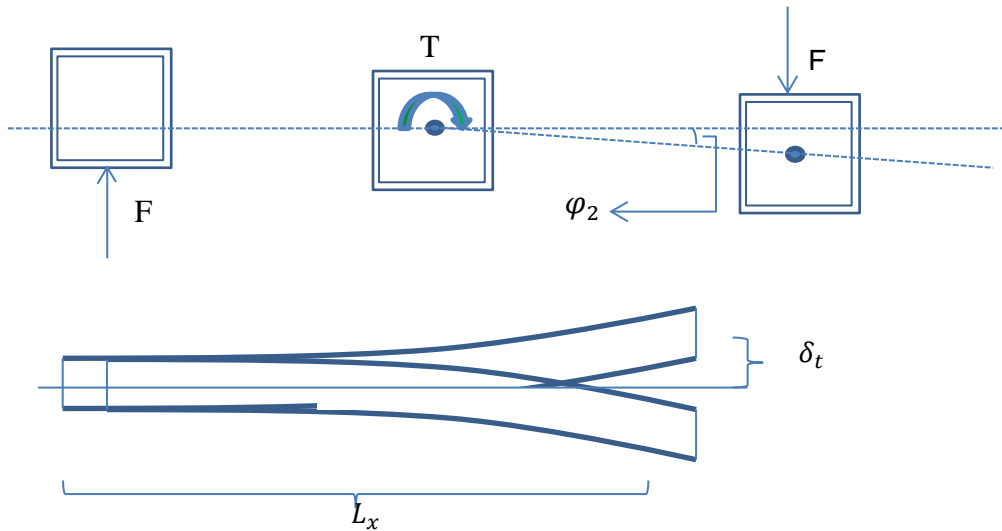


Figure 4.4: Torsion stiffness geometry

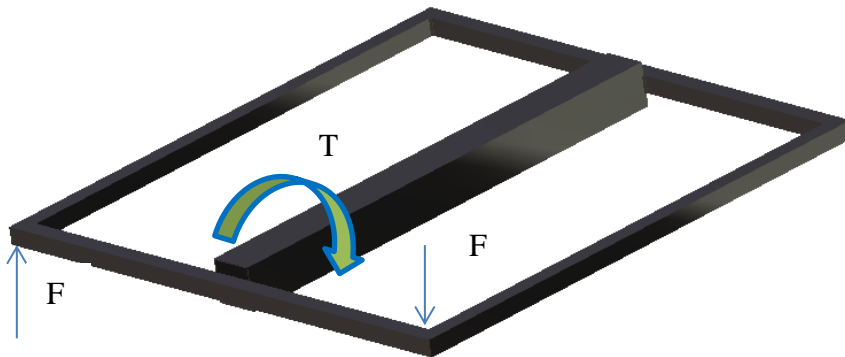


Figure 4.5: 3D view of geometry of the floor structure

The strength relation shown in Figure 4.4 are presented by (4. 8)-(4. 17)<sup>2</sup>.

<sup>2</sup> Page 75 in [16] gives equation (4. 8)- (4. 12) is from page 364 in [16] In (4. 11)0,  $v \approx 0.3$ .

$$ts = \frac{T}{\varphi_2} \quad (4. 8)$$

$$T = T_1 + T_2 + T_3 \quad (4. 9)$$

$$\varphi_2 = T_2 \cdot \frac{L_x}{G \cdot K_t} \quad (4. 10)$$

$$G = \frac{E}{2 \cdot (1 + \nu)} \quad (4. 11)$$

$$K_t = t_2 \cdot H_2^3 \quad (4. 12)$$

$$\delta_{13} = \frac{F \cdot L_x^3}{3 \cdot E \cdot I_{13}} \quad (4. 13)$$

$$I_{13} = \frac{B_{13} \cdot H_{13}^3 - b_{13} \cdot h_{13}^3}{12} \quad (4. 14)$$

$$\delta_{13} = \frac{L_y}{2} \cdot \varphi_2 \quad (4. 15)$$

$$F = \frac{T_1}{L_y/2} \quad (4. 16)$$

$$F = \frac{T_3}{L_y/2} \quad (4. 17)$$

By combining the six equations: (4. 8), (4. 9), (4. 13), (4. 15), (4. 16) and (4. 17) the linear equation system described by (4. 18) is derived.  $T$  can be seen as an input to the system and  $\varphi_2$  as the interesting output. Hence, the torsion stiffness (4. 8) can be derived from the quote between  $T$  and  $\varphi_2$ .

$$A \cdot x = b \quad (4. 18)$$

$$x = [T_1 \ T_2 \ T_3 \ \varphi_2 \ \delta_{13} \ F] \quad (4. 19)$$

$$b = [T \ 0 \ 0 \ 0 \ 0 \ 0] \quad (4. 20)$$



## 4.2 Data setting

Figure 4.6 present other data setting used. The setting of the parameter minimum torsional stiffness (tstifmin) is motivated from [19] and [20]. The assumption of a heavy (150 kg) driver motivates  $F_v$ . The beam dimensions are motivated in Table 4.1. The data setting for the target values and assigned values are given by Table 4.2.

Table 4.1: Beam dimensions.

H	Beam height (m)	0.03	0.04	0.08	0.05	0.07	0.1	0.05	0.1
B	Beam weight (m)	0.03	0.04	0.04	0.05	0.07	0.05	0.1	0.1
t	Beam thickness (m)	0.002	0.0025	0.0025	0.003	0.003	0.004	0.004	0.003

Table 4.2: Data setting

Parameter	Description	Value	Reference
$\rho$	Density (kg/m <sup>3</sup> )	7800	[21] [22]
sigmmax	Max yield stress (Pa)	7.5E+08	[21] [22] Docol 800
$E$	Young's modulus (Pa)	2.00E+11	<a href="http://en.wikipedia.org/wiki/Young_modulus">http://en.wikipedia.org/wiki/Young_modulus</a>
$\nu$	Poisson's number	0.3	[18]
$L_x$	Floor length (m)	1.2	[1]
alpha	$F_v$ position from front axle	1	[1]
$L_y$	Floor width (m)	1.2	[1]
$F_v$	Vertical force on mid beam (N)	1471.5	150 kg driver [23]
deflectionmax	Max deflection of mid beam (m)	0.001	Report author estimation
tstifmin	Min torsional stiffness (Nm/deg)	800	[19, 20]

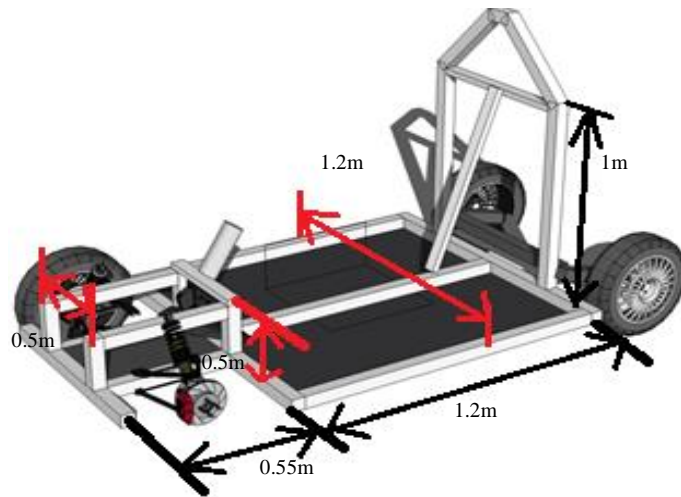


Figure 4.6: Frame beam dimensions

### 4.3 Results

When choosing beam design one should keep in mind that for the complete frame, the number of differing frame dimensions shall be minimized. Table 4.3 presents a limited portion of feasible beam design candidates sorted on mass. The term Tstifmid is the torsional stiffness with only the mid-beam present, just for comparison. Reflections:

- The design number 42 is very interesting. The mid beam height is 100 mm but only 50 mm in width. The side beams are 30x30x2 mm. The mid-beam can handle the bending stress due to driver mass in an efficient manner due to its high “height-width ratio”. The torsional stiffness is 4475 Nm/rad. Using this design shall imply that all other beams (not floor beams) should be 30x30x2 dimensions to simplify welding and minimize the number of differing beam dimensions.
- The initial middle beam design of 30x30x2 is not feasible, see Table D.2 in Appendix D. It does not comply with the torsional stiffness requirements.
- The design number 42 is very similar to number 58. The width of middle beam mid-beam is however larger, giving an increased stiffness. Also a very interesting design but with a compromise of added mass.

Table 4.3: Results- Top five light weight feasible designs

No	H2 mm	B2 mm	t2 mm	H13 mm	B13 mm	t13 mm	$\sigma$ MPa	Deflection mm	Tstif Nm/deg	Tstifmid Nm/rad	feas	Mass kg
26	50	50	3	30	30	2	169,4	0,52	776	420	1	9,5
34	70	70	3	30	30	2	82,1	0,18	1508	1151	1	11,7
42	100	50	4	30	30	2	49,0	0,08	4832	4475	1	14,8
50	50	100	4	30	30	2	74,6	0,23	916	559	1	14,8
58	100	100	3	30	30	2	38,7	0,06	3713	3356	1	15,1

- An example of a very stiff and interesting design is number 34. Shall be regarded as a “safe bet”. It has optimized weight, stiffness and stress generated.
- Refer Appendix D for a detailed version of feasible and non-feasible results.

#### 4.3.1 Total frame mass

This section evaluates the total frame mass, also including non-floor beams. It is defined by (4. 21).

$$m_{frame} = m_{floor} + \rho_{steel} \cdot L_{other} \cdot (B_{13} \cdot H_{13} - b_{13} \cdot h_{13}) \quad (4. 21)$$

where  $L_{other}$  is estimated as ~12.6 m. Table 4.4 show the frame mass for some especially interesting floor designs.

Table 4.4: Interesting designs and proposal

Option	H2 (mm)	B2 (mm)	t2 (mm)	H13 (mm)	B13 (mm)	t13 (mm)	Mass floor (kg)	Tstif (Nm/deg)	Mass frame (kg)
34	70	70	3	30	30	2	11,72	1507,81	33,73
42	100	50	4	30	30	2	14,83	4831,77	36,84
58	100	100	3	30	30	2	15,09	3712,97	37,10

## 5 FEM based frame strength evaluation

The objective of this chapter is to design an appropriate (refer Table 5.2) tubular space frame, using finite element analysis (FEA) calculations. The simulations are carried out for the whole frame to evaluate the torsional stiffness, vertical bending stiffness, mass, von Mises stress developed and packaging space (generalized). The results presented are of three different frame variants optimizing for the torsional stiffness, vertical bending stiffness and von Mises stress generated. Terms and definitions used in this chapter are defined in Table 5.1. It is to be noted that the strength analysis performed here pertains to static load case scenarios and no vehicle handling tests are performed on the chassis.

Table 5.1: Terms and definitions

Terms	Definition
Stress	stress is a physical quantity that expresses the internal forces that neighboring particles of a continuous material exert on each other
Yield strength ( $\sigma_y$ )	Yield strength, in material science engineering, is the stress up to, which the deformation of the material is elastic and above which the deformation of the material becomes plastic.
Ultimate tensile strength (UTS)	UTS, in material science engineering, is the stress up to which the material can withstand while being stretched or pulled before breaking or failing.
von Mises stress ( $\sigma_v$ )	In material sciences engineering, the von Mises yield criterion can be also formulated in terms of the von Mises stress or equivalent tensile stress, $\sigma_v$ . In this case, a material is said to start yielding when its von Mises stress reaches a critical value known as the yield strength, $\sigma_y$ .
Mesh generation	It is the practice of generating a polygonal or polyhedral blocks approximate the geometry of the domain i.e. frame, in this scenario.
Stress optimization	Optimize the structure to make the stress fall below $\sigma_y$ .

### 5.1 Methodology

The objective of this section is to describe the methodology used in Chapter 5 .

#### 5.1.1 Approach

The approach to finalize solutions is given by the flowchart in Figure 5.2. Refer Appendix E for a detailed flowchart.



Figure 5.1: Left- Basic frame structure; Right- Rolling frame model with highlighted middle floor beam

From the given base frame model as shown in Figure 5.1(left), three variants as shown in Figure 5.3, Figure 5.4 and Figure 5.5, are designed and are tested for torsional stiffness, vertical bending stiffness, mass,  $\sigma_v$ , developed and packaging space.

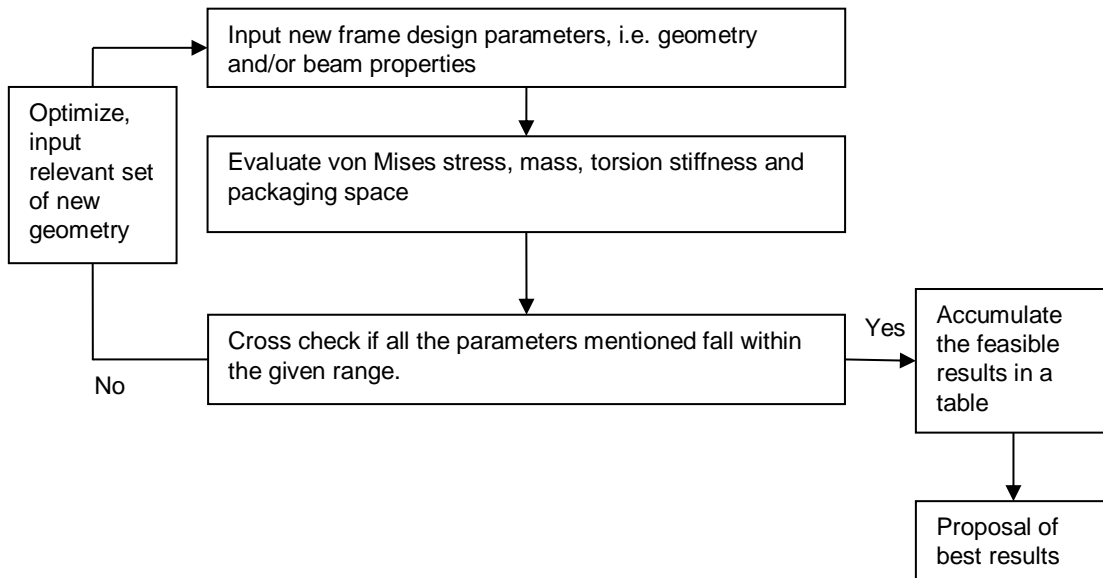


Figure 5.2: Methodology flowchart

### 5.1.2 Target criteria

The target strength criteria of the frame are shown in Table 5.2. All the optimizations on the frame variants shown in Table 5.3 are designed to meet the target given in Table 5.2.




Table 5.2: Target criteria

S.no	Property	Value	Reference/Comment
1	Torsional stiffness	~500-1000 Nm/deg	[19] [20] [24] States that for a formula SAE car of suspension stiffness from 500-1000Nm/deg the chassis should be between 300-1000Nm/deg for the handling to be tuned. It also states that the cornering performance of the car increases with increase in torsional stiffness.
2	Bending stiffness	~4000-8000 N/mm	[24] States that the bending stiffness of a chassis, of a medium sized passenger falls between 4000-8000 N/mm.
3	Maximum von Mises stress( $\sigma_v$ ) developed	$\leq 350$ MPa	[22] and [25] state that the von Mises stress developed should be less than the yield strength of the material. For better fatigue life, the max ( $\sigma_v$ ) $\leq (0.45 \cdot UTS)$ [26]. The material to be utilized to develop the chassis is considered to have $\sigma_y = 700MPa$ . [22] [21]. The Material considered is Docol 800.

### 5.1.3 Frame variants

The analysis is performed in all the three variants developed as shown in Table 5.3. The development explanation of the space frame variants are given in Table 5.3.

Table 5.3: Frame variants table

Variant	Figures	Comments
1	 <p style="text-align: center;"><i>Figure 5.3: Variant 1</i></p>	<p>Variant 1 is developed from the base frame model, as shown in Figure 5.1 (left), aiming for optimal torsional stiffness, bending stiffness and developed <math>\sigma_v</math>. The enhancements made to variant 1 from base frame model are shown in Appendix E. Additional features such as support structures for the roll hoop, support structures for the front hoop structure, support structures for the rear hoop structure, fillets and gussets are provided. This frame was proposed by [1].</p>
2	 <p style="text-align: center;"><i>Figure 5.4: Variant 2</i></p>	<p>Variant 2 is developed from variant 1 by extending the middle floor beam for harnessing purposes. This frame was proposed by [1].</p>
3	 <p style="text-align: center;"><i>Figure 5.5: Variant 3</i></p>	<p>Variant 3 is developed from variant 2, optimizing for the packaging space for batteries, power electronics, driver's seat position, suspension packaging and roll protection enhancement. This frame design was optimized and proposed by [7] and [27].</p>

### 5.1.4 Frame features

The frame is developed with various features that enhance better stress resistance and better strength. Certain features are mentioned below in this section.

#### Gussets

A gusset plate is a triangular insert that are used to connect beams, girders, columns to strengthen the joints and are fixed permanently either by using welding, rivets or bolts. The thickness of gussets is analyzed here having other dimensions constant as shown in Figure 5.6(extreme right).

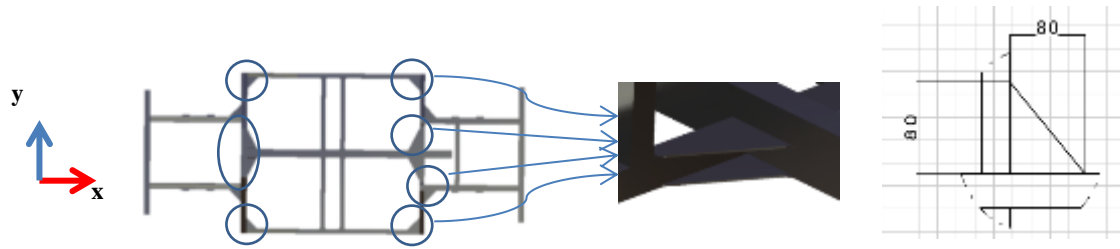


Figure 5.6: Left-Gusset plates on frame represented by blue circles (top view); Right-Dimensions

Gusset plates helped in improving the torsional stiffness of the frame and reducing the  $\sigma_v$  generated at point of connection of beams. A series of iterations on gusset thickness was performed on the frame. The highlighted option in Table 5.4 is selected for the design of the frame and was used in all the analysis performed on all the variants. Gusset thickness of 3mm was finalized. This was based on [26] who stated that  $\sigma_v < 0.45 \sigma_y$  for high durability and fatigue life. Hence, the iteration was set to halt when  $\sigma_v$  reached a value below 300MPa.

Table 5.4: Gusset thickness shortlist table

S.no	Thickness of gussets(mm)	von Mises stress (MPa)	Comment
1	1	568	High $\sigma_v$
2	2	395	High $\sigma_v$
3	3	254	Safe

### Fillets

Abrupt change in cross section area of the beam increases the  $\sigma_v$  concentration in the corners as the  $\sigma_v$  fields are more accumulated. By providing with fillet, the stress concentration factor reduces by a significant amount as the  $\sigma_v$  field becomes less accumulated due to a gradual change in  $\sigma_v$  field.

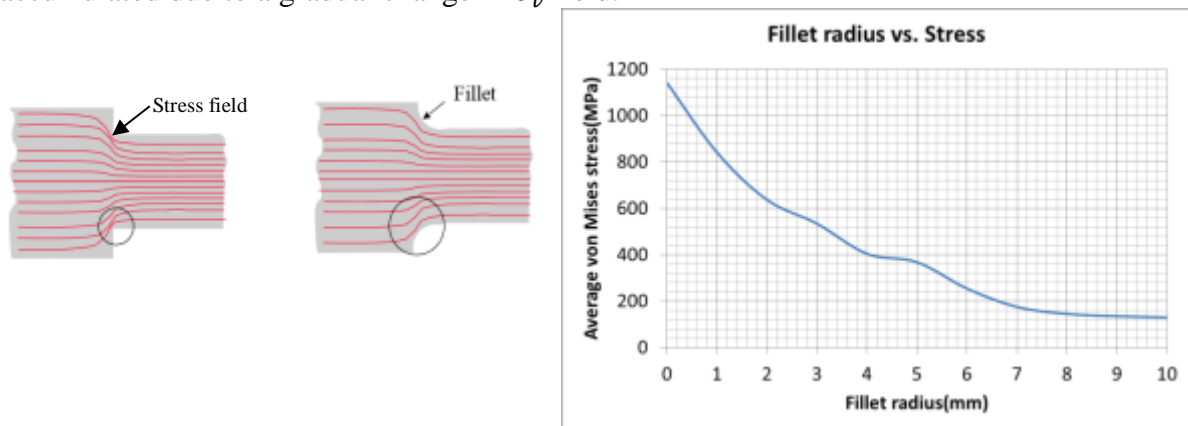


Figure 5.7: Left- Fillet concept; Right- Fillet radius vs. von Mises stress

To select the radius of the fillet, several iterations were performed on the frame variant 2, as shown in Figure 5.4, to select the best fillet radius. The average stress value on the fillets was calculated using FEA and the best fillet radius was considered for the frame development.

The fillet was provided in the following regions

- Intersection of the middle floor beam with other beams.
- Seat support structure's connection with middle floor beams and other beams.
- Intersection of front hoop structure and the rear hoop structure with the floor structure.

From it can be seen in Figure 5.7 (right), that  $\sigma_v$  increases with a decrease in radius. For the development of EDV frame, a fillet radius of 10mm was used in all the variants as it showed a significant reduction in  $\sigma_v$  generated and was finalized. Fillets were used in specific positions in geometry as mentioned below. This experiment was conducted with other beam dimensions of 30x30x2mm and middle floor beam of 60x100x2mm as per load case given in (5. 2).

### 5.1.5 Boundary conditions

This Section gives a better understanding of the boundary conditions used for the Chapter 5 .

#### Torsional stiffness

The worst-case scenario for the torsional load considered was Scenario 1 (refer Appendix E). It is riding over a speed bump with 1.5\*g of deceleration in a down slope grade of 30% at 80Kmph, with one wheel. This was concluded from comparison between the above mentioned case and situation where the vehicle is cornering.

For more reference on boundary conditions for torsional stiffness, refer Appendix E.

$$T_{simulation} = 4.438kNm$$

According to [24],  $K_t$  is given by Equation (5. 1).

$$K_t = \frac{T_{simulation}}{\arctg[(\Delta\delta_{lz} + \Delta\delta_{rz})/L]} \quad (5. 1)$$

Where ,  $\Delta\delta_{lz}$  and  $\Delta\delta_{rz}$  represent the vertical displacement of load points on left and right side of the chassis respectively and L is the distance between load points(distance between suspension hard points). Refer Appendix E for more motivation and sample evaluation.

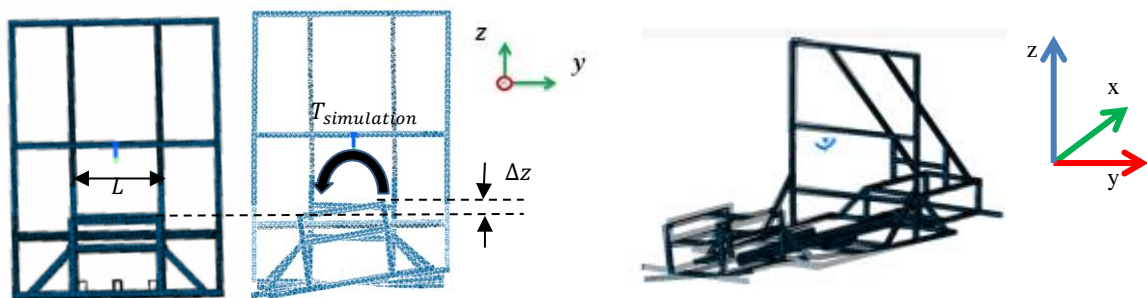


Figure 5.8: Left- Torsional unloaded and loaded frame; Right- Single picture representing deflection due to torsional loading

#### Bending stiffness

The worst case scenario for bending is given by [28] that, the maximum vertical force a human body can take is 3g of down force (negative Z direction) or 3g of up force



(positive Z direction). A similar situation is considered for all the important mass modules, which represent the sprung mass.

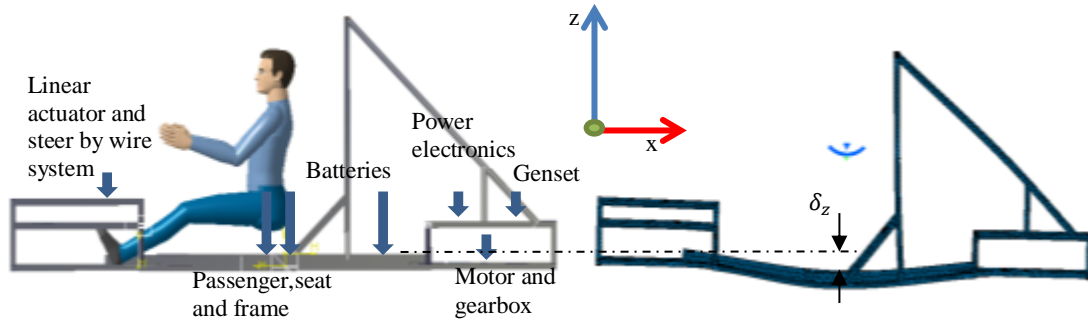


Figure 5.9: Left – Frame before vertical loading; Right-Frame after vertical loading

Table 5.5 gives the maximum vertical forces of every mass module with 3g of force in the negative Z-axis. The masses of all the component modules (apart from driver's mass) are taken from the Chapter 1 . The driver's mass is considered as 200kg to consider the worst case scenario.

Table 5.5: Vertical force for various mass modules with 3g of down force

Mass module(i)	Force (N) $F_z$
Passenger	5500
Frame	2900
Seat	630
Timing belt transmission	1000
Motor	650
Genset	840
Power electronics	180
Batteries	1200

Vertical bending stiffness of the frame is given by (5. 2).

$$K_b = \frac{\sum F_{z,i}}{\delta_z} \quad (5. 2)$$

Where,  $\delta$  is the vertical deflection of the chassis as shown in Figure 5.9.

Refer Appendix E for sample evaluation

## 5.2 Results

The results presented are for three different frame variants, as mentioned in Table 5.3, optimizing for the torsional stiffness, vertical bending stiffness,  $\sigma_v$  generated and mass. Differences between feasible and non-feasible options are mentioned in Table 5.6.

Table 5.6: Feasible and non-feasible options

Feasible option	Non-feasible option
$500 \leq K_t$ ; $4000 \leq K_b \leq 8000$ ; $\sigma_v \leq 350 \text{ MPa}$	$500 > K_t$ ; $4000 > K_b > 8000$ ; $\sigma_v > 350 \text{ MPa}$

The results shown below in Table 5.7 correspond to three variants as described in Table 5.3. Only feasible solutions are given below. Each variant is tested with nine beam options and the motivation behind selecting the nine options are given in Appendix E.

Table 5.7: Feasible results table (B- width; H-height; T-Thickness)

	Option	Middle Beam			Other Beams			Results				
		B(mm)	H(mm)	t(mm)	B(mm)	H(mm)	t(mm)	$K_t$ (Nm/deg)	$K_b$ (N/mm)	Weight(kg)	$\sigma_v$ (Mpa)	Feasible
Variant 1	1	60	100	2,5	30	30	2	1190	6970	53,9	330	yes
	2	70	70	2,5	30	30	2	1160	6270	52,3	345	yes
	3	50	100	2,5	30	30	2	1114	6888	53,4	317	yes
	4	60	80	2,5	30	30	2	1114	6510	52,8	326	yes
	5	40	100	2,5	30	30	2	996	6820	52,9	328	yes
	6	50	70	2,5	30	30	2	990	5800	51,8	305	yes
	7	60	60	2,5	30	30	2	975	5410	51,2	337	yes
	8	60	60	2	30	30	2	940	5080	50,0	341	yes
	9	40	80	2,5	30	30	2	940	6715	51,8	336	yes
Variant 2	1	60	100	2,5	30	30	2	1143	6970	55,9	316	yes
	2	70	70	2,5	30	30	2	1081	6270	54,3	348	yes
	3	50	100	2,5	30	30	2	1073	6888	55,4	321	yes
	4	60	80	2,5	30	30	2	1073	6510	54,8	323	yes
	5	40	100	2,5	30	30	2	996	6820	54,9	336	yes
	6	50	70	2,5	30	30	2	975	5800	53,8	315	yes
	7	60	60	2,5	30	30	2	962	5410	53,2	340	yes
	8	60	60	2	30	30	2	930	5080	52,0	332	yes
	9	40	80	2,5	30	30	2	930	6715	53,8	331	yes
Variant 3	1	60	100	2,5	30	30	2	1010	7650	76,3	338	yes
	2	70	70	2,5	30	30	2	995	7120	74,3	348	yes
	3	50	100	2,5	30	30	2	990	6995	75,4	326	yes
	4	60	80	2,5	30	30	2	980	6436	74,4	318	yes
	5	40	100	2,5	30	30	2	955	7054	74,5	342	yes
	6	50	70	2,5	30	30	2	942	6300	72,5	319	yes
	7	60	60	2,5	30	30	2	935	6216	72	347	yes
	8	60	60	2	30	30	2	878	6100	70	326	yes
	9	40	80	2,5	30	30	2	878	7458	73	320	yes

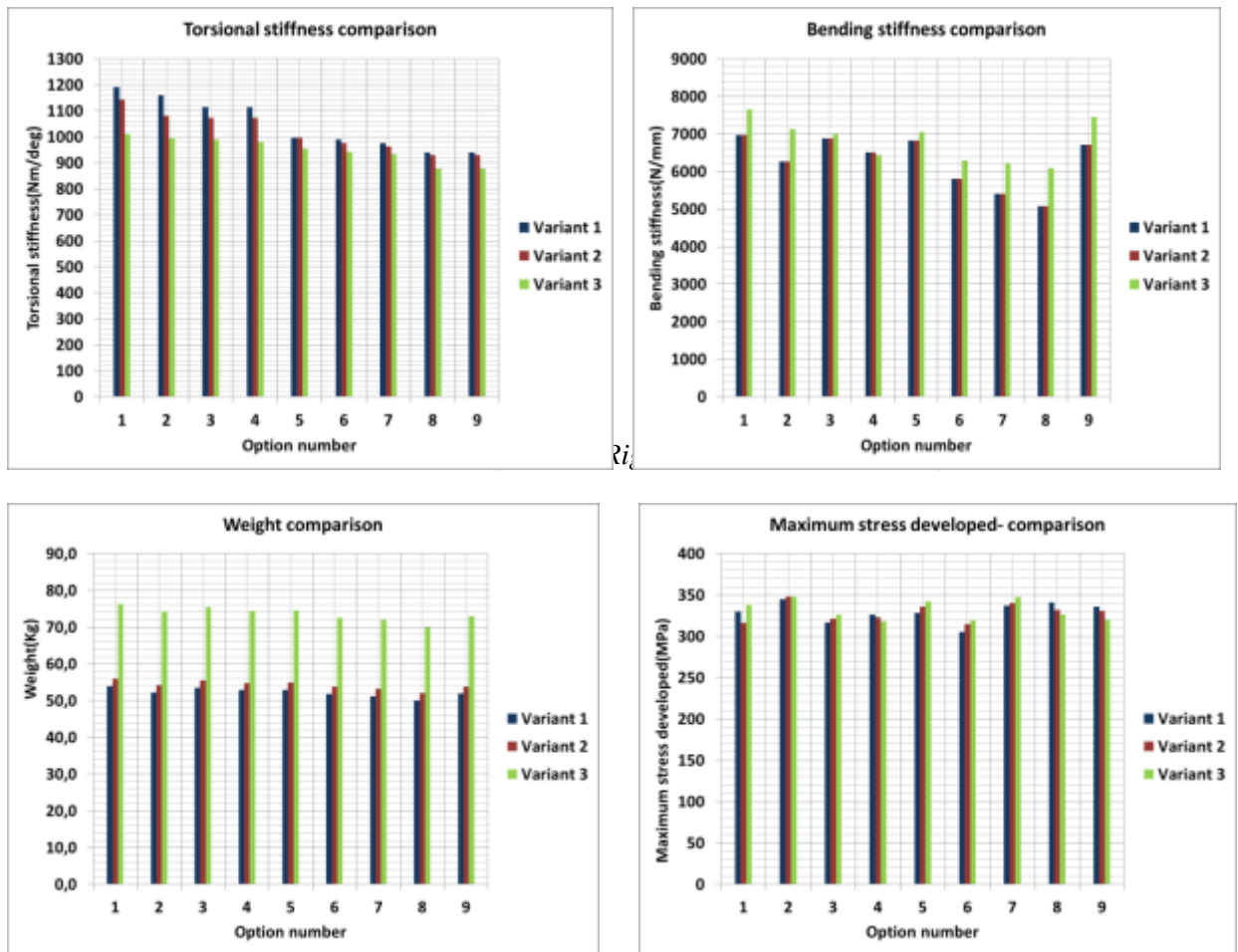


Figure 5.11: Left- Weight comparison; Right- Stress developed comparison

It can be seen from Figure 5.10 that, the torsional stiffness and the bending stiffness of all the variants with the given beam configuration and geometry, according to Table 5.7, show safe values within the limits as mentioned in Table 5.2.

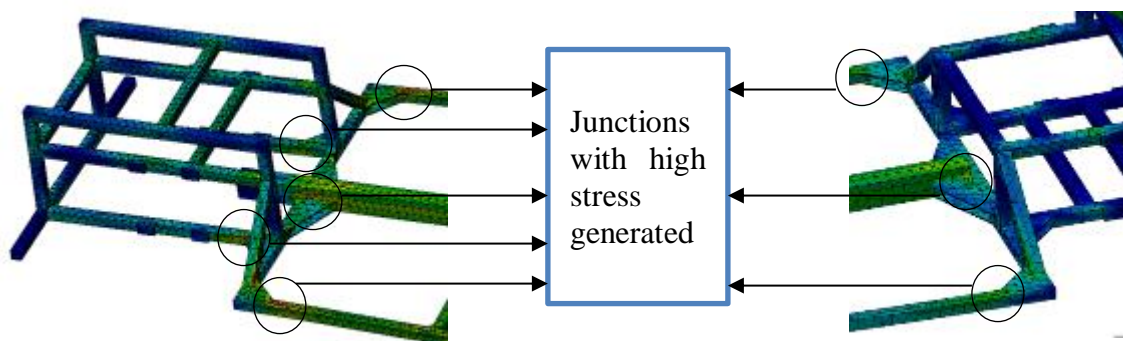


Figure 5.12: Junctions with high stress concentration; Left- Front hoop junction; Right- rear hoop junction

It is observed that the stress generated was higher in torsional test when compared to bending test. Hence, all the results pertaining to von Mises stress formation corresponds to the stress generated in the junctions as shown in Figure 5.12 from torsional test.

### 5.3 Discussion

Variants 1, 2 and 3 are compared for torsional stiffness, bending stiffness, weight and maximum stress developed in Figure 5.10 and Figure 5.11. Since variant 3 (Figure 5.5) is optimized for packaging space for all the mass modules, variant 3 is the best choice of all the options available (shaded in Table 5.7). For a detailed view of variant 3, refer Figure 5.13.

For the selection of beams, the choice depends on the beam dimensions that could be availed and the convenience of the welder.

Comparing variant 2 (Figure 5.4) and variant 3 (Figure 5.5), the torsional stiffness and the bending stiffness of the frame increases, with an increase in the number of structural members. By adding material to the beams, the torsional stiffness and stress gets optimized. But, this has a compromise on the weight of the frame.

By comparing Figure 5.10 and Figure 5.11 most competitive results compromising on weight, torsional stiffness, bending stiffness and stress of the analyzed beam options of Variant 3 is given in Table 5.8.

Table 5.8: Best options

Middle beam			Other beams			Results			
B(mm)	H(mm)	T(mm)	B(mm)	H(mm)	T(mm)	$K_t$ (Nm/deg)	$K_b$ (N/mm)	Weight(kg)	$\sigma_v$ (Mpa)
50	70	2,5	30	30	2	942	6300	72,5	319
60	60	2,5	30	30	2	935	6216	72	347
40	80	2,5	30	30	2	878	7458	73	320

Figure 5.13 gives the dimensions of basic construction of the highlighted option in Table 5.8. The dimensions are non-exhaustive.

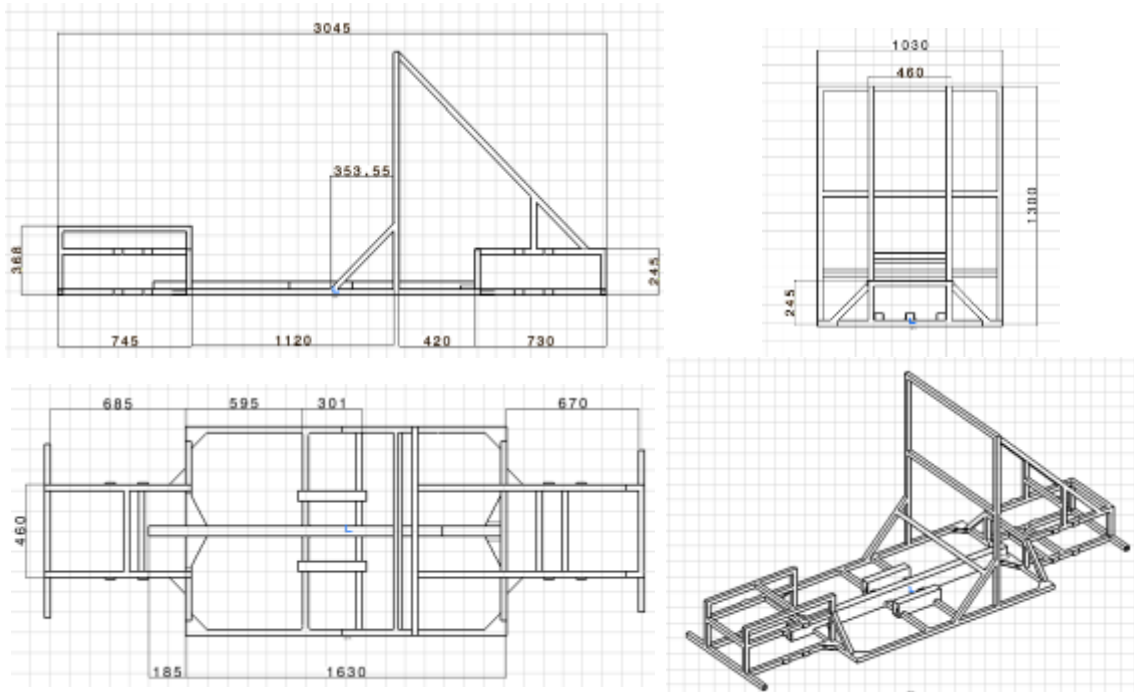


Figure 5.13: Dimensions of the frame in millimeters. Top left- Side view; Top right- Front view; Bottom left- Top view; Bottom right- Isometric view

## 6 Result summary

The objective of this section is to summarize all the results of this thesis work. Few important results of this thesis are,

- The curb mass of the vehicle (mass of the vehicle without the mass of driver and baggage) is  $m_{curb} = 307kg$  and expected gross vehicle mass is 418kg.
- The height of CoG for the current vehicle setup is 0.45m and the load distribution is 63% percent in the rear axle and 37% in the front axle. It is also being noted that the height of CoG increases with an increase driver's mass.
- For a stable car (doesn't rollover in normal road conditions) the height of CoG is preferred to be below 0.45m and outward banking has an adverse effect on rollover threshold. Vehicle spins out earlier with a drop in road tire friction. Since heavy driver's increase the height of CoG, it is advised to not evasively maneuver if the driver's weight is more than 100Kg.
- The proposed frame design is given in Figure 6.1.

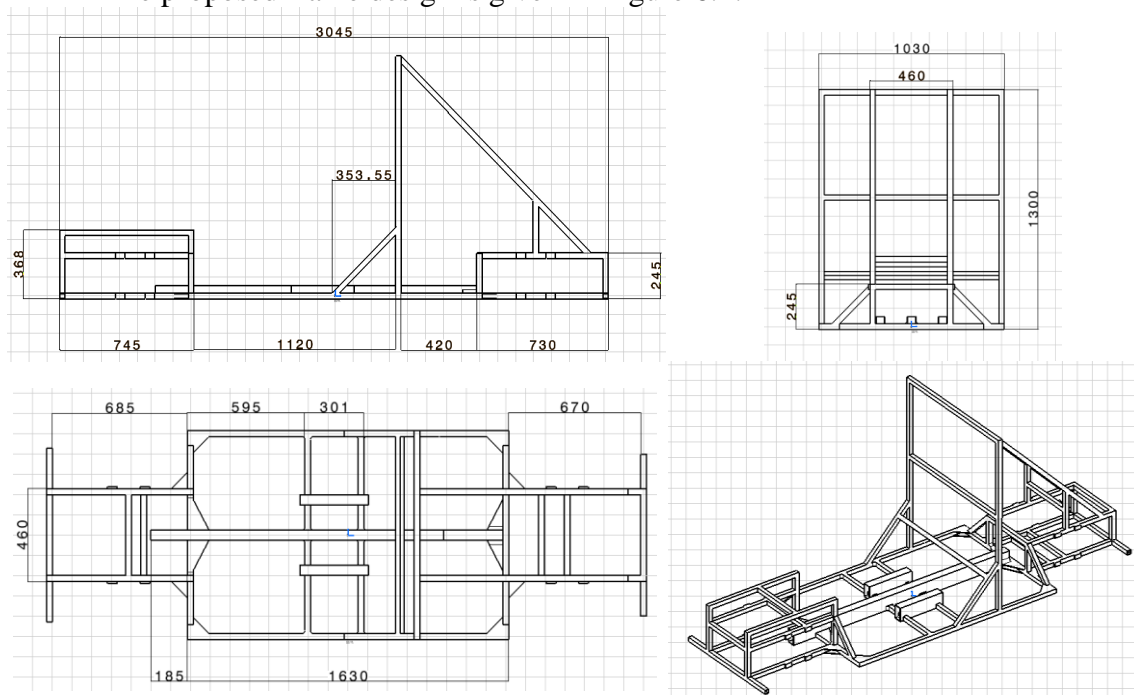


Figure 6.1: Proposed frame design (Non-exhaustive dimensions)



## Appendix A

This appendix corresponds to the Chapter 1 . The objective of this chapter is to motivate on the masses of various component modules. Table A.1 gives an overall view of the weights of different component modules.

Table A.1: Mass estimation on component modules- Curb mass

		Without Genset			With Genset		
		WM torsion	WM wishbone	AM wishbone	WM torsion	WM wishbone	AM wishbone
memexp	Expected EM(electric motor) mass (kg)	48	48	22	48	48	22
memdev	Max deviation of EM mass (kg)	2	2	0	2	2	0
mtransexp	Expected Timing belt transmission mass (kg)	0	0	11	0	0	11
mtransdev	Max deviation of Timing belt transmission mass (kg)	0	0	2	0	0	2
mpeexp	Expected power elec. mass (kg)	6	6	6	6	6	6
mpedev	Max deviation of power elec. mass (kg)	0	0	0	0	0	0
mgensetexp	Expected genset mass (kg)	0	0	0	28.5	28.5	28.5
mgensetdev	Max deviation of genset mass (kg)	0	0	0	0	0	0
mbatteryexp	Expected battery mass (kg)	72.5	72.5	72.5	72.5	72.5	72.5
mbatterydev	Max deviation of battery mass (kg)	2.5	2.5	2.5	2.5	2.5	2.5
mframeexp	Expected frame mass (kg)	73	73	73	73	73	73
mframedev	Max deviation of frame mass (kg)	3	3	3	3	3	3
mseatexp	Expected seat mass (kg)	21.3	21.3	21.3	21.3	21.3	21.3
mseatdev	Max deviation of seat mass (kg)	0	0	0	0	0	0
mtireexp	Expected tire mass (kg)	26	26	26	26	26	26
mtiredev	Max deviation of tire mass (kg)	3	3	3	3	3	3
mrिमexp	Expected rim mass (kg)	22	22	12	22	22	12
mrिमdev	Max deviation of rim mass (kg)	1	1	1	1	1	1
mfrontsuspep	Expected front suspension mass (kg)	12	12	12	12	12	12
mfrontsuspdev	Max deviation of front suspension mass (kg)	2	2	2	2	2	2
mrearsuspep	Expected rear suspension mass (kg)	15	13	13	15	13	13
mrearsuspdev	Max deviation of rear suspension mass (kg)	3	3	3	3	3	3
mmiscelexp	Expected miscellaneous mass (kg)	25	25	25	25	25	25
mmiscelddev	Max deviation of miscellaneous mass (kg)	4	4	4	4	4	4
msprungexp	Expected sprung mass(kg)	189	189	245	217	217	217
msprungdev	Max deviation of sprung mass(kg)	7	7	7	7	7	7
munsprungexp	Expected unsprung mass(kg)	123	121	63	123	121	63
munsprungdev	Maximum deviation in unsprung mass(kg)	11	11	9	11	11	9

Table A.2: Cargo mass estimation

mdriverexp	Expected driver mass (kg)	80
mdriverdev	Max deviation of driver mass (kg)	30
muggageexp	Expected baggage mass (kg)	20
muggagedev	Max deviation of baggage mass (kg)	10

### A.1 Fixed mass values of components

Mass of certain components are fixed and do not vary and is shown in Table A.3.

Table A.3: Fixed component's mass table

S.no	Part	Mass/pc.(kg)	Pieces	Overall mass
1	Power electronics [4], Kelly electronics	6	1	6 kg
2	Seat mass [4]	21.3	1	21.3 kg

### A.2 Mass estimation of battery pack

The battery pack used here are in modules and the weight of each module is 16.2kg [4] [29]. The proposed plan to accommodate battery in EDV consists 4 battery modules [4].

Table A.4: Battery module mass table

Number of packs	Weight per pack(kg)	Overall weight(kg)
4	16.2	65

Average variance mass of the batteries is given by,

$$m_{battery}^e = \mu_{battery} = \frac{1}{n} \sum_{i=1}^n (m_{battery})_i = 65 \text{ Kg}$$

Where, n stands for number of number of battery packs.

Table A.5: Battery packaging mass table

$m_{battery\text{pack}}^{\min}$ (kg)	$m_{battery\text{pack}}^{\max}$ (kg)	Comments
5	10	approximation

Where  $m_{package}^{\min}$  is the minimum weight of packaging material and  $m_{package}^{\max}$  is the maximum weight of packaging material.

To include overall mass of the battery module, the weight of cooling package needs to be added

Average variance mass of the battery packaging module is given by

$$m_{package}^e = \mu_{package} = \frac{(m_{package}^{\min} + m_{package}^{\max})}{2} = 7.5 \text{ Kg}$$

$$m_{battery\text{module}}^e = m_{package}^e + m_{battery}^e = 72.5 \text{ Kg}$$

Standard deviation of total battery mass module,



$$\sigma_{mass,batterymodule} = \sqrt{\frac{1}{n} \sum_{i=1}^n ((m_{batterymodule})_i - \mu_{batterymodule})^2} \approx 2.5 \text{ Kg}$$

Table A.6: Overall Battery module mass estimation

$m_{batterymodule}^e$ (average weight variance)	67.5 kg
$m_{batterymodule}^{max} - m_{batterymodule}^e$ (Standard deviation)	2.5 kg

### A.3 Mass estimation of electric motor module

This chapter motivates on the mass of the electric motor for both the axle mounted motor configuration and wheel motor configuration.

Table A.7: Wheel motor mass table

S.no(n)	Electric motor	Mass(kg)/piece	Pieces	Overall mass(kg)
1	Proud eagle [4]	23	2	46
2	Chennic [4]	25	2	50

Average variance mass (expected weight of wheel motor module,  $m_{electricmotor}^e$ ),

$$m_{electricmotor,wm}^e = \mu_{electricmotor,wm} = \frac{1}{n} \sum_{i=1}^n (m_{electricmotor,wm})_i = 48 \text{ Kg}$$

Standard deviation of mass of wheel motor,

$$\sigma_{mass,electricmoto,wm} = \sqrt{\frac{1}{n} \sum_{i=1}^n ((m_{electricmotor,wm})_i - \mu_{electricmotor,wm})^2} \approx 2 \text{ Kg}$$

Where n is total number electric motors variants, i is the index and  $m_{electricmotor,wm}$  is the mass of electric wheel motor module.

Table A.8: Wheel motor mass estimation

$m_{electricmotor,wm}^e$ (average weight variance)	48 kg
$m_{electricmotor,wm}^{max} - m_{electricmotor,wm}^e$ (Standard deviation)	2 kg

It is to be noted that, Table A.8 is valid only for wheel hub motors and not for axle-mounted motors.

For Axle mounted motors,

Table A.9: Axle mounted motors table

Motor	Weight/piece(kg)	Pieces	Overall mass(kg)
Golden Motors(HPM 500B) [4]	11	2	22



Figure A.1: Golden motor [4]

Using similar formula for average variance and standard deviation,

Table A.10: Axle mounted motor mass estimation

$m_{electricmotor,am}^e$ (average weight variance)	22kg
$m_{electricmotor,am}^{max} - m_{electricmotor,am}^e$ (Standard deviation)	0kg

Where,  $m_{electricmotor,am}$  is the weight of axle motor module.

#### A.4 Mass estimation of passenger module

According to [23] the mean body mass index (BMI) of Swedish population in the year 2008 is approximately  $26 \text{ kg/m}^2$  (for men) and  $25 \text{ kg/m}^2$  (for women). Average height of Swedish population is approximately 1.779 m [30] for male and 1.646m for female [30].

$$BMI_i = \frac{weight_i(Kg)}{height_i(m) \cdot height_i(m)} \quad (A. 1)$$

Where,  $i$  stands for a specific person.

From the given data and using equation (A. 1),

Average weight of Swedish male driver  $\approx 80 \text{ Kg}$

Average weight of Swedish female driver  $\approx 70 \text{ Kg}$

From [23] it is also noted that 60.2 per cent of the Sweden male population and 40.6 per cent of female population are overweight.

Considering the universal body mass index for obesity, [23] states that  $30 \text{ kg/m}^2$  is the BMI threshold for obesity. For safety purpose, assuming a BMI of  $35 \text{ kg/m}^2$  and using equation (A. 1), we have a maximum weight of 110kg for obese men and 105kg for obese women. This was taken from a sample of 100,000 people out of which 19.9% fell under this scale [23].

Using the maximum weight from male and female population, we have the expected weight of Swedish driver ( $m_{driver}^e$ )  $\approx 80\text{kg}$  and maximum Swedish driver's weight ( $m_{driver}^{max}$ )  $\approx 110 \text{ kg}$ .

Table A.11: Passenger mass estimation

$m_{driver}^e$ (average weight variance)	80 kg
$m_{driver}^{max} - m_{driver}^e$ (Standard deviation)	30 kg

## A.5 Mass estimation of front suspension module

The front suspension module is adapted from ATV Linhai 600 [4].

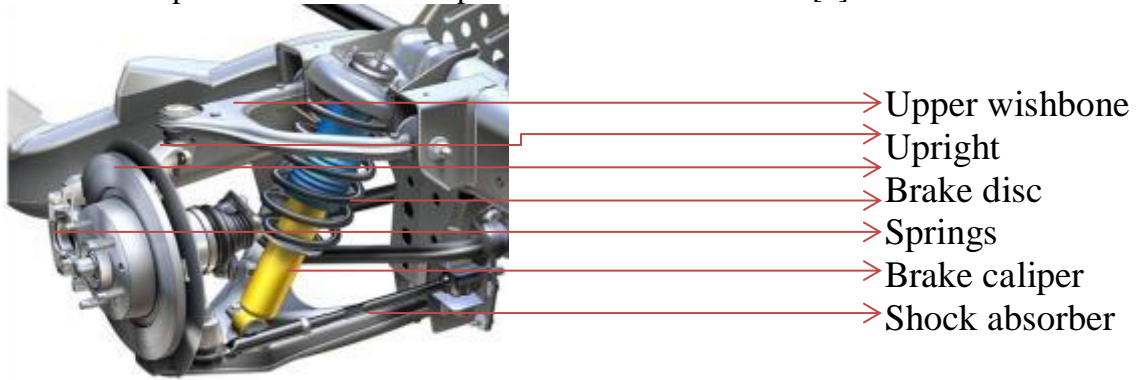


Figure A.2: Front end wishbone suspension setup

Table A.12: Front suspension module parts and weights table

S.no	Part and reference	Weight/piece (kg)	Pieces	Overall weight(kg)	Comment
1	Wishbones	2	2	4	[31] [4]
2	Springs	0.3	2	0.6	[31] [4]
3	dampers	0.5	2	1	[31] [4]
4	Uprights	1	2	2	[31] [4]
5	Brake calipers	0.8	2	1.6	[31] [4]
6	Brake disc	0.1	2	0.2	[31] [4]
7	Assorted screws and nuts	0.1	1	0.1	Assumption

The front suspension module is considered adapted with double wishbone suspensions [4]. The double wishbone suspension adaption is from Honda all-terrain vehicle Linhai 600. The weight of the wishbones, according to the selection, is assumed to be  $\approx 14Kg$ . As the number of options is restricted to two, the average variance (expected mass of front suspension module,  $m_{frontsusp}^e$ ) is given by

$$m_{frontsusp}^e = \mu_{frontsusp} = \frac{1}{t} \sum_{j=1}^t (m_{frontsusp})_j = 12 Kg$$

Standard deviation of the front suspension module mass is given by,

$$\sigma_{mass,frontsusp} = \sqrt{\frac{1}{t} \sum_{j=1}^t ((m_{frontsusp})_j - \mu_{frontsusp})^2} \approx 2 Kg$$

Where, t is total number of front suspension configuration variants, j is the index and  $m_{frontsusp}$  is the mass of front suspension module.

Table A.13: Front suspension module mass estimation

$m_{frontsusp}^e$ (Average variance)	12 kg
$m_{frontsusp}^{max} - m_{frontsusp}^e$ (standard deviation)	2 kg

## A.6 Mass estimation of rear suspension module

The rear suspension module consists of two configurations. The first type includes the approximated mass of uprights, brake components, shock absorbers, springs and a-arms (double wishbone suspension type). The second type is torsion beam suspension.

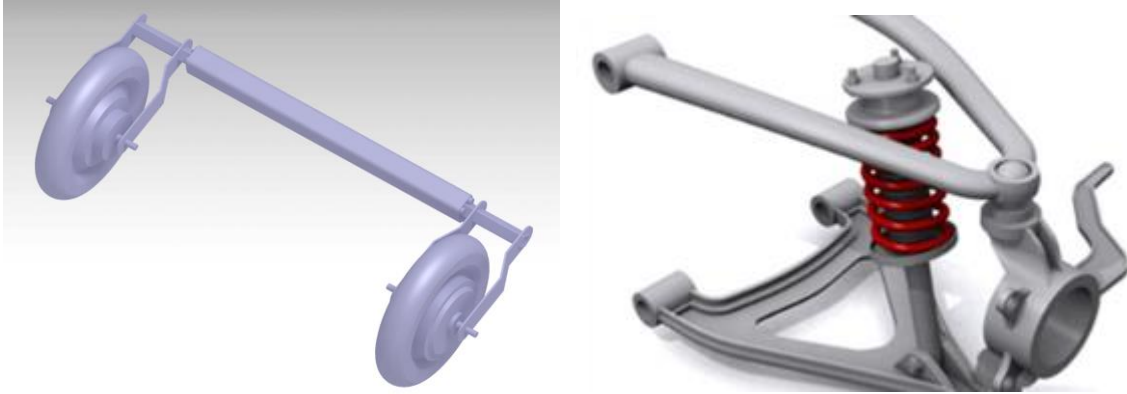


Figure A.3: Rear end torsion beam suspension set up(left) and wishbone setup(right)

It is of prime importance to note that the torsion beam suspension just supports wheel hub motors and not axle-mounted motors, whereas, double wishbone supports either. For the wishbone suspension type

Table A.14: Wishbone type rear suspension module table

S.no	Part	Weight/piece (kg)	Pieces	Overall weight(kg)	Comment
1	Wishbones	2	2	4	[31] [4]
2	Springs	0.3	2	0.6	[31] [4]
3	dampers	0.5	2	1	[31] [4]
4	Uprights	1.5	2	3	[4]
5	Brake calipers	0.8	2	1.6	[4]
6	Brake disc	0.1	2	0.2	[4]
7	Assorted screws and nuts	0.1	1	0.1	Assumption
8	Constant velocity joints and live axle	2	2	4	Assumption

Expected mass of rear suspension module,

$$m_{rearsusp}^e = \sum_{i \in n} (m_{rsuspcomp}^e)_i \approx 12 \text{ Kg}$$

Where,  $i$  is the index count;  $m_{rsuspcomp}^e$  is the expected mass of rear suspension module component;  $n$  is the rear suspension module component as shown in Table A.14.

For torsion beam suspension,

Weight of torsion beam suspension= 18 kg [4]

Average variance of rear suspension module (expected mass of Timing belt transmission module,  $m_{rearsusp}^e$ ),

$$m_{rearsusp}^e = \mu_{rearsusp} = \frac{1}{t} \sum_{j=1}^t (m_{rearsusp})_j = 15 \text{ Kg}$$

Where t is total number of rear suspension configuration variants, j is the index and  $m_{rearsusp}$  is the mass of rear suspension module.  
Standard deviation for the configuration types,

$$\sigma_{mass,rearsusp} = \sqrt{\frac{1}{t} \sum_{j=1}^t ((m_{rearsusp})_j - \mu_{rearsusp})^2} \approx 3 \text{ Kg}$$

Table A.15: Rear suspension module mass estimation

$m_{rearsusp}^e$ (Average variance)	15 kg
$m_{rearsusp}^{max} - m_{rearsusp}^e$ (standard deviation)	3 kg

## A.7 Mass estimation of transmission module

List of timing belt transmission module suppliers is given in Table A.16

Table A.16: Timing belt transmission module

S.no	Timing belt transmission	Supplier	Mass (kg)	Reference
1	(R039110163)	Rexroth	5.4	[32]
2	PD120	Mekanex	6.3	[4]
3	Rexroth(R039110165)	Rexroth	4.8	[32]

Average variance of Timing belt transmission module weight (expected Timing belt transmission module mass,  $m_{gearbox}^e$ )

For the current vehicle setup, Timing belt transmission is used from Table A.16. Since two timing belt transmissions are used,

$$m_{gearbox}^e = \mu_{gearbox} = \frac{1}{t} \sum_{j=1}^t (m_{gearbox})_j = 5.5 * 2 = 11 \text{ Kg}$$

Where t is total number of Timing belt transmission variants, j is the index and  $m_{gearbox}$  is the mass of Timing belt transmission module

Standard deviation of Timing belt transmission module is given by

$$\sigma_{mass,gearbox} = 2 * \sqrt{\frac{1}{t} \sum_{j=1}^t ((m_{gearbox})_j - \mu_{gearbox})^2} = 2 \text{ Kg}$$

Table A.17: Timing belt transmission module mass estimation

$m_{gearbox}^e$ (Average variance)	11 kg
$m_{gearbox}^{max} - m_{gearbox}^e$ (standard deviation)	2 kg

This mass strictly restricted to axle mounted motor configuration.

### A.8 Mass estimation of genset module

Generator set is set aside as an option for EDV project. Never the less, it is critical to analyze the mass of the vehicle with and without the genset.

The available options are

Table A.18: Genset module mass table

Company/model	Weight(kg)	Comment
Hyundai HY3000SEi	28.5	

For option given in Table A.18,

$$m_{genset}^e = \mu_{genset} = \frac{1}{t} \sum_{j=1}^t (m_{genset})_j \approx 28.5 \text{ Kg}$$

Where t is total number of genset variants, j is the index and  $m_{genset}$  is the mass of genset module

Standard deviation of genset module is given by

$$\sigma_{mass,genset} = \sqrt{\frac{1}{t} \sum_{j=1}^t ((m_{genset})_j - \mu_{genset})^2} = 0 \text{ Kg}$$

Table A.19: Genset module mass estimation

$m_{genset}^e$ (Average variance)	28.5 kg
$m_{genset}^{max} - m_{genset}^e$ (standard deviation)	0 kg

### A.9 Mass estimation of frame module

The objective of this session is to provide a rough estimate on mass of the chassis module. Since the construction of the frame has not been completed, a rough estimation has been done from the proposed frame.

A few considerations are

$$\rho_{steel} \quad (\text{Density of steel}) = 7850 \frac{\text{Kg}}{\text{m}^3}$$

Table A.20: Frame mass table

Middle beams			Other beams			Weight
Width(mm)	Depth(mm)	Thickness(mm)	Width(mm)	Depth(mm)	Thickness(mm)	(kg)
60	100	2,5	30	30	2	76,3
70	70	2,5	30	30	2	74,3
50	100	2,5	30	30	2	75,4
60	80	2,5	30	30	2	74,4
40	100	2,5	30	30	2	74,5
50	70	2,5	30	30	2	72,5
60	60	2,5	30	30	2	72

60	60	2	30	30	2	70
40	80	2,5	30	30	2	73

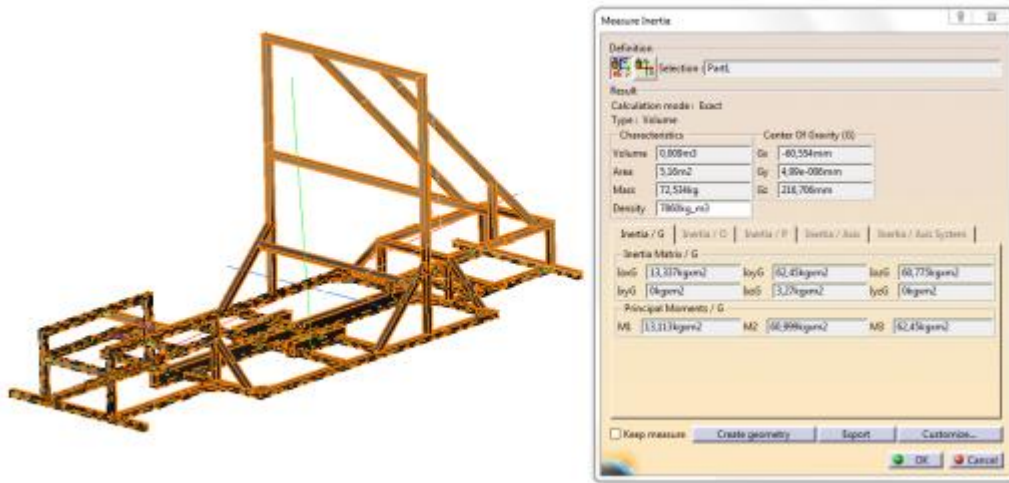


Figure A.4: Frame weight from CAD

Based on similar procedure of extracting weight from the CAD (generated by [1]) model shown in Figure A.4, Table A.20 is used for further analysis. Table A.20 is generated from Variant 3 from Chapter 5 (refer Table 5.7).

Average variance of frame module weight (expected frame module mass,  $m_{frame}^e$ )

$$m_{frame}^e = \mu_{frame} = \frac{1}{t} \sum_{j=1}^t (m_{frame})_j \approx 73 \text{ Kg}$$

Where t is total number of frame variants, j is the index and  $m_{frame}$  is the mass of frame module

Standard deviation of frame module is given by

$$\sigma_{mass,frame} = \sqrt{\frac{1}{t} \sum_{j=1}^t ((m_{frame})_j - \mu_{frame})^2} \approx 3 \text{ Kg}$$

Table A.21: Frame module mass estimation

$m_{frame}^e$ (Average variance)	73.5 kg
$m_{frame}^{max} - m_{frame}^e$ (standard deviation)	3 kg

## A.10 Miscellaneous mass module estimation

The miscellaneous mass includes the mass of wires, pedals, weld materials, assorted screws, nuts, bolts, steer by wire system and other minor electronic components.

The mass of linear actuator was the average mass of linear actuator taken from three samples from [32]. The selection of linear actuator from the website is dependent on travel length and force generation requirement, which were restricted to 100mm and 1000N, respectively [8].

Table A.22: Linear actuator mass table

S.No	Company and model number	Mass(kg)
1	Wittenstein TRBA046AA* [32]	2.3
2	Thomson PR12-02-2A65 [32]	3.9
3	Rexroth Bosch MSK030C-0900 [32]	1.9

Average mass of linear actuator is  $\sim 3Kg$

Standard deviation of linear actuators  $\sim 1Kg$

For the average weight of the steer by wire HMI (including the pedal console), samples were taken on few criteria. Considering the steering ratio to be between 12 and 15 (as for the normal passenger cars [33]) and the maximum wheel steering angle sweep (either side) for the wheel is 60 degrees [8], the required steering angle on the console would be around 900 degrees. The two samples were,

Table A.23: HMI steering and gas pedal console mass estimation

S.no	Company and model number	Mass(kg)
1	Logitech G27	18.3
2	Logitech Driving Force GT	12.3

Average mass of the steering HMI  $\sim 15Kg$

Average variance of the steering HMI  $\sim 3Kg$

Mass corresponding to assorted bolts, nuts, screws and washers  $\sim 2Kg$

Mass corresponding to weld material  $\sim 5Kg$

$$\begin{aligned}
 m_{miscellaneous}^e &= \text{Average mass of the steering HMI} \\
 &+ \text{Average mass of the assorted bolts, nuts, screws and washers} \\
 &+ \text{Average mass of weld material} \\
 &+ \text{Average mass of linear actuator}
 \end{aligned}$$

Table A.24: Miscellaneous mass module estimation

$m_{miscellaneous}^e$ (Average variance)	25 kg
$m_{miscellaneous}^{max} - m_{miscellaneous}^e$ (standard deviation)	4 kg

## A.11 Mass estimation of the rims

It is to be noted that, the wheel/hub motor includes the weight of the rims. Hence, the mass of the rims for the rear axle in wheel motor configuration will not be included. For axle motor configuration, the rim mass of the rear axle will also be included.

The selection of rims was made based on the size of the tires, which were 145/80R13 [4]. This gives a rim dimension of about  $13 \times 5.5$  (inches). To have it cost effective, only cast rims were taken into consideration when compared with forged rims [21]. The samples for rims were taken from [34].

Table A.25: Weight of rims

S.no	Company and model number	Mass (kg)/pc.
1	Konig Diva	5.7
2	Superlight ML	5.81
3	American Racing Libre	5.81



4	Copomotive ML	6
---	---------------	---

Average mass of rims  $\sim 5.83 \text{ Kg}$

Standard deviation of rims  $\sim 0.14 \text{ Kg}$

For axle motor configuration, the approximate weight of four rims were

*Table A.26: Rim module mass estimation (Axle motor configuration)*

$m_{rims}^e$ (Average variance)	23 kg
$m_{rims}^{max} - m_{rims}^e$ (standard deviation)	1 kg

For Wheel motor configuration, the approximate mass of two rims were

*Table A.27: Rim module mass estimation (wheel motor configuration)*

$m_{rims}^e$ (Average variance)	12 kg
$m_{rims}^{max} - m_{rims}^e$ (standard deviation)	1 kg

## A.12 Mass estimation of tire module

The tire mass varies with the compound used and the purpose of the tire. For the given tire specification [4]

*Table A.28: Tire module mass estimation*

S.no	Company and model number	Mass (kg)/pc.
1	Michelin 185/65 R15	6.7

Average mass of the tires  $\sim 26 \text{ Kg}$

Standard deviation of the tire mass  $\sim 3 \text{ Kg}$

*Table A.29: Tire module mass estimation*

$m_{tire}^e$ (Average variance)	26 kg
$m_{tire}^{max} - m_{tire}^e$ (standard deviation)	3 kg

As per the empirical rule, the results are formulated assuming 68 % probability ( $\mu \pm \sigma$ ) to be enough for a near-precise estimation of the GVW.



## Appendix B

This appendix corresponds to the Chapter 2 . Current position of parts on the vehicle is shown in.

*Table B.1: Position of mass modules on the frame*

Mass module	X position(m)	Y position(m)	Z Position(m)
Battery module 1	1.41	0.22	0.335
Battery module 2	1.41	0.38	0.3350
Battery module 3	1.41	0.82	0.335
Battery module 4	1.41	0.98	0.335
Frame module	0.95	0.7	0.28
Front rims module	0	0.7	0.3
Front suspension module	0	0.7	0.3
Front tire module	0	0.7	0.3
Timing belt transmission module	1.75	0.7	0.35
Genset module	2.3	0.7	0.5
Miscellaneous module	0.95	0.7	0.3
Motor module	1.65	0.7	0.35
Passenger module	1.005	0.7	0.7 to 0.9
Power electronics module	2.3	0.7	0.6
Rear rims module	2.3	0.7	0.3
Rear suspension module	2.3	0.7	0.3
Rear tire module	2.3	0.7	0.3
Seat module	1.005	0.7	0.45



## Appendix C

This appendix corresponds to the Chapter 3 .

### C.1 Suspension kinematics

The aim of this section was to estimate the roll center height (from ground) of the front and rear suspension and to determine the change in half-track width of the vehicle under suspension bump and rebound. Another aspect of this chapter was to roughly estimate the suspension hard points which help in strength analysis of frame.

Assumptions for suspension kinematics are given in Table C.1.

Table C.1: Assumption to suspension kinematics

S.no	Property	Value	Comment
1	Unloaded tire radius	283mm	(175/60R14)
2	Loaded tire radius	283mm	(175/60R14)
3	Spring radius	30mm	From ATV(measured)
4	Number of coils	16	Approximated
5	Vertical stiffness of the tire	180515(N/m)	95 / 80 R 16 tire file
6	Bump travel	76,5mm	(Suspension Travel)/2
7	Rebound travel	76,5mm	(Suspension Travel)/2
8	Body roll	3-5 degrees	Assumption
9	Wheelbase	1800mm	Given
10	Total mass center of gravity(critical)	300mm	Assumption
11	Braking percentage front(not critical)	80%	Assumption
12	Sprung mass front (%)	345kg	Chapter 1
13	Rim offset	0mm	Assumption

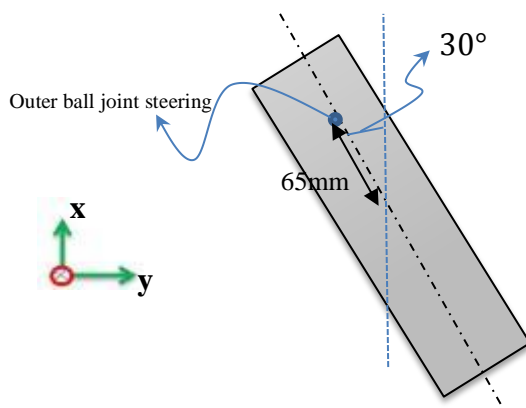


Figure C.1: Maximum steering angle steer input reference figure

Required steering input

$$\sin(30) = \frac{\text{Required steering input distance}}{65}$$

Required steering input= 32.5 mm [8]

This analysis is required to know the maximum steering wheel angle movement of the wheel based on a step steer input

## Suspension kinematics model

Based on the “zero caster setup” proposed by [8], the suspension was setup as shown in Figure C.2. A parallel and unequal arm setup was implemented using a suspension analysis tool, ‘Lotus Shark-suspension interactive’, commercially available software.

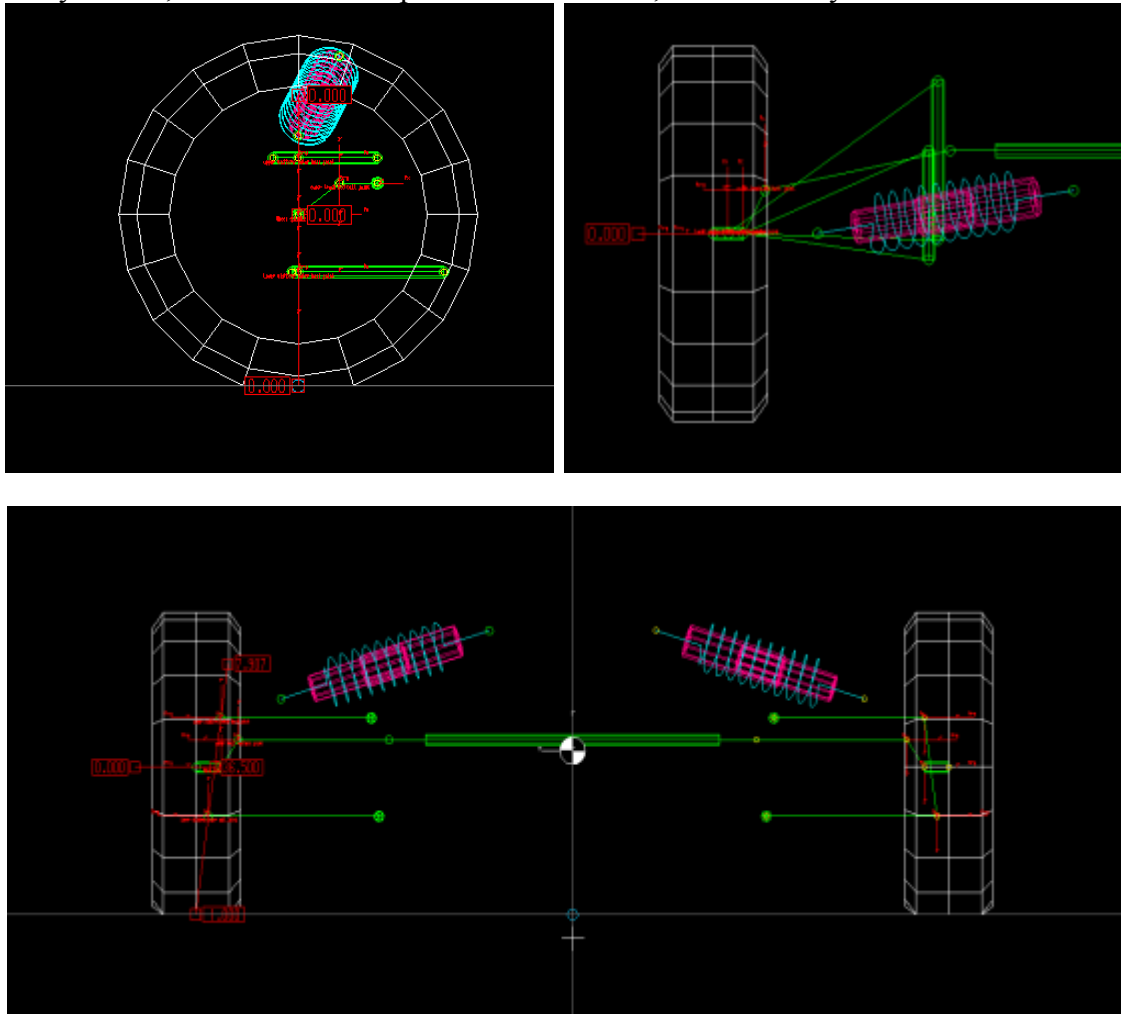


Figure C.2: Suspension Kinematics model; Top left (XZ plane) - Caster setup; Top right (XY plane) - Toe angle setup; Bottom (YZ plane) - Camber setup

Table C.2: Static values (both front and rear suspension is considered symmetric)

STATIC VALUES	Reference	Unit	Value
Camber Angle		(deg)	0.00
Toe Angle	{SAE}	(deg)	0.00
Caster Angle		(deg)	0.00
Caster Trail	(hub)	(mm)	0.000
Caster Offset	(grnd)	(mm)	0.000
Kingpin Angle		(deg)	7.91
Kingpin Offset	(w/c)	(mm)	36.500
Kingpin Offset	(grnd)	(mm)	-1.000
Mechanical Trail	(grnd)	(mm)	0.000
ROLL CENTRE HEIGHT	(grnd)	(mm)	0.041

After, setting up the suspension system, the following graphs were obtained as shown in Figure C.3. For definitions and further information on the “zero caster setup”, refer [8].

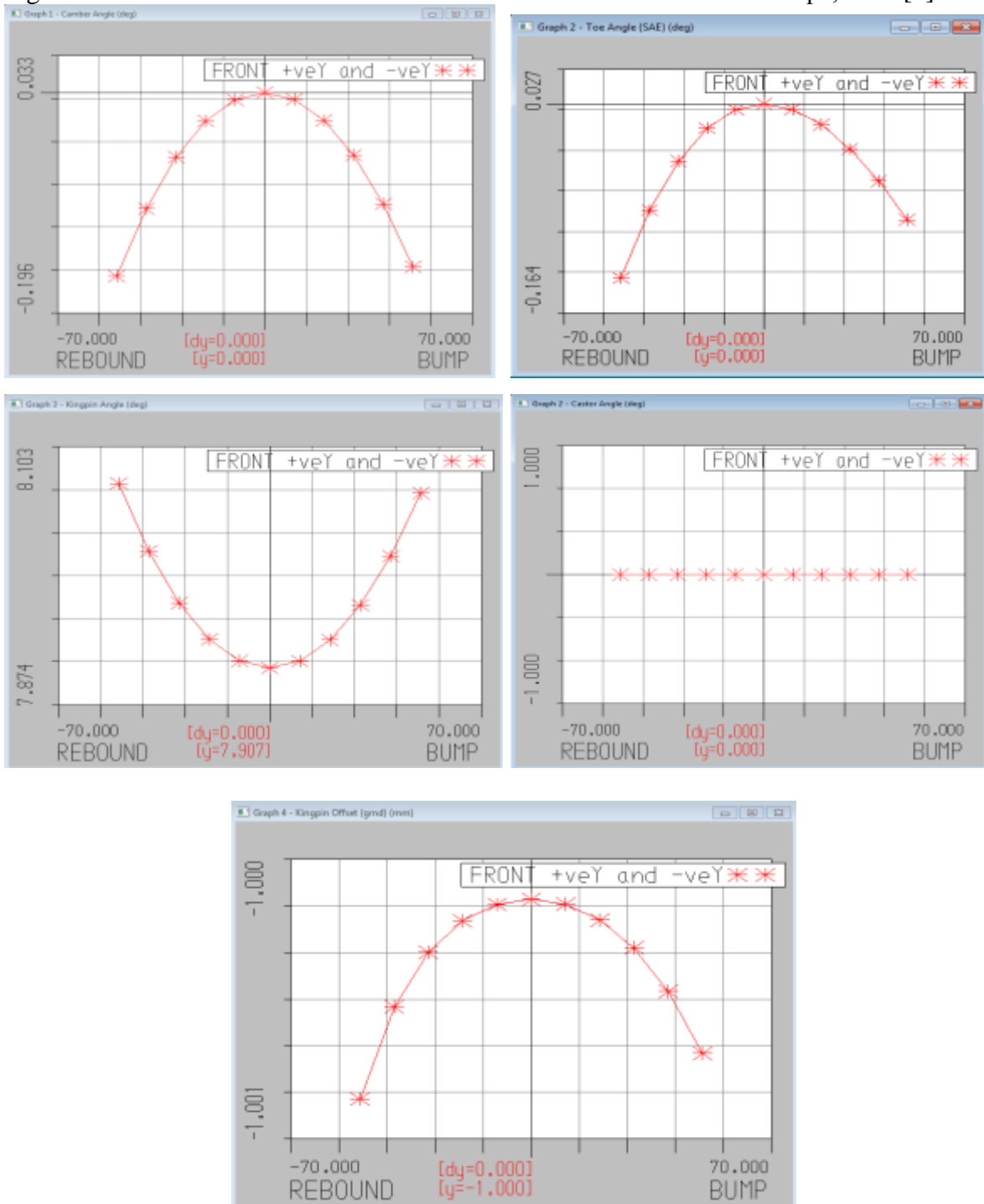


Figure C.3: Camber (top left), toe (top right), Kingpin angle (middle left), caster (middle right) and Kingpin offset (bottom) curves during bump and rebound for the zero caster setup proposed by [8].

Since the camber and toe changes are very small in the order of tenths decimal place, it can be neglected. From Figure C.3 it is seen that the roll centers lies on the ground and the change in camber and toe is negligible which results in negligible change in half-track width.

Table C.3:  $\Delta t_w$  and  $h_{rollc_j}$  values (where  $j$  stands for front or rear axle)

S.no	value
$\Delta t_w$	0
$h_{rollc_j}$	0

## C.2 Roll stiffness estimation

Figure C.4 defines roll stiffness of an axle.

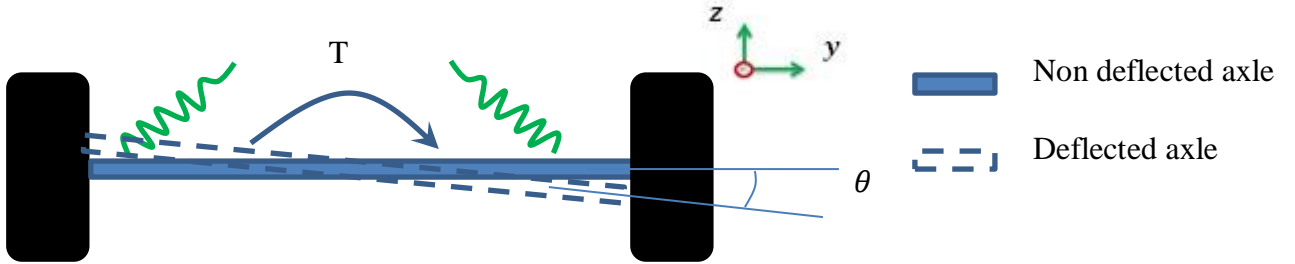


Figure C.4: Definition of roll stiffness

The deflection of the springs considered here are linear. The definition of roll stiffness is given by

$$K_{\varphi} = \frac{T}{\theta} \quad (C. 1)$$

In order to estimate the roll stiffness of the vehicle, wheel motion ratio analysis of every wheel is performed.

Using simple lever arm equations on Figure C.5 (right),

$$F_B = F_A \left[ \frac{a}{b} \right] \quad (C. 2)$$

$$d_B = d_A \left[ \frac{b}{a} \right] \quad (C. 3)$$

Dividing (C. 2) by (C. 3), wheel rate can be obtained.  $F_B$  is the vertical force acting on the point B,  $d_B$  is the vertical displacement of the point B,  $b$  is the distance between the pivot point C and lever point B,  $a$  is the distance between the pivot point C and spring mount A.

To derive the wheel rate, Figure C.5(left) gives

$$\frac{F_B}{d_B} = K_B = \frac{F_A \left[ \frac{a}{b} \right]}{d_A \left[ \frac{b}{a} \right]} = K_A \left[ \frac{a}{b} \right]^2 \quad (C. 4)$$

$$K_w = K_s \cdot \left( \frac{a}{b} \right)^2 \quad (C. 5)$$

Where  $K_w$  is the wheel rate and  $K_s$  is the spring rate of one wheel end. To have a linear spring rate, we consider that the springs are mounted perpendicular to the wishbones.



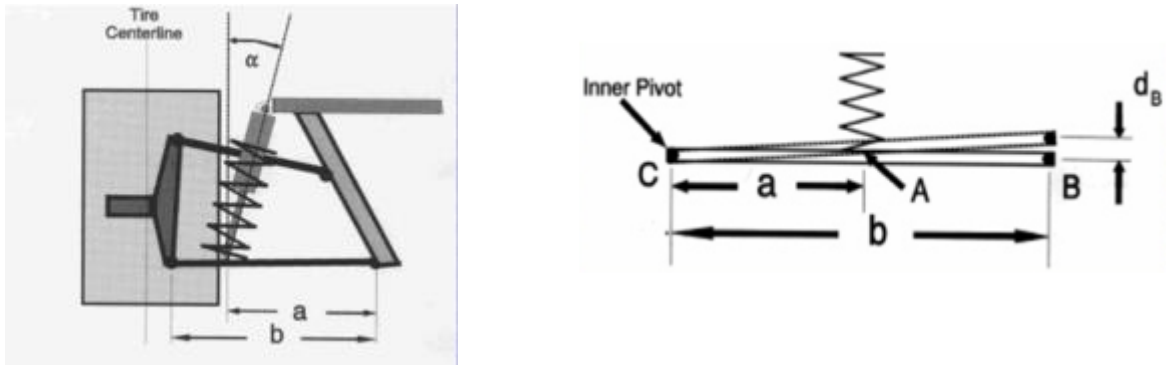


Figure C.5: Left- wheel motion ratio; right- motion ratio of a simple lever arm

Suspension roll stiffness of an axle is given by

$$K_{\phi} = K_{fs} + K_{rs} + K_{auxiliary} \quad (C. 6)$$

$$K_{fs} = \frac{T}{\theta} = \frac{t^2}{4} \cdot K_{fwl} + \frac{t^2}{4} \cdot K_{fwr} \quad (C. 7)$$

$$K_{rs} = \frac{T}{\theta} = \frac{t^2}{4} \cdot K_{rwl} + \frac{t^2}{4} \cdot K_{rwr} \quad (C. 8)$$

Where  $K_{\phi}$  is the total roll stiffness of the vehicle,  $K_{fs}$  is the front suspension roll stiffness,  $K_{rs}$  is the rear suspension roll stiffness,  $K_{auxiliary}$  is the roll stiffness due to auxiliary components such as antiroll bars,  $K_{fwl}$  is the front left wheel rate,  $K_{fwr}$  is the front right wheel rate,  $K_{rwl}$  is the rear left wheel rate,  $K_{rwr}$  is the rear right wheel rate and  $t$  is the track width . All the wheel rates are given in N/m.

It is assumed in design, all the wheels have the same wheel rate and the vehicle is symmetric.

Table C.4: Dimensions of suspension for motion ratio analysis

	Front suspension	Rear suspension	Comment/reference
a	0.145	0.18	[4]
b	0.37	0.32	[4]

Using the spring stiffness values mentioned in Table 3.2 ( $10 \text{ kN}/\text{rad}$ ), the roll stiffness of the front suspension and the rear suspension are given in Table C.5.

Table C.5: Roll stiffness measures

	$K_{\phi}(t_w = 1.2m)$	$K_{\phi}(t_w = 1.3m)$	$K_{\phi}(t_w = 1.4m)$
Units	$\text{kN}/\text{rad}$	$\text{kN}/\text{rad}$	$\text{kN}/\text{rad}$
Front suspension	1.106	1.297	1.505
Rear suspension	2.278	2.673	3.100

The highlighted option in Table C.5 is the roll stiffness of the current vehicle specification.

### C.3 Road bank angle modeling

According to [35] and [3] the height of a curb in a highway lies between 100 and 400 mm in height. Refer Figure C.6.

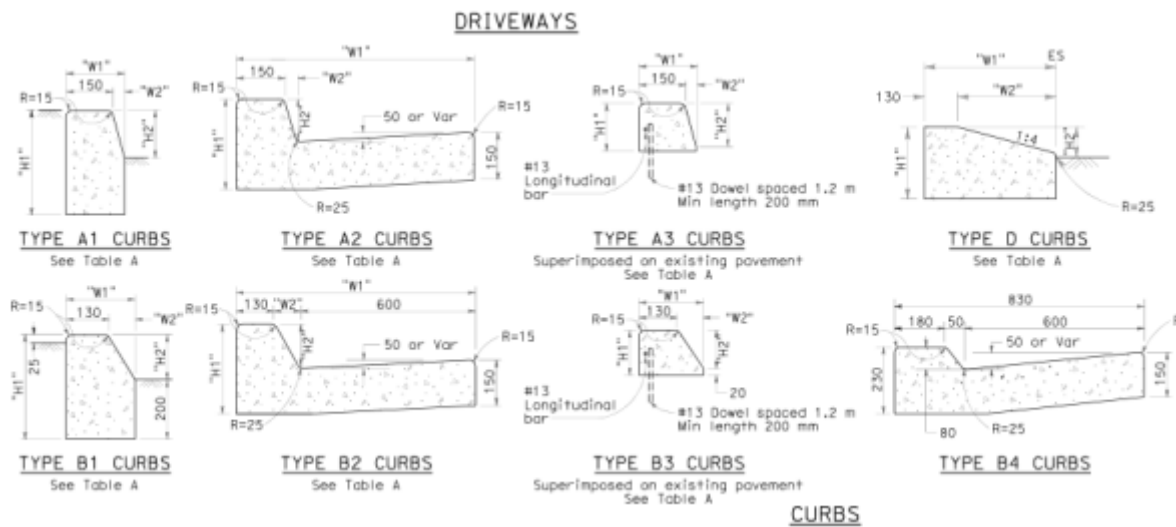


Figure C.6: Curb height dimensions picture [3]

Refer Table C.6 for the unknown dimension on Figure C.6.

Table C.6: Dimensions of the curb [3]

CURB TYPE	DIMENSIONS			
	"H1"	"H2"	"W1"	"W2"
A1-150	350	150	190	40
A1-200	400	200	200	50
A2-150	300	150	290	40
A2-200	350	200	800	50
A3-150	150	130	185	35
A3-200	200	180	198	48
B1-100	300	100	200	70
B1-150	350	150	230	100
B2-100	250	100	800	70
B2-150	300	150	830	100
B3-100	100	80	185	55
B3-150	150	130	217	87
D-100	250	100	452	322
D-150	300	150	652	522

Now, it is considered that “worst case scenario” is when the EDV rides with inner wheel (in the corner) on the curb with a maximum height and the outer wheel on the ground in a circular track. Refer Figure C.7 and Figure C.8 for more details.

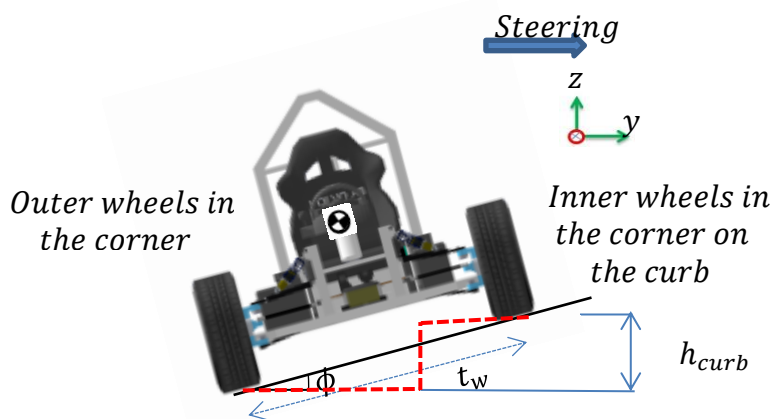


Figure C.7: Bank angle

$$\phi = \sin^{-1} \left( \frac{h_{curb}}{t_w} \right) \quad (C. 9)$$

The bank angle is given by (C. 9). Hence for varying  $h_{curb}$ , it is safe to consider the minimum road elevation as flat road and the highest road elevation as 400mm.



Figure C.8: Corner with a curb

Table C.7: Minimum and maximum banking angles

Parameter	Minimum	Maximum
Bank angle ( $\phi$ )(degrees)	0	11

#### C.4 Steady state rollover simulation results

This section corresponds to results from steady state modeling.

Table C.8: Steady state results comparison with  $h_{cog}^{vehicle}=0.4, \mu = 1.3$

Road friction ( $\mu$ )	$h_{cog}^{vehicle}$ (m)	$h_{curb}$ (mm)	$\phi$ (degrees)	Plots
1.3	0.4	No curb	0	
		200	5.5	

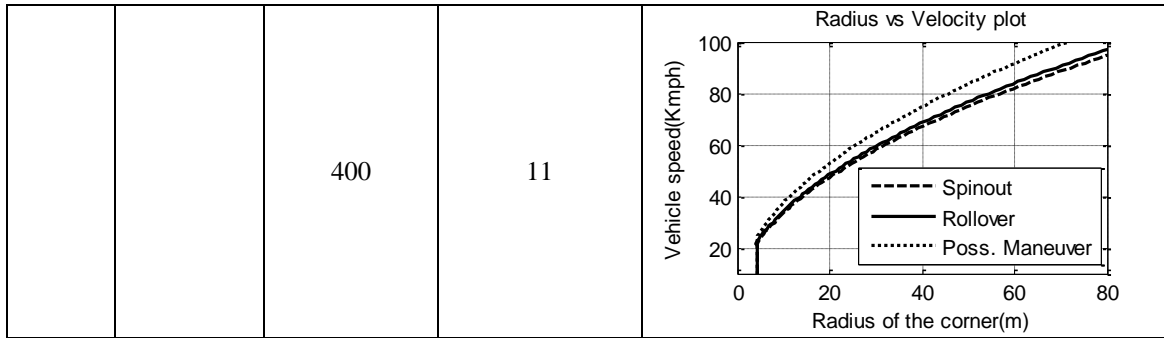


Table C.9: Steady state results comparison with  $h_{cog}^{vehicle}=0.45, \mu = 1.3$

Road friction ( $\mu$ )	$h_{cog}^{vehicle}$ (m)	$h_{curb}$ (mm)	$\phi$ (degrees)	Plots
1.3	0.45	No curb	0	
		200	5.5	
		400	11	

Table C.10: Steady state results comparison with  $h_{cog}^{vehicle}=0.4, \mu = 0.8$

Road friction ( $\mu$ )	$h_{cog}^{vehicle}$ (m)	$h_{curb}$ (mm)	$\phi$ (degrees)	Plots
0.8	0.4	No curb	0	
		200	5.5	
		400	11	

Table C.11: Steady state results comparison with  $h_{cog}^{vehicle}=0.45, \mu = 0.8$

Road friction ( $\mu$ )	$h_{cog}^{vehicle}$ (m)	$h_{curb}$ (mm)	$\phi$ (degrees)	Plots
0.8	0.45	No curb	0	

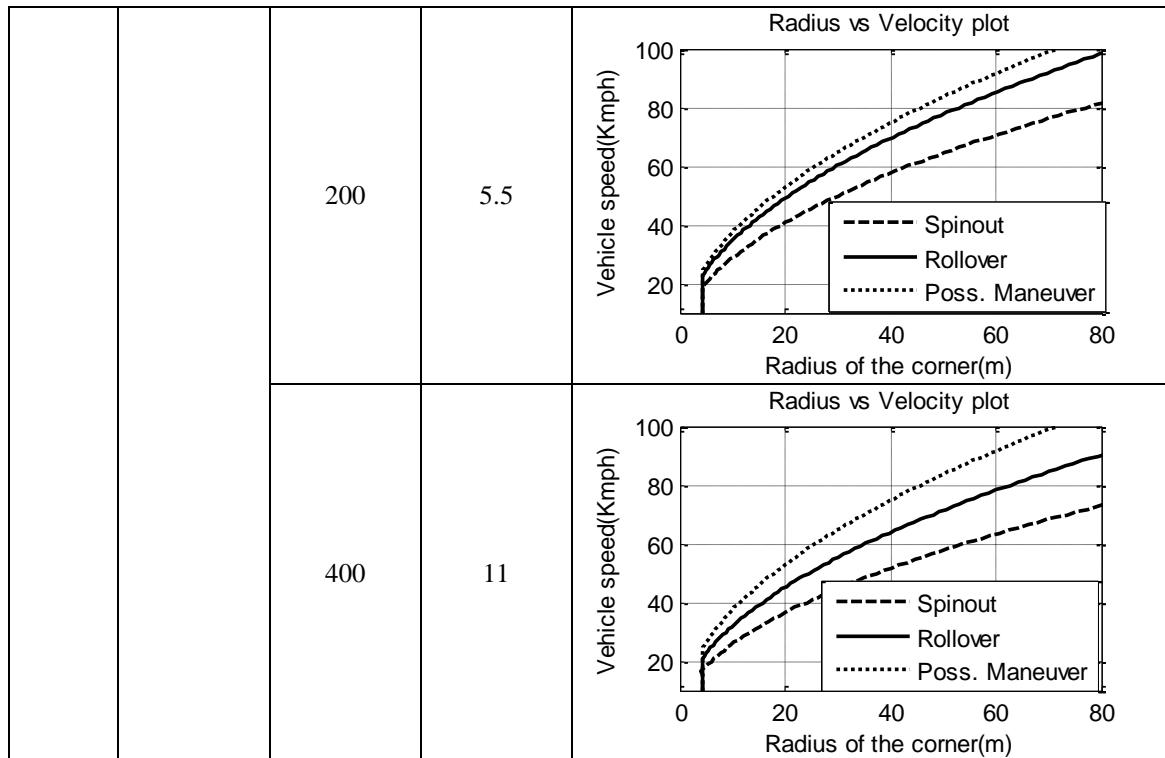
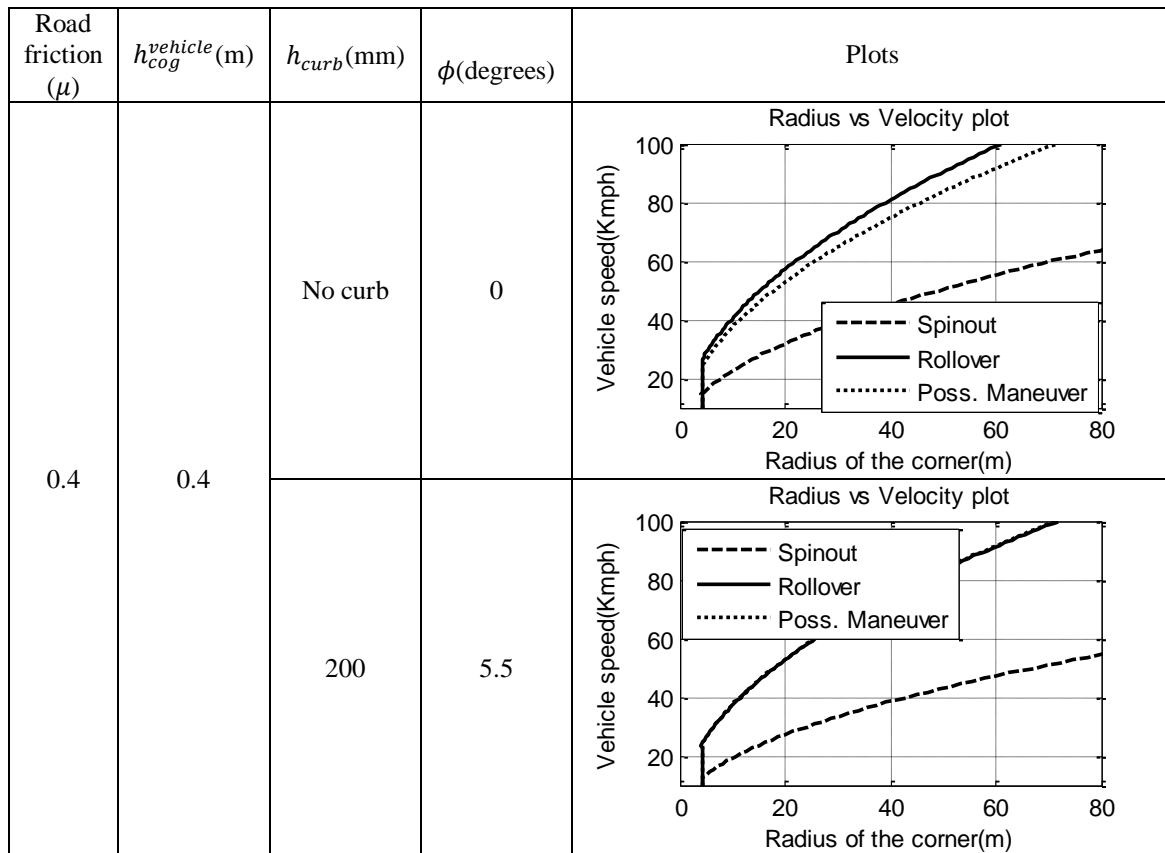


Table C.12: Steady state results comparison with  $h_{cog}^{vehicle}=0.4, \mu = 0.4$



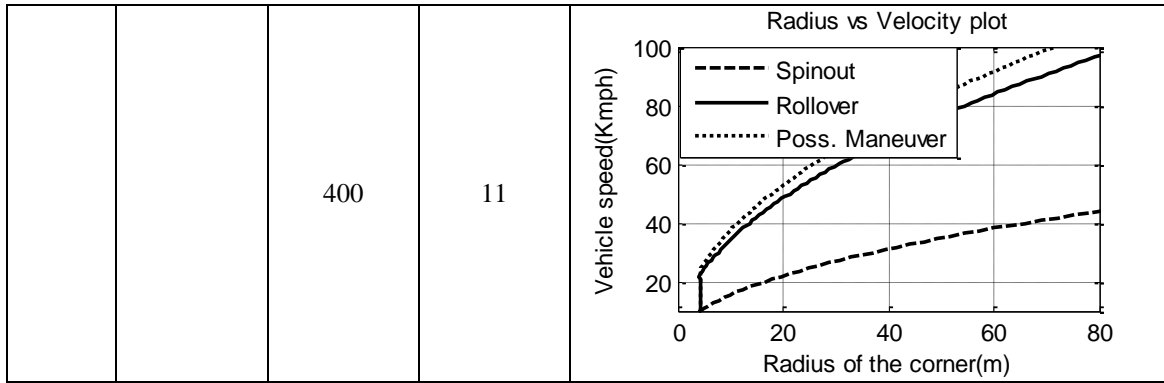


Table C.13: Steady state results comparison with  $h_{cog}^{vehicle}=0.45, \mu = 0.4$

Road friction ( $\mu$ )	$h_{cog}^{vehicle}$ (m)	$h_{curb}$ (mm)	$\phi$ (degrees)	Plots
0.4	0.45	No curb	0	
		200	5.5	
		400	11	

Table C.14: Steady state results comparison with  $h_{cog}^{vehicle}=0.5 \mu = 0.4$

Road friction ( $\mu$ )	$h_{cog}^{vehicle}$ (m)	$h_{curb}$ (mm)	$\phi$ (degrees)	Plots
0.4	0.5	No curb	0	
		200	5.5	
		400	11	

## C.5 Transient rollover modeling

The transient model was a just another method of predicting the rollover. This method could be further developed in the future with various maneuver inputs.

### Transient maneuver modeling

A bicycle model with lateral and longitudinal load transfer was utilized to model the transient behavior of the vehicle.

### Vehicle coordinate system

ISO vehicle coordinate system was used to model the vehicle. Figure C.9 shows a pictorial representation of the vehicle coordinate system.



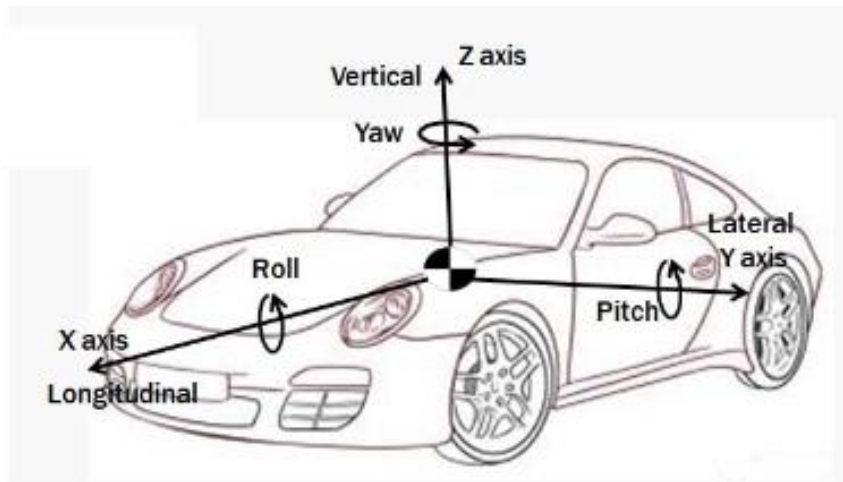


Figure C.9: ISO vehicle coordinate system

### Wheel coordinate system

The purpose of this session is to show the significance of understanding a tire model in rollover analysis. Figure C.10 gives a clear idea on the tire co-ordinate system when talking about longitudinal and lateral forces. From here, all the vectors will follow ISO co-ordinate system as shown in Figure C.10.

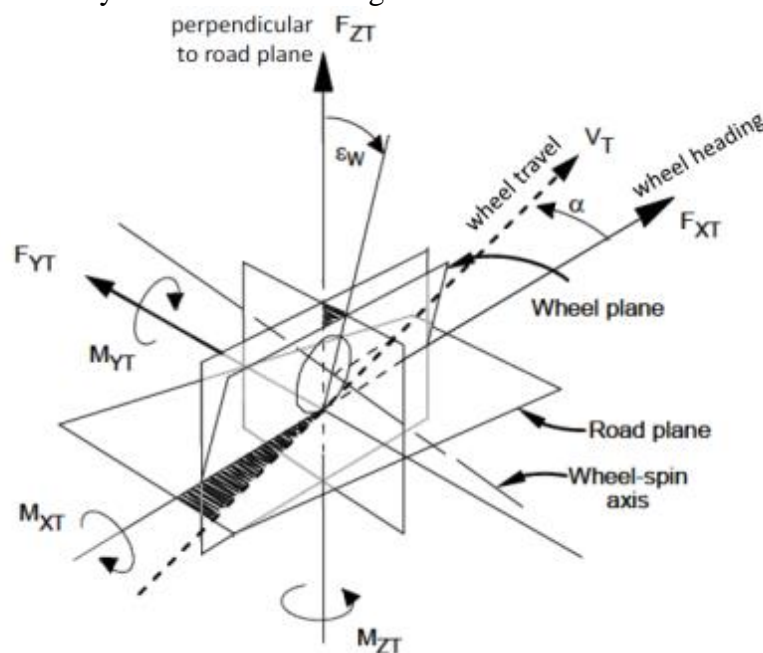


Figure C.10: ISO wheel co-ordinate system

### Tire model

When a tire is orientated at an angle not equal to its direction of its motion, a side force acts perpendicular to the plane of the wheel. This relation is nearly linear for small slip angles. The relationship that defines lateral force as a function of slip angle makes use of the tire cornering stiffness. Friction rollover, usually takes place when the road tire friction coefficient peaks as shown in Figure C.11, i.e.  $> \frac{F_{yij}}{\mu \cdot F_{zij}}$ . Just the peak friction coefficients for interesting road tire conditions are modeled i.e. the lateral acceleration of the axles are limited to the friction coefficient of the tire. Modeling lateral tire

stiffness/ compliance was from [33]. A linear tire model was used to calculate the lateral stiffness of the wheels.

$$C_{\alpha} = c_0 \cdot f_{zi} + c_1 \cdot f_{zi}^2 \quad (3.14)$$

Where  $C_{\alpha}$  is the cornering stiffness,  $c_0$  is the cornering stiffness parameter,  $c_1$  is the cornering coefficient.

Table C.15: Cornering stiffness coefficients [33]

$c_0$	30.7	$rad^{-1}$
$c_1$	-0.00235	$(N.rad)^{-1}$

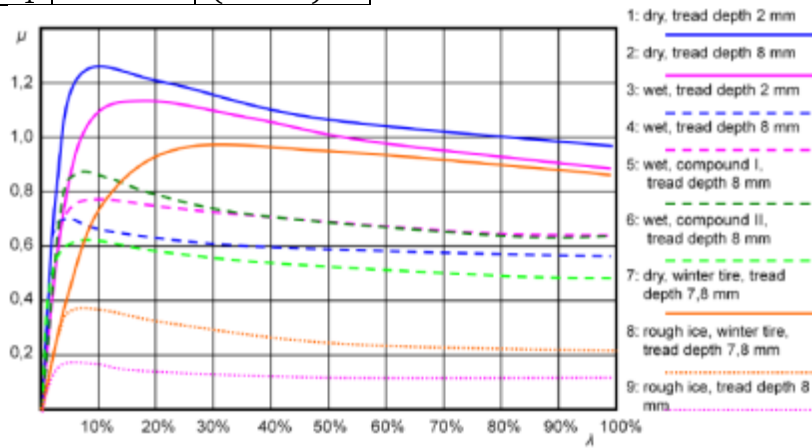


Figure C.11: Slip vs. Friction coefficient curve; Nonlinear curves for different tire models from [11].

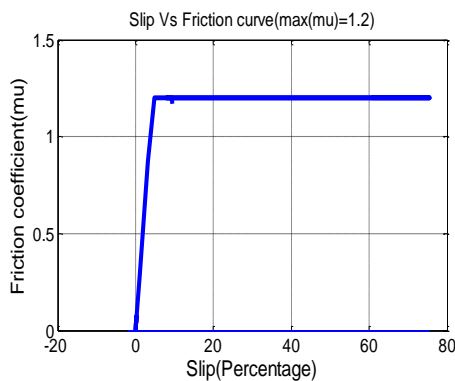


Figure C.12: Linear tire model for the current vehicle limited by maximum friction road-tire friction coefficient

Table C.16: Peak friction coefficient consideration for different tire-road conditions

	Dry road with high friction coefficient	Normal dry road	Reference
Peak friction value	1.5	1.2	[11]

The road tire friction coefficient increases, with an increase in slip angle (refer Appendix C), in a linear fashion for small values of slip angles. At a certain slip angle for a particular road-tire friction peak, the tire reaches saturation region. This causes the

vehicle to spinout rather than rollover. Such a driving situation is not critical from a rollover stability perspective.

### Combined wheel slip

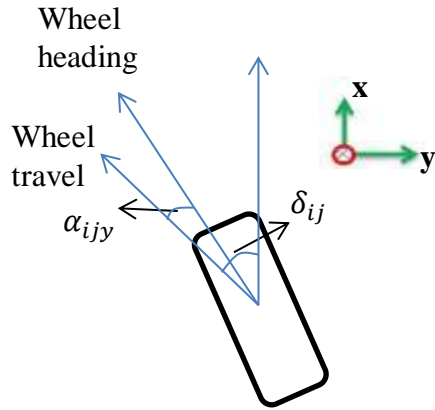


Figure C.13: Wheel lateral slip model

$$\alpha_{ijy} = \delta_{ij} \pm \tan^{-1}\left(\frac{v_y + \dot{\psi} \cdot l_j}{v_x}\right) \quad (3.15)$$

(3.15) gives the equation for lateral wheel slip in degrees where  $\alpha$  is the slip angle,  $\delta$  is the steering angle,  $v_x$  is the longitudinal velocity,  $v_y$  is the lateral velocity,  $i$  is either left wheel or right wheel and  $j$  is either front axle or the rear axle. For combined slip conditions,

$$F_{yij} = K_{yt} \cdot \alpha_{ijy} \quad (3.16)$$

$$\max(F_{yij}) = \sqrt{(\mu \cdot F_{zij})^2 - (F_{xij})^2} \quad (3.17)$$

(3.17) gives the combined slip equation.

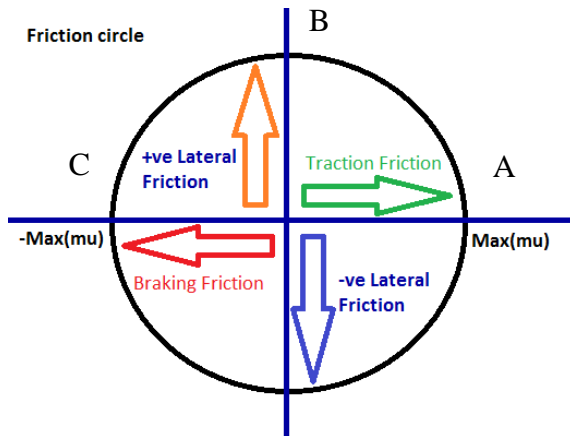


Figure C.14: Friction circle for combined slip equation

The friction circle gives the dynamic interaction between tire and the road surface. This friction limit diagram varies for various road surface conditions. The circle gets smaller with reduction in  $\max(\mu)$ . A, shows the maximum traction friction available to propel the car. B shows the maximum lateral friction available while cornering (without propulsion or braking). C shows the maximum braking force available without cornering. The most important point of this chapter's interest is the point B.

### Steering input

The steering input given to this model was a step steer input as shown in Figure C.15. Since finding the best rollover maneuver wasn't in the scope of the thesis, step steer input was taken in order to easily parameterize the steering input and path of the vehicle.

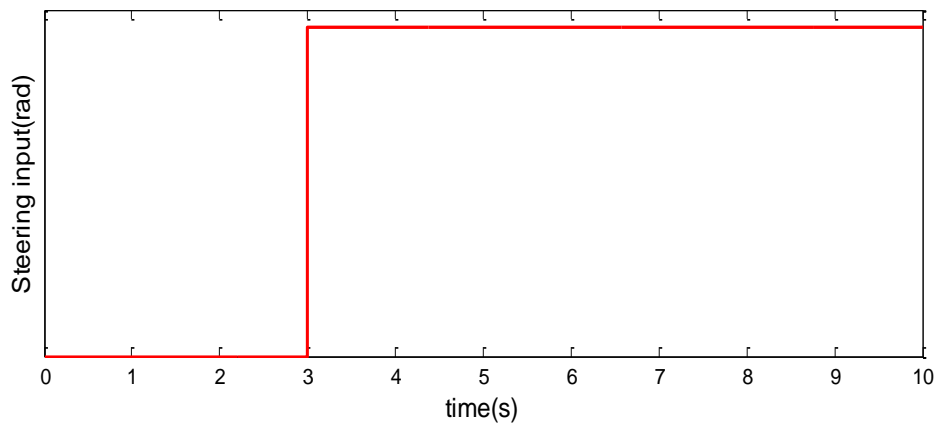


Figure C.15: Steering input for transient model

### Rollover event

The rollover event is said to occur if either of the inner wheels lift off. That is, the sum of normal forces on both the inner wheels of the corner is zero ( $F_{z1l} + F_{z2l} = 0$ ) i.e. the wheels lose contact with the ground.

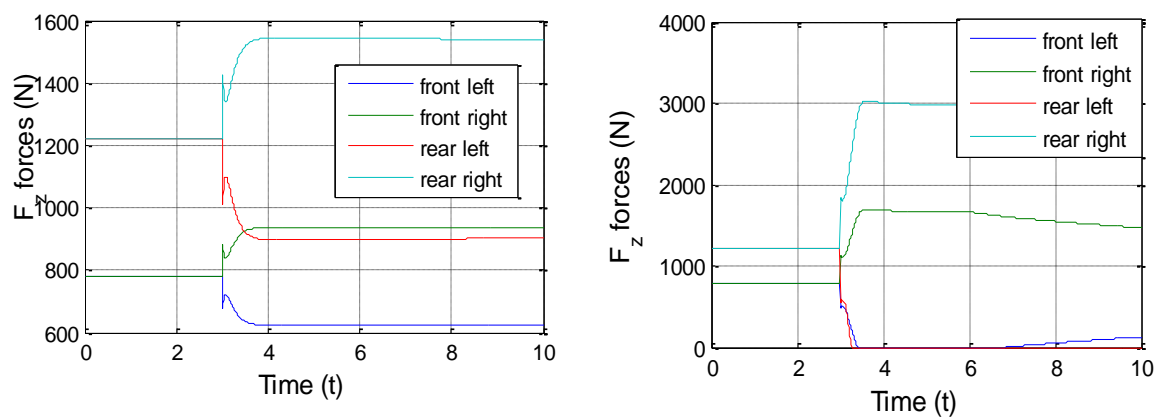


Figure C.16: Left- Maneuver without rollover; Right- Maneuver resulting in rollover

The difference between a maneuver without and with rollover can be seen from Figure C.16 (left and right respectively). Figure C.16 (right) shows that the both the inner wheels of the vehicle in the corner have lifted of resulting in vehicle rollover.

### Chassis Model

A bicycle model was converted into a two-track model with lateral and longitudinal load transfer with body roll.

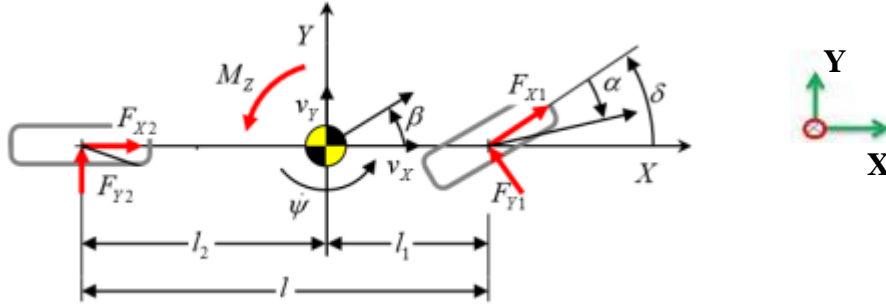


Figure C.17: Bicycle model

The equations of motion of a bicycle model are given by (3. 18), (3. 19) and (3. 20)

$$\dot{v}_x = \frac{(F_{X1} \cdot \cos \delta - F_{Y1} \cdot \sin \delta + F_{X2})}{m} + \dot{\psi} \cdot v_y \quad (3. 18)$$

$$\dot{v}_y = \frac{(F_{X1} \cdot \sin \delta - F_{Y1} \cdot \cos \delta + F_{Y2})}{m} - \dot{\psi} \cdot v_x \quad (3. 19)$$

$$\ddot{\psi} = \frac{(F_{X1} \cdot \sin \delta + F_{Y1} \cdot \cos \delta) \cdot l_1 - F_{Y2} \cdot l_2}{J_{zz}} \quad (3. 20)$$

### Load transfer model

Longitudinal load transfer taken from [33] is given by (3. 21)

$$\Delta F_{z,long} = \pm GVW^e \cdot a_x \cdot \frac{h}{2 \cdot l} \quad (3. 21)$$

Lateral load transfer is given [33] by (3. 22)

$$\Delta F_{z,lat} = \pm GVW^e \cdot a_y \cdot \left( \frac{h_{roll} \cdot (l - l_j)}{l \cdot t_w} + \frac{\Delta h}{t_w} \cdot \frac{c_{jw}}{c_{fw} + c_{rw}} \right) \quad (3. 22)$$

Where , j stands for either front or rear axle respectively.

$$\Delta F_z = \Delta F_{z,long} + \Delta F_{z,lat} \quad (3. 23)$$

Equation (3. 23) gives the net load transfer.

## C.6 Transient maneuver results

Transient maneuver rollover analysis includes the time factor for rollover. The main objective of transient model is to study the comparison between steady state models and motivate on the results. This chapter also throws light on how quick the rollover event occurs (how fast wheels lose contact with the ground). Vehicle model described in Figure C.17 is used in transient maneuver rollover. The rollover plot is a contour plot of sum of  $F_z$  forces of inner wheels of the vehicle in a corner. The rollover event occurs for the specific configuration when the contour ( $F_{zlr} + F_{zlf}$ ) value reaches zero (refer Section 0 for further details on how the event is considered). If there contour shows a positive value, the vehicle has not rolled over. Since friction is modeled as a limiting parameter here, comparatively accurate results are available in this section. The radius mentioned in all graphs is the intended radius ( $\delta \cdot L$ ) of the vehicle. Vehicle spin out is not modeled here as rollover is the main criteria in this section. It is also to be noted that this transient model has a drawback as suspension effects are not modeled here.

It can be seen in Table C.17 that the vehicle rolls over only with high coefficient of friction and high  $h_{cog}^{vehicle}$ . At low  $h_{cog}^{vehicle}$  and low  $\mu$  levels, the  $F_z$  forces still exist which either means that the vehicle has either spun out (high lateral slip levels) or is running stable i.e. the tires are still in contact with the ground.

Table C.17: Transient maneuver rollover plots for  $t_w = 1.4m$

$t_w$ (m)	$h_{cog}^{vehicle}$ (m)	$\mu$ or $\frac{a_y}{g}$ limit	Rollover plot (contour = $F_{zlr} + F_{zlf}$ )	General comment
1.4	0.4	1.3		Safe
		1.5		Safe

0.45	1.3		Safe
	1.5		Safe
0.5	1.3		Safe
	1.5		Safe/marginal

### Observations for transient maneuver cornering

From Table C.17, it can be seen that, for the current vehicle specification, high amount of  $\mu$  and  $a_y$  is required for the vehicle to rollover. Though the friction limits modeled here are very high, the limitations of tire are predictably less i.e., the tire saturates before  $\mu$  of 1.5 [11]. Hence, using higher friction limits to model rollover has an added advantage as the friction limits of the tire cannot reach such high friction levels (refer [11], [13] and [14]). This also means that the probability of vehicle spinning out is higher than a rollover event.





## Appendix D

This appendix corresponds to the Chapter 4 and Table D.2 shows the non-feasible frame dimensions.

Table D.1: Feasible results

H2 (mm)	B2 (mm)	t2 (mm)	H13 (mm)	B13 (mm)	t13 (mm)	Sigm (MPa)	Deflection (mm)	Tstif (Nm/rad)	Tstifmid (Nm/deg)	feas	Mass (kg)	Mass of the frame
30	30	2	40	40	2,5	720,3	3,6	1130,4	60,4	1	9,1	46,0
30	30	2	80	40	2,5	720,3	3,7	5832,1	60,4	1	12,9	69,4
30	30	2	50	50	3	720,3	3,7	2587,4	60,4	1	12,7	68,1
30	30	2	70	70	3	720,3	3,7	7365,7	60,4	1	17,1	96,2
30	30	2	100	50	4	720,3	3,7	17529,0	60,4	1	23,4	135,0
30	30	2	50	100	4	720,3	3,7	5801,3	60,4	1	23,4	135,0
30	30	2	100	100	3	720,3	3,7	22205,4	60,4	1	23,9	138,3
40	40	2,5	40	40	2,5	320,1	1,2	1249,0	179,0	1	10,5	47,4
40	40	2,5	80	40	2,5	320,1	1,2	5950,7	179,0	1	14,3	70,8
40	40	2,5	50	50	3	320,1	1,2	2706,0	179,0	1	14,1	69,5
40	40	2,5	70	70	3	320,1	1,2	7484,3	179,0	1	18,6	97,6
40	40	2,5	100	50	4	320,1	1,2	17647,6	179,0	1	24,8	136,4
40	40	2,5	50	100	4	320,1	1,2	5919,9	179,0	1	24,8	136,4
40	40	2,5	100	100	3	320,1	1,2	22324,0	179,0	1	25,3	139,7
80	40	2,5	40	40	2,5	118,7	0,2	2502,1	1432,1	1	12,4	49,3
80	40	2,5	80	40	2,5	118,7	0,2	7203,7	1432,1	1	16,1	72,7
80	40	2,5	50	50	3	118,7	0,2	3959,1	1432,1	1	15,9	71,4
80	40	2,5	70	70	3	118,7	0,2	8737,4	1432,1	1	20,4	99,5
80	40	2,5	100	50	4	118,7	0,2	18900,6	1432,1	1	26,6	138,3
80	40	2,5	50	100	4	118,7	0,2	7173,0	1432,1	1	26,6	138,3
80	40	2,5	100	100	3	118,7	0,2	23577,0	1432,1	1	27,2	141,6
50	50	3	30	30	2	169,4	0,5	776,1	419,6	1	9,5	31,5
50	50	3	40	40	2,5	169,4	0,5	1489,5	419,6	1	12,3	49,2
50	50	3	80	40	2,5	169,4	0,5	6191,2	419,6	1	16,0	72,6
50	50	3	50	50	3	169,4	0,5	2946,5	419,6	1	15,8	71,3
50	50	3	70	70	3	169,4	0,5	7724,9	419,6	1	20,3	99,3
50	50	3	100	50	4	169,4	0,5	17888,1	419,6	1	26,5	138,2
50	50	3	50	100	4	169,4	0,5	6160,5	419,6	1	26,5	138,2
50	50	3	100	100	3	169,4	0,5	22564,5	419,6	1	27,1	141,5
70	70	3	30	30	2	82,1	0,2	1507,8	1151,2	1	11,7	33,7
70	70	3	40	40	2,5	82,1	0,2	2221,2	1151,2	1	14,5	51,4
70	70	3	80	40	2,5	82,1	0,2	6922,9	1151,2	1	18,3	74,8
70	70	3	50	50	3	82,1	0,2	3678,2	1151,2	1	18,1	73,5
70	70	3	70	70	3	82,1	0,2	8456,6	1151,2	1	22,6	101,6
70	70	3	100	50	4	82,1	0,2	18619,8	1151,2	1	28,8	140,4
70	70	3	50	100	4	82,1	0,2	6892,2	1151,2	1	28,8	140,4
70	70	3	100	100	3	82,1	0,2	23296,2	1151,2	1	29,3	143,7
100	50	4	30	30	2	49,0	0,1	4831,8	4475,2	1	14,8	36,8

100	50	4	40	40	2,5	49,0	0,1	5545,2	4475,2	1	17,7	54,5
100	50	4	80	40	2,5	49,0	0,1	10246,9	4475,2	1	21,4	77,9
100	50	4	50	50	3	49,0	0,1	7002,2	4475,2	1	21,2	76,6
100	50	4	70	70	3	49,0	0,1	11780,5	4475,2	1	25,7	104,7
100	50	4	100	50	4	49,0	0,1	21943,8	4475,2	1	31,9	143,5
100	50	4	50	100	4	49,0	0,1	10216,1	4475,2	1	31,9	143,5
100	50	4	100	100	3	49,0	0,1	26620,2	4475,2	1	32,4	146,8
50	100	4	30	30	2	74,6	0,2	916,0	559,4	1	14,8	36,8
50	100	4	40	40	2,5	74,6	0,2	1629,4	559,4	1	17,7	54,5
50	100	4	80	40	2,5	74,6	0,2	6331,1	559,4	1	21,4	77,9
50	100	4	50	50	3	74,6	0,2	3086,4	559,4	1	21,2	76,6
50	100	4	70	70	3	74,6	0,2	7864,7	559,4	1	25,7	104,7
50	100	4	100	50	4	74,6	0,2	18027,9	559,4	1	31,9	143,5
50	100	4	50	100	4	74,6	0,2	6300,3	559,4	1	31,9	143,5
50	100	4	100	100	3	74,6	0,2	22704,4	559,4	1	32,4	146,8
100	100	3	30	30	2	38,7	0,1	3713,0	3356,4	1	15,1	37,1
100	100	3	40	40	2,5	38,7	0,1	4426,4	3356,4	1	17,9	54,8
100	100	3	80	40	2,5	38,7	0,1	9128,1	3356,4	1	21,7	78,2
100	100	3	50	50	3	38,7	0,1	5883,4	3356,4	1	21,5	76,9
100	100	3	70	70	3	38,7	0,1	10661,7	3356,4	1	25,9	105,0
100	100	3	100	50	4	38,7	0,1	20825,0	3356,4	1	32,2	143,8
100	100	3	50	100	4	38,7	0,1	9097,3	3356,4	1	32,2	143,8
100	100	3	100	100	3	38,7	0,1	25501,4	3356,4	1	32,7	147,1

Table D.2: Non feasible frame dimensions

H2 (mm)	B2 (mm)	t2 (mm)	H13 (mm)	B13 (mm)	t13 (mm)	Sigm (MPa)	Deflection (mm)	Tstif (Nm/rad)	Tstifmid (Nm/deg)	feas	Mass (kg)
30	30	2	30	30	2	720,3	3,7	417,0	60,4	0	28,30464
40	40	2,5	30	30	2	320,1	1,2	535,6	179,0	0	29,718
50	50	3	30	30	2	169,4	0,5	776,1	419,6	0	31,48704

## Appendix E

This appendix corresponds to the chapter 5 .

### E.1 Approach

This section provides information on the FEM approach adapted for evaluating the strength of the frame structure. This version is a much more detailed version of Figure 5.2.

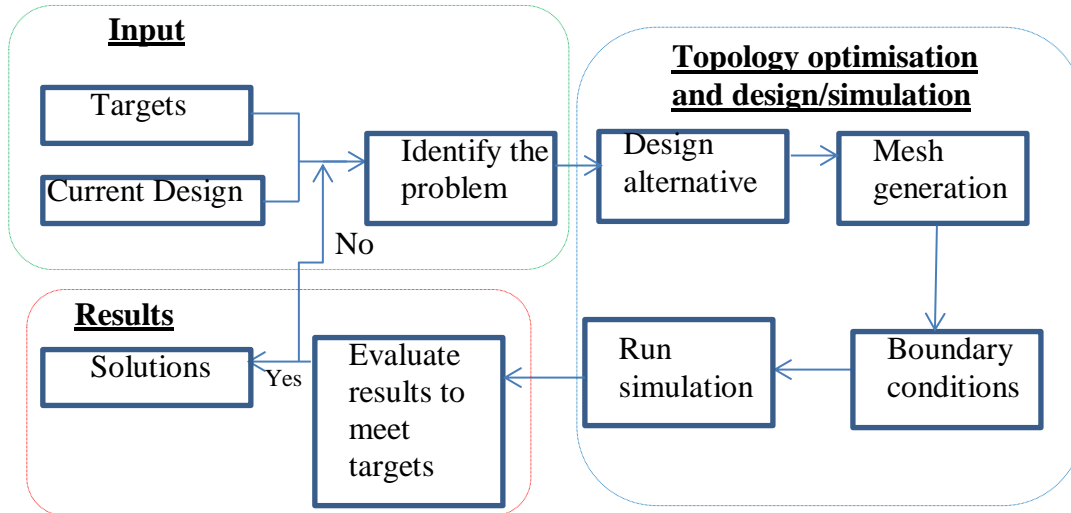


Figure E.1: Flow chart for FEM approach on methodology

### E.2 Boundary conditions

This section gives a clear description on the boundary condition for strength evaluation of the EDV frame.

#### E.2.1 Torsional stiffness

The worst case scenario considered was going over a speed bump with 1.5g of deceleration force in a down slope grade of 30% at 80Kmph, with one wheel. This was considered after comparing this case scenario with cornering.

Table E.1: Boundary conditions input value

Variable	Value	Reference
Weight distribution (front/rear)	67/33 %	[1]
Deceleration	$-14.71 \text{ m/s}^2$	-
Mass of the vehicle	418 Kg	[1]
Velocity of the car	$22.22 \text{ m/s}$	[4]
Distance b/w CoG and front axle	1.514 m	[1]
Wheel base	2.3 m	[1]
Radius of the bump	14.102 m	[36]
Grade of the slope	$16.70^\circ$	[36]
Acceleration due to gravity	$9.81 \text{ m/s}^2$	-
Height of CoG	0.42m	[1]
Track width	1.4 m	[7]

## Scenario 1

Calculating the moment equilibrium around rear contact to the ground around the front axle using [33],

$$N_f = m \cdot \left( g \cdot \frac{l_r \cdot \cos \varphi + h \cdot \sin \varphi}{l_r + l_f} + a_x \cdot \frac{h}{l_r + l_f} \right) \quad (E. 1)$$

(E. 1) includes equal mass distribution of left and right wheels on axles and excludes rolling resistance, air resistance and suspension effects.

$$N_f = 2.605 \text{ kN}$$

$$N_f^{wheel} = \frac{N_f}{2} = \text{Normal force / wheel.}$$

$$N_f^{wheel} \sim 1.3 \text{ kN};$$

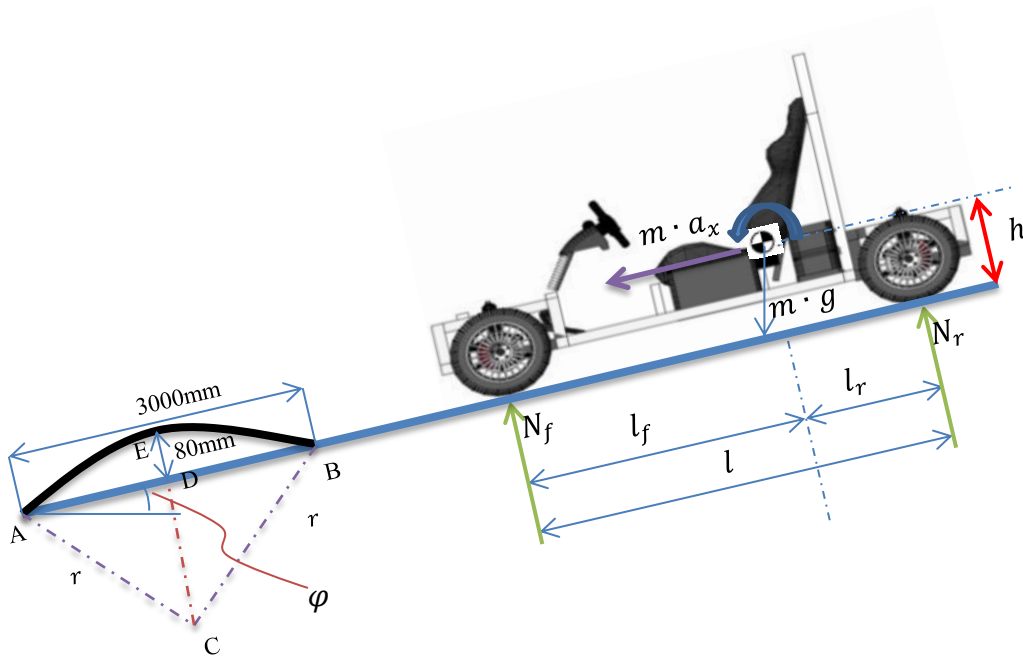


Figure E.2: Free body diagram for torsional case boundary conditions

The normal force on the top of the bump is given by (E. 2).

$$f_{normal}^{net} = N_f^{wheel} - \frac{mv_x^2}{r} = 3.326 \text{ kN} \quad (E. 2)$$

$f_{normal}^{net}$  is the force acting on the frame.

Torque acting about the vehicle's front axle is given by equation (E. 3).

$$T_{simulation} = f_{normal}^{net} \cdot t_w = 4.3238 \text{ kNm} \quad (E. 3)$$

## Scenario 2 – Load transfer ratio

Load transfer ratio is given by (E. 4).

$$LTR = \frac{Sum(F_{zl} - F_{zr})}{Sum(F_{zl} + F_{zr})} \quad (E. 4)$$

When LTR reaches 1 or -1, it means that the right hand side tires or left hand side tires have lost their contact patch with the ground respectively. If LTR is 0, then the vehicle is going in a straight line without any load transfer (no acceleration or deceleration). [37] States that the frame experiences the maximum torsion when  $LTR \rightarrow 1$ .

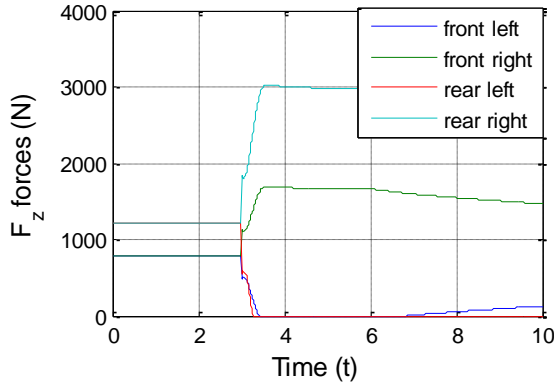


Figure E.3: Graph for load transfer ratio

LTR in this situation between 4<sup>th</sup> and 5<sup>th</sup> second in the X-axis is 1. The force acting on the front hoop of the frame (LHS) is given by  $F_{z1l}$  which sums up to be 1800N.

Hence, the force acting on the frame is

$$T_{simulation} = t_w \cdot F_{z1l} = 2.52 \text{ kNm}$$

Comparing Scenario 1 and Scenario 2, the worst case condition is taken as the boundary condition (scenario 1).

Figure E.4 pictorially represent the torsional loading condition. Here the rear roll hoop is clamped (fixed) and the torque ( $T_{simulation}$ ) is given to the front roll hoop.

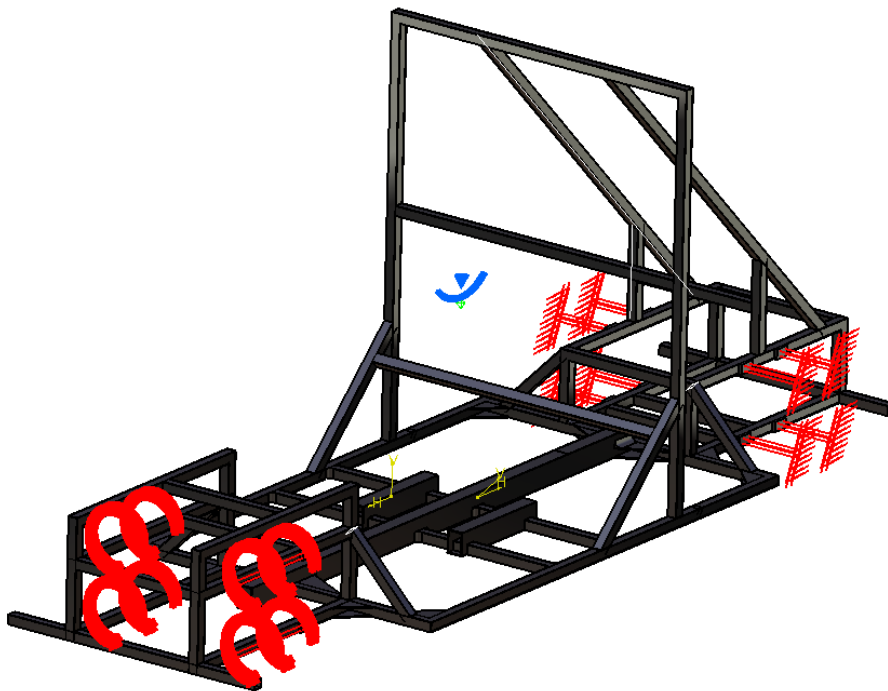


Figure E.4: Sample boundary condition for torsional load

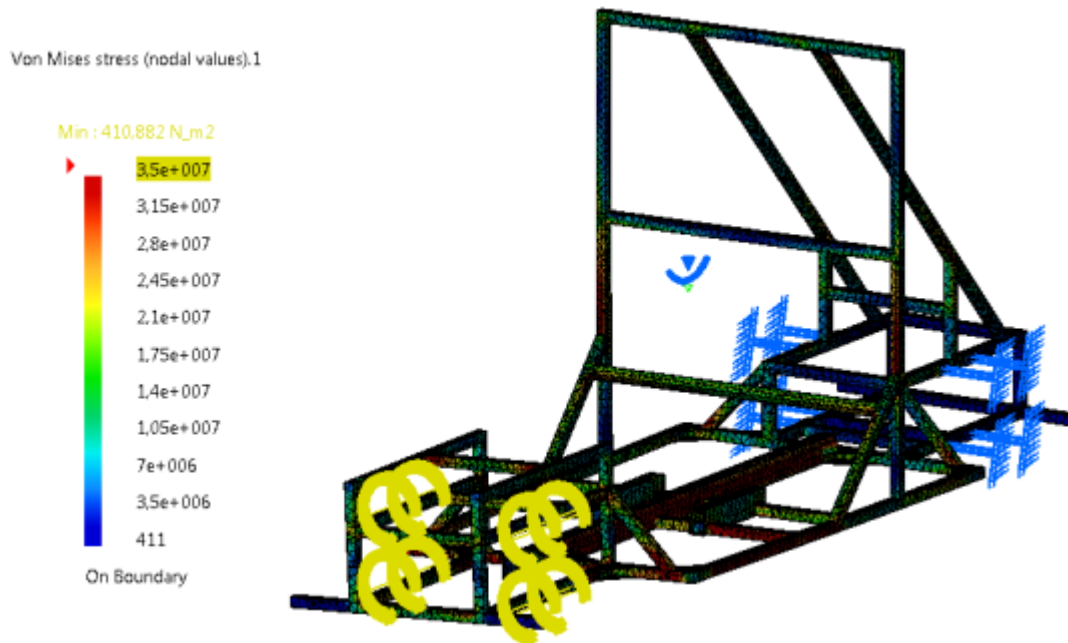


Figure E.5: FEM model after applying torsional load

### E.2.2 Bending stiffness

Pictorial representation of vertical bending load boundary condition is given by Figure E.6.

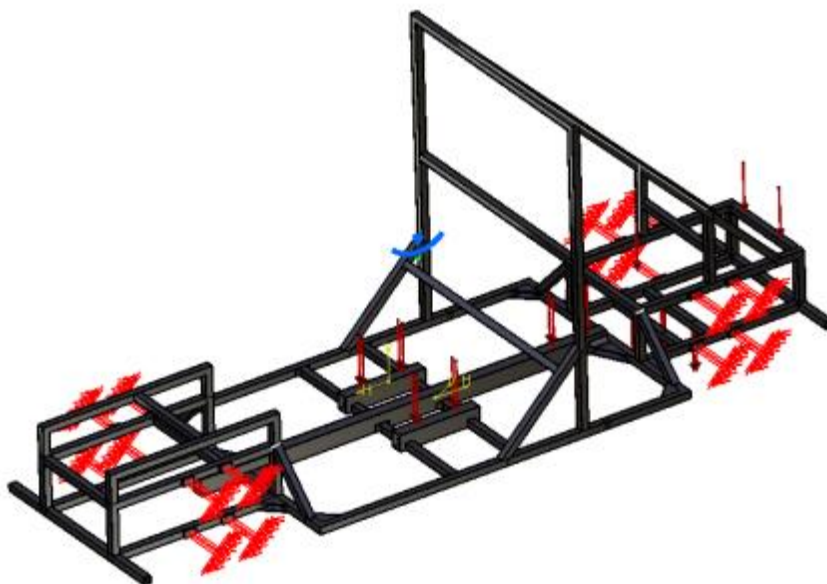
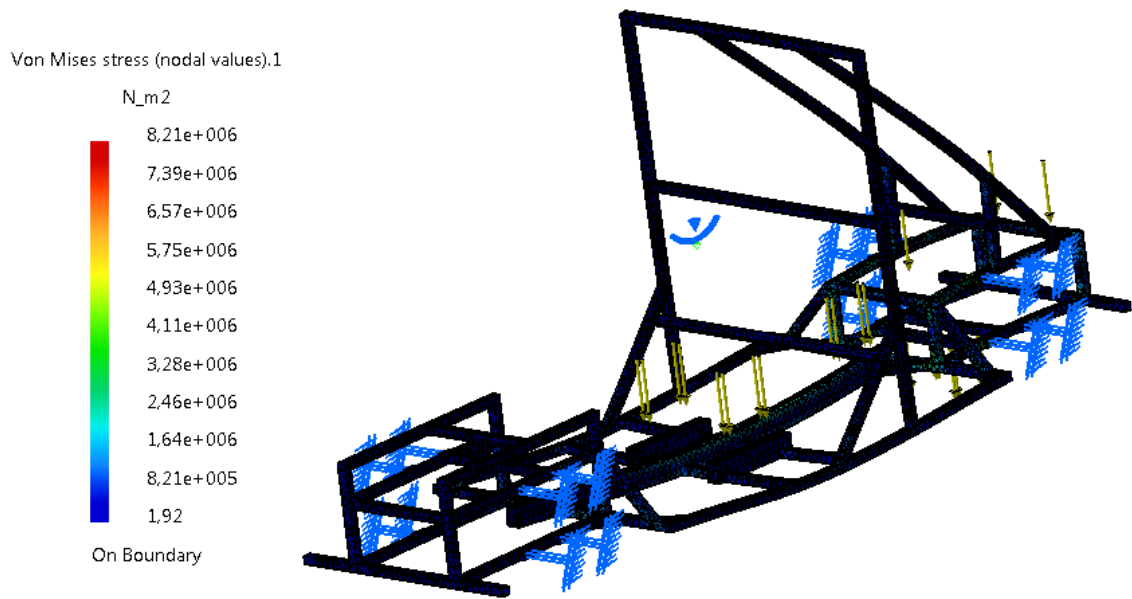


Figure E.6: Bending load boundary conditions

The front and rear roll hoops are clamped and the loads were applied as per Chapter 2 .



*Figure E.7: FEM model after applying bending load*

### E.3 Beam shortlist

Table E.2: Beam shortlists

S.no	Middle beam of floor structure			Other beams			$K_t$	$\sigma_v$ (torsion)	Weight	$\delta_z$	$\sigma_v$ (Bending)	$K_b$
	W(mm)	H(mm)	T(mm)	W(mm)	H(mm)	T(mm)	Nm/deg	(Mpa)	(kg)	(mm)	(MPa)	(N/mm)
1	40	40	2	30	30	2	632	786	48,37	1,59	75,4	3036,9
2	40	40	2	20	40	2	797	767	54,431	1,26	85	3832,3
3	40	40	2,5	30	30	2	751	446	49,137	1,26	68	3832,3
4	40	40	2,5	20	40	2	930	358	55,204	1,19	80	4057,7
5	50	50	2	30	30	2	840	358	49,171	1,16	60,5	4162,6
6	50	50	2	20	40	2	1033	315	56,149	0,943	75,6	5120,5
7	50	50	2,5	30	30	2	872	352	50,159	1,09	57	4429,9
8	50	50	2,5	20	40	2	1057	330	57,141	0,88	66	5487,1
9	60	60	2	30	30	2	930	332	49,99	0,951	53	5077,4
10	60	60	2	20	40	2	1142	254	56,982	0,742	69	6507,6
11	60	60	2,5	30	30	2	962	340	51,205	0,893	54,2	5407,2
12	60	60	2,5	20	40	2	1202	268	58,192	0,69	59,8	6998,0
13	70	70	2,5	30	30	2	1081	348	52,25	0,77	47,9	6271,0
14	70	70	2,5	20	40	2	1367	358	59,243	0,56	60	8622,6
15	80	80	2,5	30	30	2	1171	350	53,345	0,718	52	6725,1
16	80	80	2,5	20	40	2	1510	302	60,343	0,491	49,7	9834,3
17	90	90	2,5	30	30	2	1510	393	54,391	0,7	43,2	6898,1
18	90	90	2,5	20	40	2	1712	266	61,394	0,444	44,5	10875,3
19	100	100	2,5	30	30	2	1513	344	55,739	0,67	46,9	7206,9
20	100	100	2,5	20	40	2	1896	233	62,227	0,432	34,3	11177,4
21	30	50	2	30	30	2	758	485	48,966	1,29	61,2	3743,1
22	30	50	2	20	40	2	917	392	55,382	1,04	56,2	4642,9
23	30	50	2,5	30	30	2	771	385	49,703	1,23	59,1	3925,7
24	30	50	2,5	20	40	2	930	345	56,156	1,01	51,4	4780,8
25	40	60	2	30	30	2	825	401	49,76	1,06	55,8	4555,3
26	40	60	2	20	40	2	1018	304	56,215	0,86	52	5614,7
27	40	60	2,5	30	30	2	856	388	50,749	0,99	54	4877,4
28	40	60	2,5	20	40	2	1049	316	57,207	0,799	48,9	6043,4
29	40	80	2	30	30	2	889	350	50,631	0,838	50,5	5762,1
30	40	80	2	20	40	2	1098	364	57,089	0,629	40,1	7676,7
31	40	80	2,5	30	30	2	930	331	51,837	0,719	51,2	6715,8
32	40	80	2,5	20	40	2	1134	287	58,299	0,59	40,9	8184,1
33	40	100	2,5	30	30	2	996	336	52,926	0,708	48,7	6820,1
34	40	100	2,5	20	40	2	1212	289	59,392	0,487	36,1	9915,1
35	50	70	2	30	30	2	930	372	50,588	0,873	48	5531,1
36	50	70	2	20	40	2	1152	322	57,047	0,685	61,4	7049,1
37	50	70	2,5	30	30	2	975	315	51,794	0,832	50,6	5803,7
38	50	70	2,5	20	40	2	1182	306	58,258	0,631	60	7652,4
39	50	90	2,5	30	30	2	1065	366	52,883	0,726	47,1	6651,0
40	50	90	2,5	20	40	2	1303	258	59,35	0,508	53,9	9505,2



41	50	100	2,5	30	30	2	1073	321	53,427	0,701	50,5	6888,2
42	50	100	2,5	20	40	2	1340	246	59,897	0,468	57,6	10317,6
43	60	80	2,5	30	30	2	1073	323	52,84	0,742	49,3	6507,6
44	60	80	2,5	20	40	2	1353	239	59,309	0,53	64,6	9110,6
45	60	100	2,5	30	30	2	1143	316	53,928	0,693	49,6	6967,7
46	60	100	2,5	20	40	2	1473	282	60,401	0,453	58,7	10659,2
47	80	100	2,5	30	30	2	1609	420	54,931	0,683	59,7	7069,8
48	80	100	2,5	20	40	2	1671	493	61,411	0,444	87,5	10875,3

Based on weight, torsional stiffness, bending stiffness and the stress developed nine best options were selected from Table E.2. It was assumed that the shortlisted options would have the same effect on all the other variants in the terms of weight, torsional stiffness and bending stiffness. All the nine options are highlighted in green in Table E.2.

## REFERENCES

- [1] E. Vijayakumar, Chassis strength evaluation and rollover analysis of a single seat electric car, Gothenburg: Volvo group trucks technology, 2013.
- [2] "[http://en.wikipedia.org/wiki/Speed\\_bump](http://en.wikipedia.org/wiki/Speed_bump)," 2013. [Online].
- [3] "Curbs and Driveways," State of California Department of Transportation, California, 2006.
- [4] Tobias Rattfelt, "Preparatory Component Selection for Design of Prototype Electric One-Seater Car," Volvo group trucks technology, Gothenburg, 2013.
- [5] A. R. a. R. Prathap, Introduction to statics and dynamics, Oxford University press, 2002.
- [6] T. D. C. I. K. C. E. J. C. John T. McConville, "Anthropometric Relationships of Body and Body Segment Moments of Inertia," Air Force Aerospace Medical Research Laboratory, Ohio, 1980.
- [7] Joakim, "Subsystem Design and Packaging of Electric One Seater Car," Volvo Group Trucks Technology, Gothenburg, 2013.
- [8] G. Werum, "Steering actuator sizing of electric demonstration vehicle," Volvo AB, Gothenburg, 2013.
- [9] N. D. Smith, "Understanding Parameters Influencing Tire Modeling," Department of Mechanical Engineering, Colorado State University, Colorado, 2004.
- [10] J.-W. K. J. O. Y. Z. a. A. D. Chang-Ro Lee, "Validation of a FEA Tire Model for Vehicle Dynamic Analysis and Full Vehicle Real Time Proving Ground Simulations," *NHCRP*, vol. Paper number 971100.
- [11] P. D. r. n. H. Winner, Fahrndynamik und Fahrkomfort, Darmstadt: Technische Universität Darmstadt, 2013.
- [12] A. Hac, "Rollover Stability Index Including Effects of Suspension Design," *SAE technical paper series*, no. 2002-01-0965, 2002.
- [13] M. P. a. A. S. M. P. Daniel A. Fittanto, "Passenger Vehicle Steady-State Directional Stability Analysis Utilizing EDVSM and SIMON," Engineering Dynamics corporation and Daniel A. Fittanto, P.E., 2004.
- [14] A. Roberts, "Dynamic Analysis of Side-by-Side Utility and Recreational Vehicle," The Engineering Institute, USA.
- [15] Y.-H. J. Hsu, "Estimation and Control of Lateral Tire Forces using Steering Torque," Stanford University, California, 2009.
- [16] B. M. E. R. L. Baudille Riccardo, "An Integrated Tool for Competition Go-Kart Track Analysis," Department of Mechanical Engineering, "Tor Vergata" University, Rome.
- [17] G. Lind, "Weather and Traffic Controlled Variable Speed Limits in Sweden," Movea Traffikkonsult AB, Stockholm, 2007.
- [18] Tefyma, ISBN 91-87234-13-0.
- [19] D. C. J. P. R. R. H. Andrew Deakin, "The effect of chassis stiffness on race car handling balance," *SAE Technical paper*, vol. 01, no. 3554, p. 10.4271, 2000.
- [20] R. P. Singh, "Structural Performance Analysis of Formula SAE Car," *Jurnal Mkanikal*, vol. 31, pp. 46-61, 2010.
- [21] R. steels, "Ruuki steels," 20 05 2013. [Online]. Available: [www.ruuki.com](http://www.ruuki.com).

- [22] SSAB, SSAB steel profilers, 11 June 2013. [Online]. Available: <http://www.ssab.com/en/Products--Services/>.
- [23] W. h. organisation, *NCD country profiles*, World health organisation, 2011.
- [24] L. M. Giancarlo Genta, *Automotive Chassis Design*, Torino: Springer, 2009.
- [25] J. E. J. Charles G.Salmon, *Steel Structures: Design and behavior*, Harper & Row, 1980.
- [26] C. S. N.C. Pandya, *Machine design*, Charotar book house, 1974.
- [27] T. Rattfelt, "Construction Description of Electric One Seater Car," Volvo Group Trucks Technology, Gothenburg, 2013.
- [28] C. M.Harris, *Shock and Vibration Handbook*, California: McGraw- Hill, 2002.
- [29] H. H. Jonas Hellgren, "Electric Demonstration Vehicle- Battery and Genset System Design," Volvo Group Trucks Technology, Gothenburg, 2013.
- [30] L. W. B. S. T. P. L. Anders Gustafsson, "Stature and sexual stature dimorphism in Sweden, from the 10th to the end of 20th century," *American journal of human biology*, no. 19, pp. 861-870, 2007.
- [31] C. f. student, Interviewee, *Suspension system*. [Interview]. 18 February 2012.
- [32] 02 03 2013. [Online]. Available: <http://www.directindustry.com/industrial-manufacturer/linear-actuator-61042.html>.
- [33] B. H.Jacobson, *Vehicle Dynamics Compendium*, Gothenburg: Chalmers University of Technology, 2012.
- [34] "Wheel Weights," 29 06 2010. [Online]. Available: [www.wheelweights.net](http://www.wheelweights.net). [Accessed 22 04 2013].
- [35] M. R. J. W. F. P. H. M. F. a. K. C.A. Plaxico, "Recommended Guidelines for Curb and Curb-Barrier Installation," NHCRP(National Co-operation Highway Research), Washington D.C., 2005.
- [36] E. a. e. s. department, *Design specification and requirements manual*, London, 2010.
- [37] D. P. V. T. a. R. R. Chad Larish, " A New Predictive Lateral Load Transfer Ratio for Rollover Prevention System," IEEE, Minnessota, 2012.